General Diffusions: Financial Applications, Analysis and Extension

ZHAO, Jing

A Thesis Submitted in Partial Fulfillment
of the Requirements for the Degree of
Doctor of Philosophy
in
Statistics

The Chinese University of Hong Kong
May 2010

Thesis/Assessment Committee

Professor Chan Ngai-Hang (Chair)
Professor Wong Hoi-Ying (Thesis Supervisor)
Professor Chan Ping-Shing (Committee Member)
Professor Gu Ming-Gao (Committee Member)
Professor Kwok Yue-Kuen (External Examiner)

The Chinese University of Hong Kong

The undersigned certify that we have read a thesis, entitled "General Diffusions: Financial Applications, Analysis and Extension" submitted to the Graduate School by ZHAO Jing ( ) in partial fulfillment of the requirements for the degree of Doctor of Philosophy in Statistics. We recommend that it be accepted.

Prof. Wong Hoi-Ying
Supervisor

Prof. Chan Ngai-Hang

Prof. Chan Ping-Shing

Prof. Gu Ming-Gao

Prof. Kwok Yue-Kuen
External Examiner

Declaration

No portion of the work referred to in this thesis has been submitted in support of an application for another degree or qualification of this or any other university or other institution of learning.

Abstract of thesis entitled:
General Diffusions: Financial Applications, Analysis and Extension
Submitted by ZHAO Jing
for the degree of Doctor of Philosophy in Statistics
at The Chinese University of Hong Kong in May 2010.

ABSTRACT

General diffusion processes (GDP), or Itô's processes, are potential candidates for the modeling of asset prices, interest rates and other financial quantities to cope with empirical evidence. This thesis considers the applications of general diffusions in finance and potential extensions. In particular, we focus on financial problems involving (optimal) stopping times. A typical example is the valuation of American options. We investigate the use of Laplace-Carson transform (LCT) in valuing American options, and discuss its strengthen and weaknesses. Homotopy analysis from topology is then introduced to derive closed-form American option pricing formulas under GDP. Another example is taken from optimal dividend policies with bankruptcy procedures, which is closely related to excursion time and occupation time of a general diffusion. With the aid of Fourier transform, we further extend the analysis to the case of multi-dimensional GDP by considering the currency option pricing with mean reversion and multi-scale stochastic volatility.

摘要

為了兼顧大量的經驗證據, 一般擴散過程或者Ito過程是模擬資產價格, 利率水平和其它金融數量的潛在模型. 本文探討了一般擴散過程在金融的方面的應用以及潛在的推廣. 具體地説, 我們集中研究涉及最優停時的金融問題. 美式期權定價是一個典型的例子. 我們探討了拉普拉斯-卡森變換在分析美式期權方面的作用和弱點. 為了推導一般擴散過程下面的美式期權的解析解, 我們採用了來源于拓撲學中的同倫分析. 另一個例子考慮了破産過程對最優派息策略的影響. 這個問題與一個一般擴散過程的巡潛時和佔位時緊密相關. 在傅立葉變換的幫助下, 我們通過研究自回歸和多尺度隨機波動下面的外匯期權定價, 將分析擴展到了多維一般擴散過程.

ACKNOWLEDGEMENT

I would like to express my deepest gratitude to my supervisor, Prof. Wong, Hoi-Ying, for his vision, guidance, motivation, availability, help and generous support throughout the period of my PhD program. Special thanks should go to Prof. Chan Ngai-Hang, Prof. Chan Ping-Shing, Prof. Gu Ming-Gao, and Prof. Kwok Yue-Kuen for their service as committee members and giving valuable comments on my research. I am also thankful for the assistance from the faculty of the Department of Statistics. Finally, I owe a debt of gratitude to my parents and friends for their love, support and encouragement over the years.

Contents

List of Figures

List of Tables

Chapter 1

Introduction

General diffusion processes are potential candidates for the modeling of asset prices, interest rates and other financial quantities. Specifically, let $\{X_t \in \mathbb{R} : t \in [0,\infty)\}$ be a stochastic process defined on a probability space $(\Omega, \mathcal{F}, P)$ with a filtration $\{\mathcal{F}_t\}_{t\geq 0}$, meaning a family of sub-σ-algebras of $\mathcal{F}$ with $\mathcal{F}_s \subseteq \mathcal{F}_t$ whenever $s \leq t$. One-factor general diffusion process (GDP) is described by the stochastic differential equation (SDE)

$$\mathrm{d}X_t = \widetilde{\mu}(X_t, t)\mathrm{d}t + \widetilde{\sigma}(X_t, t)\mathrm{d}W_t^P, \quad X_0 = x_0, \tag{1.1}$$

where the drift $\widetilde{\mu}(x,t) : \mathbb{R}\times[0,\infty) \to \mathbb{R}$ and diffusion coefficient $\widetilde{\sigma}(x,t) : \mathbb{R}\times[0,\infty) \to \mathbb{R}_+$ are real, deterministic functions and $\{W_t^P, t \geq 0\}$ is the standard Brownian motion process, representing the uncertainty in the economy, defined on $(\Omega, \mathcal{F}, P)$. The representative investor is assumed to have access only to the information contained in the historical data, which can be modeled by the σ-field generated by $\mathcal{F}_t = \sigma\{X_s : 0 \leq s \leq t\}$. In order for the SDE (1.1) to admit unique solution, throughout the thesis we assume generally that $\widetilde{\mu}(x,t)$ and $\widetilde{\sigma}(x,t)$ are measurable functions and satisfy the following Lipschitz and growth conditions: for any $t \geq 0$,

$$|\widetilde{\mu}(x,t) - \widetilde{\mu}(y,t)| + |\widetilde{\sigma}(x,t) - \widetilde{\sigma}(y,t)| \leq L|x-y|, \forall x, y \in \mathbb{R}, \tag{1.2}$$

and for any $x \in \mathbb{R}$,

$$|\widetilde{\mu}(x,t)| + |\widetilde{\sigma}(x,t)| \leq K(1+|x|), \forall t \geq 0, \tag{1.3}$$

where $L > 0$ and $K > 0$ are constants.

1.1 American Options under General Diffusions

General diffusions have been commonly used to model stochastic dynamics of financial securities following the works of Black and Scholes (1973) and Merton (1973) which established the foundation of option pricing theory in finance. Under the one-factor general diffusion process, the underlying asset price S_t evolves according to the SDE

$$\mathrm{d}S_t = (\mu(S_t, t) - D(S_t, t))S_t\mathrm{d}t + \sigma(S_t, t)S_t\mathrm{d}W_t^P, \tag{1.4}$$

where $\mu(S_t, t)$, $D(S_t, t)$, and $\sigma(S_t, t)$ are deterministic functions, which represent the expected return on the asset, the dividend yield and the return volatility, respectively. We assume that $\sigma(S_t, t) > 0$ and is bounded away from zero. Given this assumption and conditions (1.2)-(1.3), Novikov (1979) showed that there exists a unique martingale measure equivalent to P, or the risk-neutral probability Q, for the asset price considered in (1.4). This equivalent martingale measure is defined as

$$Q(A) = \int_A \xi(W_t^P, t)P(\mathrm{d}W_t^P), \quad \forall A \in \mathcal{F}_t, \tag{1.5}$$

where the adapted process

$$\xi(W_t^P, t) = \exp\left\{-\int_0^t \left(\frac{\mu(S_s, s) - r}{\sigma(S_s, s)}\right)\mathrm{d}W_s^P - \frac{1}{2}\int_0^t \left(\frac{\mu(S_s, s) - r}{\sigma(S_s, s)}\right)^2 \mathrm{d}s\right\}, \tag{1.6}$$

represents the Radon-Nikodym derivative of Q with respect to P. Consider

$$\mathrm{d}W_t^Q = \mathrm{d}W_t^P + \left(\frac{\mu(S_t, t) - r}{\sigma(S_t, t)}\right)\mathrm{d}t.$$

The risk-neutral asset dynamics is given by

$$\mathrm{d}S_t = (r - D(S_t, t))S_t\mathrm{d}t + \sigma(S_t, t)S_t\mathrm{d}W_t^Q. \tag{1.7}$$

Risk neutrality asserts that the expected total return on the asset equals the risk-free interest rate: $\mathbb{E}^Q[\mathrm{d}S_t/S_t + D(S_t, t)\mathrm{d}t|\mathcal{F}_t] = r\mathrm{d}t$, and any derivative can be uniquely

priced as the expected value of its discounted payoff under the risk-neutral measure. There has been phenomenal growth in financial products and instruments powered by these processes, as documented in Sundaresan (2000). The valuation and hedging of American-style options is a challenging topic in both academic circles and the financial industry, because most liquidly traded options are American-style contracts, which allow option holders to exercise their rights before maturity. Specifically, determining the price of an American option with payoff $(g(S_t))_{0\leq t\leq T}$ until maturity T could be characterized by the optimal stopping problem

$$V_A(S_t,t) = \operatorname{ess}\sup_{\tau\in\mathcal{T}_{t,T}} \mathbb{E}^Q[e^{-r(\tau-t)}g(S_\tau)|\mathcal{F}_t], \tag{1.8}$$

where $\mathcal{T}_{t,T}$ denotes the set of all stopping times between t and T. There is not yet an analytical solution to these financial products under a more realistic situation, beyond the Black-Scholes dynamics. The principal difficulty arises from the absence of a simple expression for the optimal early exercise strategy of American options, which should be determined within the pricing mechanism.

Using Black-Scholes asset price dynamics, the valuation of American options has been studied thoroughly. The intractability of the optimal stopping approach leads McKean (1965), Merton (1973), and many others to formulate the valuation of American options as a free boundary value problem involving the solution of partial differential equations (PDEs). Possible numerical methods for American option pricing are the finite difference method (Brennan and Schwartz, 1977; Wu and Kwok, 1997), the binomial method (Cox et al.,1979), and simulation via least squares method (Longstaff and Schwartz, 2001). An alternative method uses quasi-analytical approximations (Geske and Johnson, 1984; MacMillan, 1986; Barone-Adesi and Whaley, 1987). A quasi-analytical approximation can be obtained either by considering early exercise rights at a small number of discrete time points and then projecting the result to a larger number of exercise rights, or by simplifying the Black-Scholes equation with some ad hoc approximations. Important developments include the capped option approximation of Broadie and Detemple (1996),

Table 1.1: Examples of GDP with $\mathrm{d}S_t = (r-q)S_t\mathrm{d}t + \sigma(S_t,t)S_t\mathrm{d}W_t^Q$

Model	$\sigma(S_t,t)$	Remark
CEV model	δS_t^{β}	a special case of GDP (considered in Chapter 2&3)
hyperbolic sine model	$\alpha\sqrt{1+\ \beta/(S_t e^{\mu(T-t)})\ ^2}$	a special case of GDP (considered in Chapter 3)
Black-Scholes model	σ	a special case of the CEV model
square-root model	$\sigma S_t^{-1/2}$	a special case of the CEV model

and the integral-equation method of Kim (1990), Carr et al. (1992), Huang et al. (1996), Ju (1998), and others. Under the Black-Scholes assumption, the Laplace-Carson transform (LCT) has been adopted by Carr (1998) to value American options and by Kimura (2008) to value finite-lived Russian options.

Empirical evidence, however, suggests that the Black-Scholes model is inadequate to describe asset returns and the behavior of option markets. In particular, asset return distributions exhibit excess kurtosis and fat tails, whereas the volatility implied by the option prices shows a smile or skew shape across strike prices. This leads to a practical need to establish a more flexible model to cope with the empirical facts. One popular class of models is the one-factor general diffusion processes specified in (1.7). For instance, the constant elasticity of variance (CEV) model of Cox (1975, 1996) is a special case of one-factor general diffusion processes in which the volatility of the asset is a monomial of the asset price, i.e., $\sigma(S_t,t) = \delta S_t^{\beta}$. Carr et al. (1999) characterize the entire class of volatility functions that allow the stock price to be transformed into standard Brownian motion by changing only the scale. Table 1.1 gives some examples of one-factor general diffusion processes (GDP) with constant dividend yield q under the risk-neutral measure.

In fact, one-factor general diffusion processes with deterministic volatility function of time and the underlying asset price are often called local volatility (LV) models, or deterministic volatility function (DVF) models. This class of models originates from Derman and Kani (1994), Dupire (1994), and Rubinstein (1994) to fit the observed option prices (or, equivalently, the implied volatility surface) cross-sectionally. The main advantage of one-factor general diffusion processes, compared to Lévy or stochastic volatility models, is that they avoid non-traded source of risk. Consequently, the one-factor general diffu-

sion processes satisfy the complete market assumption that allows for arbitrage pricing and hedging.

One-factor general diffusion processes are very elegant and theoretically sound, however, they may suffer from some stability issues in practice. For instance, the calibration of local volatility function is sensitive to the input data. To avoid such problems, we may specify the parametric form for the local volatility function in advance, see the CEV model and the hyperbolic sine model in Table 1.1 for examples. Unfortunately, there are significant difficulties in extending the aforementioned results of American option valuation under the Black-Scholes dynamics to the case of general diffusion processes. Even though typical present value representations of the American option price (1.8) are valid with general diffusions, little is known about the corresponding early exercise strategy. In recent years, optimal stopping problems under general diffusions have generated considerable attention. For the valuation of American options under the CEV model, Detemple and Tian (2002) derive a recursive integral equation for the exercise boundary. Wong and Zhao (2008) generalize the artificial boundary finite difference method to the CEV model. Nunes (2009) proposes an alternative characterization of the early exercise premium that is valid for the CEV model.

However, the analytical valuation of American options under the CEV model is yet to solve. In Chapter 2, we show that by the Laplace-Carson transform (LCT) the determination of the optimal early exercise boundary can be separated from the American option valuation procedure, enabling the option holders to know the early exercise strategy in advance. The LCTs of the Greeks are derived in explicit forms. This may help managing market risks through hedging. The application of the LCT, however, relies heavily on the specific parametric form of the volatility function. When the local volatility function is time-dependent such as the hyperbolic sine model in Table 1.1, Laplace-Carson transforms do not work in valuing American options. The analytical valuation of American options under a wide class of general diffusion processes calls for techniques with more degree of flexibility.

In mathematical physics, Liao (1997) has introduced the homotopy analysis method from topology (Patty, 1993, Chapters 8-9) to solve nonlinear problems. Zhu (2006) has applied this approach to derive a closed-form solution to American put options on a non-dividend paying stock using the Black-Scholes model. Although his solution is expressed in Taylor's expansion, it is exact and explicit. The closed-form solution is useful not only in determining option values quantitatively, but also in understanding American option properties qualitatively. Chapter 3 investigates the analytic valuation of American options under general diffusion processes using homotopy analysis. Although it focuses on vanilla options, the method is generally applicable to any exotic derivatives with continuous earlier exercise rights.

Chapter 3 may contribute to the literature in the following ways.

1. The homotopy analysis method in American option pricing is generalized by introducing a shape parameter and kernel function, which could be used to reduce the error for a given order of approximation. This generalization originates from Liao (2004) in the area of heat transfer and fluid mechanics.

2. The determination of the optimal early exercise boundary is separated from the American option valuation procedure for general diffusion processes of a dividend paying stock. To our knowledge, similar separation is only obtained under the Black-Scholes model with zero dividend in the literature.[1]

3. Exact and explicit solutions for American options and the early exercise boundary are obtained in Maclaurin series under general diffusion processes.

4. As the option price and exercise policy are expressed as infinite series, sequence transformations are proposed to speed up the convergence. Specifically, the Padé technique is employed to improve the accuracy and efficiency.

[1]Carr (1998) is the first one using Laplace transform to separate the optimal early exercise boundary from the valuation procedure of American put on a non-dividend paying stock. In the context of homotopy analysis method, Zhu (2006) successfully does the separation for the American put options on a non-dividend paying stock.

5. A hybrid numerical scheme of homotopy analysis and finite difference method is proposed to the American option pricing under general diffusions. This proposed scheme is unconditionally stable and efficient given that the infinite homotopic series converges.

Therefore, a unified framework for American option pricing under general diffusion processes is established in Chapter 3. Numerical examples using the CEV model and the hyperbolic sine model show the validity, effectiveness, and flexibility of the proposed homotopy analysis approach.

1.2 Application in Optimal Dividend Policies

The financial applications of general diffusion processes are not restricted to option pricing. In the asset price dynamics (1.4), the dividend yield $D(S_t, t)$ is assumed to be a deterministic function of time and the underlying asset price for the convenience of derivative pricing. In order to investigate the optimal dividend payment strategies, the firm-surplus approach is employed in Chapter 4. In particular, the optimal dividend policy aims at maximizing the expectation of the discounted total dividends until a firm becomes bankruptcy in the physical measure. Thus, the dividend policy should strike the balance between bankruptcy risk and the dividends received by shareholders.

Gerber and Shiu (2003, 2004) propose a dividend barrier strategy on the surplus, which is assumed to follow a Brownian motion, and give a comprehensive history of this topic. Their approach has been extended in various ways recently. For instance, Gerber and Shiu (2006) study the generalized barrier strategy with a refraction boundary, above which the dividends are paid at a constant dividend rate. Leung et al. (2008) consider a finite time dividend-ruin model in which the firm value, instead of the surplus, follows a geometric Brownian motion (GBM). The dividend barrier is an upside reflecting boundary on the firm value. Bankruptcy occurs when the firm value hits a downside barrier. Cai et al. (2006) show how the expectation of discounted dividends and the optimal dividend barrier can be calculated when the surplus earns investment income at

a constant force, which essentially leads to an Ornstein-Uhlenbeck (OU) process with a negative mean-reverting rate. In Chapter 4, we further assume that the firm pays a debit interest rate depending on the deficit level when it is in financial distress. The proposed model is a special case of general diffusion processes (1.1) with drift $\widetilde{\mu}(x,t) = \mu + \rho(x)x$ and diffusion coefficient $\widetilde{\sigma}(x,t) = \sigma$, where $\rho(x)$ is the surplus-dependent credit/debit interest rate.

However, there is still a gap between the theoretical results and reality, as the impact of bankruptcy procedures on optimal dividend strategy remains unclear. Chapter 4 is devoted to filling that gap. In Chapter 11 of the US Bankruptcy Code, default and liquidation are two distinguishable events. A defaulted firm is allowed to continue its business for a "grace" period of time, during which a renegotiation process can take place between shareholders and debt holders and the firm is given the chance to reorganize. If the firm is unable to recover during this period, then shareholders are forced to declare bankruptcy.

This bankruptcy procedure could be integrated into our model setting by using so-called excursion time or occupation time framework, which have appealing interpretation in a corporate bankruptcy scheme. Suppose that a regulatory authority takes its bankruptcy filing actions according to a hypothetical default clock, in the case of excursion time framework, an excursion time is counted by this default clock, which starts ticking when the surplus process breaches the default threshold and is reset to zero if the firm recovers from the default. Thus, successive defaults are possible until the underlying surplus stays consecutively below the default threshold longer than some predetermined time. In the case of occupation time framework, the default clock, corresponding to an occupation time, is not reset to zero when a firm emerges from default, but it is only halted and restarted when the surplus process goes below the default threshold again. As a result, the past defaults are never forgiven. Specifically, our model is based on the surplus of a firm. When the firm is in a creditworthy condition, the surplus generates an investment income at a constant rate of interest. Default occurs when the surplus hits a

default threshold, but the firm is allowed to continue its business for a period. Once the surplus is negative, a debit interest is charged at a rate related to the deficit level of the firm. Liquidation is triggered by an excursion time or an occupation time.

The impact of bankruptcy mechanisms has recently attracted a great deal of attention. Chen and Suchaneki (2007) show how the mentioned bankruptcy procedure affects the market value of life insurance liabilities. They also provide examples from different countries in which defaulted firms were allowed to continue operations for a period. For instance, the grace period lasts from 119 days up to 1669 days for defaulted companies in United States. In France, a legal three-month observation period before a possible liquidation is systematically granted by the courts to firms in financial distress. Similar bankruptcy mechanisms are also considered by Francois and Morellec (2004), Cetin et al. (2004), Yildirim (2006) and Broadie et al. (2007). These studies concentrate on the optimal capital structure rather than the dividend policy and are specific to Brownian motion or GBM. In Chapter 4, we consider a more general situation, in which the surplus follows an OU process. Moreover, our results are applicable to any values of mean-reverting rate. Cadenillas et al. (2007) also study optimal dividend policy with a mean-reverting cash reservoir. However, they do not consider bankruptcy procedures.

When the underlying stochastic variable follows Brownian motion or GBM, the distribution of the excursion time and occupation time has been studied thoroughly and applied to different aspects. Lau and Kwok (2004) construct valuation algorithms that price risky convertible bonds with embedded option features and explored the impact of the excursion time requirement in the soft call constraint on optimal issuer's calling policy. Galai et al. (2007) consider the liquidation is triggered when the total time that the firm's asset value spends under the distress threshold exceeds a predetermined grace period and the corresponding valuation of equity and debt. Bernard and Chen (2009) model the realistic bankruptcy procedure by an excursion time and an occupation time, respectively and investigate how the regulator can establish regulatory rules to meet some regulatory objectives. Linetsky (1999) derives the pricing formulas of step options

using the distribution of the occupation time variable under GBM. Hugonnier (1999) presents the Feynman-Kac framework to study occupation times under Brownian motion and GBM, and links up occupation time derivatives with α-quantile options. Wong and Kwok (2003) extend the aforementioned approaches to options on multiple assets with an occupation time. Beyond Brownian motion, Leung and Kwok (2007) derive the distribution of occupation time under the CEV model. To the best of our knowledge, excursion times or occupation times of (restricted) OU processes have not yet been considered in the literature. Chapter 4 thus provides a unified framework to study the related problems. For instance, our result can be applied to the valuation of Parisian options under mean reversion.

1.3 Multi-Dimensional GDP: Application in Currency Option Pricing

The OU process observed in optimal dividend problem motivates us to consider its use in option pricing. OU processes are usually linked to mean-reversion in finance. Evidence of mean reversion in financial assets is abundant. In particular, there is strong evidence of mean reversion for currencies, such as that presented by Bessembinder et al. (1995). Jorion and Sweeney (1996) show that the real exchange rates revert to their mean levels and Sweeny (2006) provides empirical evidence of mean reversion in G-10 nominal exchange rates. Theoretical results have also been presented on mean-reverting currency process. Sorensen (1997) suggests that mean reversion takes place through the dynamics of the domestic and foreign term structures of interest rates, whereas Ekvall et al. (1997) provide several explanations for mean-reverting exchange rates using an equilibrium model. One possible reason for the mean reversion witnessed in the foreign-exchange market is the intervention of central banks, which keeps the exchange rates close to desired target values. Thus, mean-reversion speed can be regarded as a measure for the magnitude of central bank intervention.

One-factor general diffusion processes are however insufficient to capture market phe-

nomena for currencies since stochastic volatility is inevitable for currency option pricing. Ekvall et al. (1997) are among the pioneers who proposed that the logarithmic currency value follows an Ornstein-Uhlenbeck process under the risk-neutral measure and who derived the closed-form solution to European options. Although their approach has been extensively applied to path-dependent currency options, such as in the studies by Hui and Lo (2006) and Wong and Lau (2008), the constant volatility assumption of their model is generally regarded as inappropriate. Not only does the implied volatility smile of the currency option market call for stochastic volatility, but there is a theoretical inconsistency in their model. As Duan and Pliska (2003)[2] point out, even though the currency exhibits mean reversion under the physical probability measure, the risk-neutral process has no mean reversion effect in a continuous-time economy if the volatility and interest rates (both domestic and foreign) are constant values. This is because the Black-Scholes (BS) delta-hedging argument sends the risk-neutral drift to a constant. A risk-neutral mean reversion process can occur only in an incomplete market in which the number of stochastic variables is larger than the number of underlying assets of the option.

A possible source of incompleteness in a financial market is stochastic volatility (SV). Wong and Lo (2009) recently incorporated the Heston (1993) SV model into a mean reversion asset price process. They then obtained a closed-form European option pricing formula and devised a numerical approach for path-dependent options. Although the Wong and Lo model may be useful for assets with mean reversion and SV, it is inadequate for the currency option market. The empirical results of Fiorentini et al. (2002) indicate that the Heston model has a tendency to overprice out-of-the money (underprice in-the-money) calls for daily data. Andersen and Bollerslev (1997) examined the intraday periodicity and the volatility in foreign exchange and equity markets, and found that several distinct component processes affected the volatility dynamics. In other words, there should be more than one factor in the SV process. The empirical study of Alizadeh

[2]Although the argument of Duan and Pliska (2004) is based on option pricing on co-integrated assets, it also holds true for mean reversion because a mean-reverting asset is co-integrated with itself.

et al. (2002) further documented that there were two dominated stochastic factors that governed the evolution of currency volatility, with one highly persistent factor and one quickly mean-reverting factor. Chernov et al. (2003) also found evidence in favor of a second volatility factor. In fact, LeBaron (2001) has documented that two-factor SV models can produce the kurtosis, fat-tailed return distribution and long memory effect that is observable in many financial times series.

Chapter 5 aims to extend one-factor general diffusion processes to multi-factor models for currency option pricing incorporating mean reversion and multi-scale stochastic volatility. In particular, multi-dimensional general diffusion process (GDP) is defined by the system of stochastic differential equations (SDEs)

$$\mathrm{d}\mathbf{X}_t^i = a^i(\mathbf{X}_t, t)\mathrm{d}t + \sum_{j=1}^{n} b^{ij}(\mathbf{X}_t, t)\mathrm{d}W_t^{P,j}, \quad \text{for } i = 1, ..., m, \tag{1.9}$$

where $a^i (i = 1, ..., m)$ and $b^{ij} (i = 1, ..., m; j = 1, ...n)$ are measurable functions from $\mathbb{R}^m \times [0, \infty)$ into $\mathbb{R}$. The process $\mathbf{W}^P = (W^{P,1}, ..., W^{P,n})^{\mathbf{T}}$, with $^{\mathbf{T}}$ denoting transposition, is an n-dimensional Brownian motion on a probability space $(\Omega, \mathcal{F}, P)$, and $\mathbb{F} = (\mathcal{F}_t)_{t\geq 0}$ is the P-augmentation of the filtration generated by $\mathbf{W}^P$. Like in the case of one-factor model, we assume that the coefficients a^i and b^{ij} satisfy appropriate growth and Lipschitz conditions. For the mean reversion and multi-scale stochastic volatility model considered in Chapter 5, the component $\mathbf{X}^1$ describes the log-currency- value process and is denoted by $X_t = \log(S_t)$. The other components of $\mathbf{X}$ can then be used to model the structure of the market in which S_t is embedded. In our case, they include a specification of stochastic volatility.

Multi-scale SV (MSV) models have gained attention in the option pricing literature. Fouque et al. (2003) proposed a two-scale SV model that was based on the suggestion of Alizadeh et al. (2002) and others, and managed to calibrate all effective parameters from volatility skews of equity options. They also obtained an asymptotic approximation of a European call option as the sum of the BS formula and the Greek correction term. The Greek correction term is a combination of the gamma, delta-gamma, vega, and delta-

vega of the option. The model developed by Fouque et al. (2003) has been applied to defaultable bonds (Fouque et al. 2006), lookback options (Wong and Chan, 2007), default correlation (Fouque et al., 2008) and turbo warrants (Wong and Chan, 2008). Despite the fact that the model of Fouque et al. (2003) does not take into account the mean reversion on the asset value process, it relies heavily on the assumption that the mean reversion rates of the two SV driving factors are close to zero and infinity, respectively, in order to derive asymptotic solutions.

Fatone et al. (2009) considered a simple MSV model that is a special case of Fouque et al. (2003), but parsimonious and analytically tractable. They have demonstrated its calibration to the implied volatilities and obtained a corresponding explicit solution for European options. Chapter 5 combines the works of Wong and Lo (2009) and Fatone et al. (2009) and extends them to currency option pricing with mean reversion and MSV. An advantage of the proposed model is that it can simultaneously fit the term structure of currency futures and the implied volatility surface of currency options. It is in fact a super-calibration to currency futures in the sense that the resulting characteristic function of the log-currency-value is expressed directly in terms of the observed term structure of the futures contracts of the underlying currency.

The proposed model in Chapter 5 is flexible enough for a financial analyst to perform scenario analysis with it. For instance, a currency option trader who is concerned about the impact of central bank intervention on option prices can examine the sensitivity of the option price to the change in mean-reversion speed. To allow seasonal volatility within derivative pricing, the mean levels of the volatility driving processes can be postulated to be a time-dependent periodic function. In such a situation, the closed-form solutions for vanilla call and put options remain available.

Once the characteristic function is derived, the fast Fourier transform (FFT) option pricing approach of Carr and Madan (1999) can be effectively carried out to value the vanilla call and put options. However, we further improve the computational efficiency by relaxing the grid size constraint within the FFT by employing the fractional FFT (FRFT)

of Bailey and Swarztrauber (1991) and Chourdakis (2004). The FRFT is extremely useful when a large number of evaluations on characteristic function are needed in case of calibration to European option prices. Using Monte Carlo simulation as a benchmark, our numerical examples show that the derived option pricing formula is accurate and efficient for practical use.

1.4 Outline of the Thesis

The remainder of the thesis is organized as follows. Chapter 2 investigates American option pricing under the CEV model by using the Laplace-Carson transform. Chapter 3 provides closed-form solutions in the sense of homotopy expansion for American options under general diffusion processes, which nest the CEV model as special cases. Chapter 4 examines the impact of bankruptcy procedures on optimal dividend barrier policies wherein generalized barrier strategies and finite time dividend-bankruptcy models are also considered. Chapter 5 extends one-factor general diffusion processes to multi-factor models for currency option pricing incorporating mean reversion and multi-scale stochastic volatility. Chapter 6 concludes the thesis.

Chapter 2

American Options under the CEV Model

In recent years, empirical evidence shows that Black-Scholes model is difficult to reconcile with both the assumptions on the process of the underlying asset and the predictions on the behavior of option prices. The constant elasticity of variance (CEV) model introduced by Cox (1975) is a popular alternative in modelling asset price dynamics in practice. The CEV model assumes that the risk-neutral process of the underlying asset price S_t evolves according to the stochastic differential equation:

$$\mathrm{d}S_t = (r-q)S_t\mathrm{d}t + \delta S_t^{\beta+1}\,\mathrm{d}W_t^Q, \tag{2.1}$$

where r is the risk-free interest rate, q is the dividend yield, and W_t^Q is the Wiener process under the risk-neutral measure. It belongs to the class of general diffusion process with $\sigma(S,t) = \delta S^{\beta}$. Thus, β can be interpreted as the elasticity of the local volatility function because $\frac{\mathrm{d}\sigma/\sigma}{\mathrm{d}S/S} = \beta$, and δ is the scale parameter fixing the initial instantaneous volatility at time $t = 0$, $\sigma_0 = \sigma(S_0) = \delta S_0^{\beta}$.

Closed-form pricing formulas of European call and put options are available for the CEV model (see Cox 1975, Emanuel and MacBeth 1982). As stated in Wong and Zhao (2008), the CEV model nests several asset price processes as special cases by setting different values of β and captures the volatility smile in the financial market.

2.1 The free-boundary problem

Let $P_A(S,\tau)$ be the American put option price with strike price K and $S_f(\tau)$ be the corresponding optimal exercise boundary, where $\tau = T - t$ is the remaining time to maturity and T is the calendar time of maturity. The valuation can be formulated as a free boundary problem. Specifically,

$$\frac{\partial P_A}{\partial \tau} = \frac{1}{2}\delta^2 S^{2\beta+2}\frac{\partial^2 P_A}{\partial S^2} + (r-q)S\frac{\partial P_A}{\partial S} - rP_A, \tag{2.2}$$

$$P_A(S,0) = \max(K-S,0), \tag{2.3}$$

$$P_A(S_f(\tau),\tau) = K - S_f(\tau), \tag{2.4}$$

$$\frac{\partial P_A(S_f(\tau),\tau)}{\partial S} = -1, \tag{2.5}$$

$$\lim_{S\to\infty} P_A(S,\tau) = 0. \tag{2.6}$$

This PDE is defined on $S \in [S_f(\tau),\infty)$ and $\tau \in [0,T]$. Equation (2.5) is known as the high-contact condition for American put options. This condition must hold for all continuous asset price processes, including the CEV model (see Carr et al. 1992). In the region $(S_f(\tau),\infty)\times[0,T]$, $P_A(S,\tau) > \max(K-S,0)$. The option should be held rather than exercised and hence it is called the continuation region. In addition, $S_f(0^+) = \min(rK/q, K)$.

According to the put-call symmetry of American options (Proposition 6 in Detemple 2001), the problem of pricing a call option can always be converted into a problem of pricing a put option and vice versa under Markovian models. Thus, it suffices to consider the valuation of either the American put option or the American call option. This chapter considers the put option value.

2.2 Valuation with Laplace-Carson transforms

For $\lambda > 0$, define the Laplace-Carson transform (LCT) of the American put option price $P_A(S,\tau)$ as

$$\widehat{P}_A(S,\lambda) = \int_0^\infty P_A(S,\tau)\lambda e^{-\lambda\tau}d\tau := \mathcal{LC}[P_A(S,\tau)](\lambda). \tag{2.7}$$

Similarly, we denote the LCTs of $S_f(\tau)$ by $\widehat{S}_f(\lambda)$. There is no essential difference between the LCT and the Laplace Transform (LT) except that the use of LCT simplifies notation in the later analysis of this chapter. Under the Black-Scholes assumption, LCT has been adopted by Carr (1998) to value American options and by Kimura (2008) to value finite-lived Russian options. From equations (2.2)–(2.6), the following proposition is obtained to describe the LCT of the optimal exercise boundary.

Proposition 2.2.1. The LCT of the early exercise boundary of the American put option under the CEV model satisfies

$$A_1\Lambda(\widehat{S}_f(\lambda)) = A_2\phi_{\lambda+r}(\widehat{S}_f(\lambda)) + A_3\widehat{S}_f(\lambda)\left.\frac{\mathrm{d}\phi_{\lambda+r}(S)}{\mathrm{d}S}\right|_{S=\widehat{S}_f(\lambda)} + A_4\left.\frac{\mathrm{d}\phi_{\lambda+r}(S)}{\mathrm{d}S}\right|_{S=\widehat{S}_f(\lambda)}, \quad (2.8)$$

where

$$A_1 = \left(\frac{\lambda K}{\lambda+r} - \frac{\lambda}{\lambda+q}K\right)\left.\frac{\mathrm{d}\phi_{\lambda+r}(S)}{\mathrm{d}S}\right|_{S=K} + \frac{\lambda\phi_{\lambda+r}(S=K)}{\lambda+q},$$
$$A_2 = -\frac{q\Lambda(S=K)}{\lambda+q}, \quad A_3 = \frac{q\Lambda(S=K)}{\lambda+q}, \quad A_4 = -\frac{rK\Lambda(S=K)}{\lambda+r},$$

the explicit forms of $\Lambda(S)$, and $\phi_{\lambda+r}(S)$ are given in Appendix A.

Proof. Taking LCTs on equations (2.2)–(2.6) gives us

$$\frac{1}{2}\delta^2 S^{2\beta+2}\frac{\partial^2\widehat{P}_A}{\partial S^2} + (r-q)S\frac{\partial\widehat{P}_A}{\partial S} - (\lambda+r)\widehat{P}_A + \lambda\max(K-S,0) = 0, \quad (2.9)$$

$$\widehat{P}_A(\widehat{S}_f(\lambda),\lambda) = K - \widehat{S}_f(\lambda), \quad (2.10)$$

$$\frac{\partial\widehat{P}_A(\widehat{S}_f(\lambda),\lambda)}{\partial S} = -1, \quad (2.11)$$

$$\lim_{S\to\infty}\widehat{P}_A(S,\lambda) = 0. \quad (2.12)$$

The solution of the governing equation (2.9) is classic:

$$\widehat{P}_A(S,\lambda) = \begin{cases} C_{11}\phi_{\lambda+r}(S) + C_{12}\psi_{\lambda+r}(S), & \text{when} \quad S\in(K,\infty), \\ C_{21}\phi_{\lambda+r}(S) + C_{22}\psi_{\lambda+r}(S) + u_{\lambda+r}(S), & \text{when} \quad S\in(\widehat{S}_f(\lambda),K), \end{cases} \quad (2.13)$$

where $\psi_{\lambda+r}(S)$ and $\phi_{\lambda+r}(S)$ are the fundamental increasing and decreasing solutions with the explicit forms given in Appendix A. Moreover, based on the results in Davydov and Linetsky (2001), the Wronskian of $\psi_{\lambda+r}(S)$ and $\phi_{\lambda+r}(S)$ is defined by

$$\phi_{\lambda+r}(S)\frac{\mathrm{d}\psi_{\lambda+r}(S)}{\mathrm{d}S} - \psi_{\lambda+r}(S)\frac{\mathrm{d}\phi_{\lambda+r}(S)}{\mathrm{d}S} = \xi(S)\omega_{\lambda+r} = \Lambda(S), \quad (2.14)$$

where

$$\xi(S) = \exp\left(\frac{r-q}{\delta^2\beta}S^{-2\beta}\right), \quad \omega_{\lambda+r} = \begin{cases} \frac{2|r-q|\Gamma(2m+1)}{\delta^2\Gamma(m-k+1/2)}, & r-q \neq 0, \\ |\beta|, & r-q=0, \end{cases} \tag{2.15}$$

and $\Gamma(x)$ is the Euler Gamma function.

To match the boundary condition (2.12), we have $C_{12} = 0$. It is easy to see that

$$u_{\lambda+r}(S) = -\frac{\lambda}{\lambda+q}S + \frac{\lambda K}{\lambda+r} \tag{2.16}$$

is a particular solution to the non-homogeneous equation.

Based on the pathwise continuity of the solution at $S = K$ and the high-contact condition specified in (2.11), we obtain

$$\begin{cases} C_{11}a_1 = C_{21}a_1 + C_{22}a_2 + b_1, \\ C_{11}a_3 = C_{21}a_3 + C_{22}a_4 + b_2, \\ C_{21}a_5 + C_{22}a_6 = b_3, \end{cases} \tag{2.17}$$

where

$$\begin{aligned} &a_1 = \phi_{\lambda+r}(S=K), \quad a_2 = \psi_{\lambda+r}(S=K), \quad a_3 = \frac{\mathrm{d}\phi_{\lambda+r}(S)}{\mathrm{d}S}\Big|_{S=K}, \\ &a_4 = \frac{\mathrm{d}\psi_{\lambda+r}(S)}{\mathrm{d}S}\Big|_{S=K}, \quad a_5 = \frac{\mathrm{d}\phi_{\lambda+r}(S)}{\mathrm{d}S}\Big|_{S=\widehat{S}_f(\lambda)}, \quad a_6 = \frac{\mathrm{d}\psi_{\lambda+r}(S)}{\mathrm{d}S}\Big|_{S=\widehat{S}_f(\lambda)}, \\ &b_1 = u_{\lambda+r}(S=K), \quad b_2 = \frac{\mathrm{d}u_{\lambda+r}(S)}{\mathrm{d}S}\Big|_{S=K}, \quad b_3 = -1 - \frac{\mathrm{d}u_{\lambda+r}(S)}{\mathrm{d}S}\Big|_{S=\widehat{S}_f(\lambda)}. \end{aligned} \tag{2.18}$$

Thus, C_{11}, C_{21} and C_{22} can be uniquely determined as

$$\begin{cases} C_{11} = \frac{a_5(a_2b_2-a_4b_1)+a_6(a_3b_1-a_1b_2)}{(a_2a_3-a1a4)a_5} + \frac{b_3}{a_5}, \\ C_{21} = \frac{a_6(a_3b_1-a_1b_2)}{(a_2a_3-a_1a_4)a_5} + \frac{b_3}{a_5}, \\ C_{22} = \frac{a_1b_2-a_3b_1}{a_2a_3-a_1a_4}. \end{cases} \tag{2.19}$$

Denote $a_7 = \phi_{\lambda+r}(S = \widehat{S}_f(\lambda))$, $a_8 = \psi_{\lambda+r}(S = \widehat{S}_f(\lambda))$, and $b_4 = u_{\lambda+r}(S = \widehat{S}_f(\lambda)) - K + \widehat{S}_f(\lambda)$, the value match condition (2.10) corresponds to

$$C_{21}a_7 + C_{22}a_8 + b_4 = 0. \tag{2.20}$$

According to equations (2.14), we recognize that

$$\begin{aligned} &a_2a_3 - a_1a_4 = -\Lambda(K), \\ &b_3 = -b_2 - 1, \\ &a_6a_7 - a_5a_8 = \Lambda(\widehat{S}_f(\lambda)), \end{aligned}$$

which yields

$$\begin{cases} C_{11} = [(a_4a_5 - a_3a_6)b_1 + (a_1a_6 - a_2a_5 - \Lambda(K))b_2 - \Lambda(K)]/[\Lambda(K)a_5], \\ C_{21} = [-a_3a_6b_1 + (a_1a_6 - \Lambda(K))b_2 - \Lambda(K)]/[\Lambda(K)a_5], \\ C_{22} = [a_3b_1 - a_1b_2]/[\Lambda(K)]. \end{cases} \tag{2.21}$$

After simplifying (2.20), the functional equation for the LCT of the optimal exercise boundary is found

$$A_1\Lambda(\widehat{S}_f(\lambda)) = A_2\phi_{\lambda+r}(\widehat{S}_f(\lambda)) + A_3\widehat{S}_f(\lambda)\left.\frac{\mathrm{d}\phi_{\lambda+r}(S)}{\mathrm{d}S}\right|_{S=\widehat{S}_f(\lambda)} + A_4\left.\frac{\mathrm{d}\phi_{\lambda+r}(S)}{\mathrm{d}S}\right|_{S=\widehat{S}_f(\lambda)},$$

where

$$A_1 = \left(\frac{\lambda K}{\lambda+r} - \frac{\lambda}{\lambda+q}K\right)\left.\frac{\mathrm{d}\phi_{\lambda+r}(S)}{\mathrm{d}S}\right|_{S=K} + \frac{\lambda\phi_{\lambda+r}(S=K)}{\lambda+q},$$
$$A_2 = -\frac{q\Lambda(S=K)}{\lambda+q}, \quad A_3 = \frac{q\Lambda(S=K)}{\lambda+q}, \quad A_4 = -\frac{rK\Lambda(S=K)}{\lambda+r}.$$

□

Remark 2.2.1. Consider the functional equation (2.8), if we set

$$f(y) = A_1\Lambda(y) - A_2\phi_{\lambda+r}(y) - A_3y\left.\frac{\mathrm{d}\phi_{\lambda+r}(y)}{\mathrm{d}S}\right|_{S=y} - A_4\left.\frac{\mathrm{d}\phi_{\lambda+r}(S)}{\mathrm{d}S}\right|_{S=y}. \tag{2.22}$$

It can be verified that there exists a unique root of the equation $f(y) = 0$ in the interval $(0, K)$ for different values of model parameters. For instance, when $\beta < 0$ and $r - q > 0$, we have $f(K) > 0$, $f(0) < 0$, and $\frac{\mathrm{d}f(y)}{\mathrm{d}y} > 0$ for $y \in (0, K)$ based on the properties of the confluent hypergeometric functions and Euler Gamma function. After specifying the interval of the root, $\widehat{S}_f(\lambda)$ could be found by secant method for different values of λ.

Proposition 2.2.2. The LCT of the American put option price under the CEV model is given by

$$\widehat{P}_A(S,\lambda) = \begin{cases} C_{11}\phi_{\lambda+r}(S), & \text{when} \quad S \in [K, \infty), \\ C_{21}\phi_{\lambda+r}(S) + C_{22}\psi_{\lambda+r}(S) + u_{\lambda+r}(S), & \text{when} \quad S \in (\widehat{S}_f(\lambda), K), \end{cases} \tag{2.23}$$

where C_{11}, C_{21}, C_{22}, $\phi_{\lambda+r}(S)$, $\psi_{\lambda+r}(S)$, and $u_{\lambda+r}(S)$ are defined in Proposition 2.2.1. Moreover, $\widehat{S}_f(\lambda) < K$ is a unique positive solution of the functional equation (2.8).

Remark 2.2.2. Proposition 2.2.1 and Proposition 2.2.2 are also useful to perpetual American put option and Canadian put option considered by Carr (1998), of which

maturity follows an exponential distribution. The perpetual American put and its early exercise boundary can be obtained by setting $\lambda = 0$; whereas, those of Canadian put can be obtained by setting $\lambda = 1/T$. Mathematically, we have $P_A^{perpetual}(S) = \widehat{P}_A(S, \lambda = 0)$, $S_f^{perpetual} = \widehat{S}_f(\lambda = 0)$, $P_A^{Canadian}(S, T) = \widehat{P}_A(S, \lambda = 1/T)$ and $S_f^{Canadian} = \widehat{S}_f(\lambda = 1/T)$.

As important as computing the prices of an option is computing the standard hedge sensitivities: Δ, Γ, and Θ. In financial markets, the aim of a trader is to manage the Greeks so that all risks are acceptable. Provided the LCTs of the optimal exercise boundary and the American put option price under the CEV model, we can derive the LCTs of the Greeks in explicit forms as follows:

Proposition 2.2.3. The LCTs of the Greeks under the CEV model

$$\widehat{\Delta}(S, \lambda) = \mathcal{LC}\left[\frac{\partial P_A(S,\tau)}{\partial S}\right](\lambda) = \frac{\partial \widehat{P}_A(S,\lambda)}{\partial S},$$

$$\widehat{\Gamma}(S, \lambda) = \mathcal{LC}\left[\frac{\partial^2 P_A(S,\tau)}{\partial S^2}\right](\lambda) = \frac{\partial^2 \widehat{P}_A(S,\lambda)}{\partial S^2},$$

$$\widehat{\Theta}(S, \lambda) = \mathcal{LC}\left[\frac{\partial P_A(S,\tau)}{\partial \tau}\right](\lambda) = \lambda[\widehat{P}_A(S,\lambda) - \max(K - S, 0)],$$

are, respectively, given by

$$\widehat{\Delta}(S,\lambda) = \begin{cases} C_{11}\frac{\mathrm{d}\phi_{\lambda+r}(S)}{\mathrm{d}S} & , \ S \in [K, \infty), \\ C_{21}\frac{\mathrm{d}\phi_{\lambda+r}(S)}{\mathrm{d}S} + C_{22}\frac{\mathrm{d}\psi_{\lambda+r}(S)}{\mathrm{d}S} - \frac{\lambda}{\lambda+q} & , \ S \in (\widehat{S}_f(\lambda), K), \end{cases}$$

$$\widehat{\Gamma}(S,\lambda) = \begin{cases} C_{11}\frac{\mathrm{d}^2\phi_{\lambda+r}(S)}{\mathrm{d}S^2} & , \ S \in [K, \infty), \\ C_{21}\frac{\mathrm{d}^2\phi_{\lambda+r}(S)}{\mathrm{d}S^2} + C_{22}\frac{\mathrm{d}^2\psi_{\lambda+r}(S)}{\mathrm{d}S^2} & , \ S \in (\widehat{S}_f(\lambda), K), \end{cases}$$

$$\widehat{\Theta}(S,\lambda) = \begin{cases} \lambda C_{11}\phi_{\lambda+r}(S) & , \ S \in [K, \infty), \\ \lambda(C_{21}\phi_{\lambda+r}(S) + C_{22}\psi_{\lambda+r}(S) + u_{\lambda+r}(S) - K + S) & , \ S \in (\widehat{S}_f(\lambda), K). \end{cases}$$

Remark 2.2.3. By recognizing the relationship between LCT and LT, i.e.,

$$\mathcal{LC}\left[W(\tau)\right](\lambda) = \lambda \mathcal{L}\left[W(\tau)\right](\lambda), \tag{2.24}$$

the optimal exercise boundary, American put option price and Greeks can be expressed in terms of Laplace inversion:

$$S_f(\tau) = \mathcal{L}^{-1}\left[\widehat{S}_f(\lambda)/\lambda\right], P_A(S,\tau) = \mathcal{L}^{-1}\left[\widehat{P}_A(S,\lambda)/\lambda\right], \Delta = \mathcal{L}^{-1}\left[\widehat{\Delta}(S,\lambda)/\lambda\right],$$
$$\Gamma = \mathcal{L}^{-1}\left[\widehat{\Gamma}(S,\lambda)/\lambda\right], \text{ and } \Theta = \mathcal{L}^{-1}\left[\widehat{\Theta}(S,\lambda)/\lambda\right]. \tag{2.25}$$

2.3 Numerical Examples

This section provides numerical examples to illustrate the American option valuation under the CEV model using the Laplace-Carson transform. In fact, the implementation of our solution is straightforward given the analytical solutions. The first step is to numerically calculate the early exercise boundary. To this end, the secant method (or any other root-finding procedure) is applied to determine the unique root of the functional equation in Proposition 2.2.1 over the interval $(0, K)$. The Gaussian quadrature scheme is then implemented to numerically calculate Laplace inversion for the optimal exercise boundary. The Gaussian quadrature scheme is adopted because Piessens (1971) shows that directly implementing Gaussian quadrature scheme to the Bromwich inversion integral is very accurate on a fairly wide range of functions.

Figures 2.1–2.4 plot the early exercise boundaries of American put options under the CEV model with specified parameters. Understanding the early exercise strategy of American option may be of great independent interest to option investors. In fact, investment agents have to provide the expected holding time of an American-style contract. Other things being fixed, Figures 2.1–2.4 show that the early exercise boundary of a put option is shifting upward when r increases, q decreases, σ_0 decreases and/or β increases. These are very natural. When interest rate increases, it is more attractive to exercise the option early for cash due to a higher return from interest rate. When the underlying asset pays more dividend, the put option holder attends to delay exercising the option for receiving dividend from the asset. The continuation value of an American put is higher for a higher volatility because its European counterpart gains values from volatility. Thus, the American put is less likely to be exercised early for a highly volatile underlying asset. Under the CEV model, the instantaneous volatility function, $\sigma(S) = \delta S^{\beta} = \sigma_0(S/S_0)^{\beta}$, is increasing with σ_0, but decreasing with β, due to the fact that $S_0 > S_f(\tau)$ for American puts. It explains the shifts for the cases of Figures 2.3–2.4.

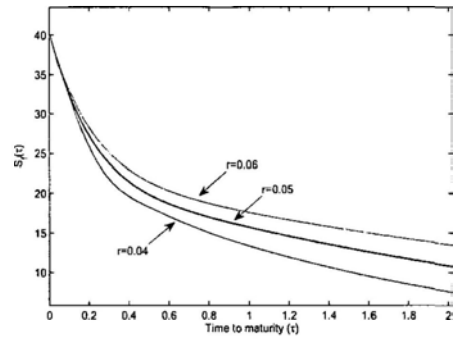

Figure 2.1: Early exercise boundaries (CEV) $(T = 2, q = 0, \sigma_0 = 0.4, \beta = -1, K = 40)$.

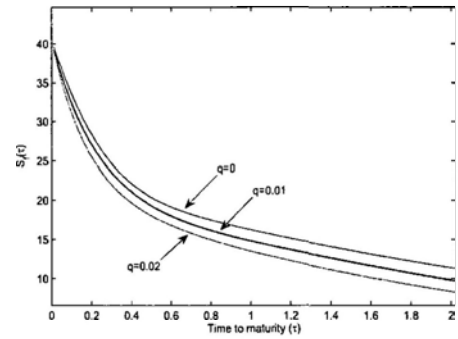

Figure 2.2: Early exercise boundaries (CEV) $(T = 2, r = 0.05, \sigma_0 = 0.4, \beta = -1, K = 40)$.

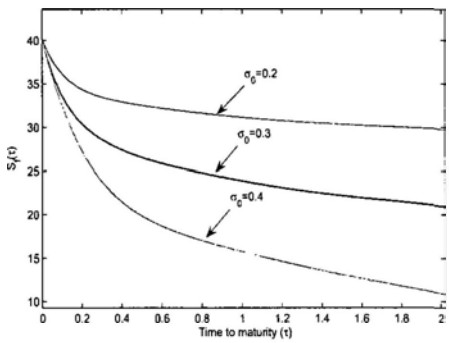

Figure 2.3: Early exercise boundaries (CEV) $(T = 2, r = 0.05, q = 0, \beta = -1, K = 40)$.

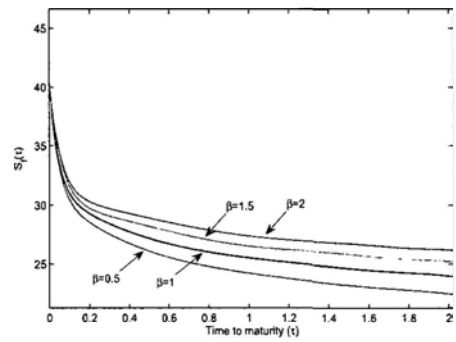

Figure 2.4: Early exercise boundaries (CEV) $(T = 2, r = 0.05, q = 0, \sigma_0 = 0.4, K = 40)$.

Despite the early exercise boundary, the Laplace-Carson transform approach also renders an efficient computation to the American option price based on the analytical solution in Proposition 2.2.2. To fairly compare the accuracy and efficiency of our numerical method, we use the binomial ap- proximation of Nelson and Ramaswamy (1990) with a large number of time steps (3000) as the benchmark and contrast our results with alternative numerical PDE methods. Specifically, the competitor approaches are the traditional Crank-Nicolson (CN) finite difference method (FDM) and the implicit FDM with an artificial boundary condition (ABC) proposed by Wong and Zhao (2008). It has been shown by Wong and Zhao (2008) that the ABC approach is an unconditionally stable FDM for CEV option pricing. Table 2.1 summarizes the computational results of American puts. The parameter values are $S_0 = 40$, $r = 5\%$, $q = 0$, and $T = 3$. The relative error (RE) shown in parentheses, which is the absolute difference between

the computed numerical values and the binomial approximation divided by the binomial approximation, is less than 1% for all cases. The computational time of the binomial approximation with large time steps (3000) is about 1035 seconds for each output, whereas the Laplace-Carson transform approach takes less than 1 seconds. Compared with FDM and ABC with 1024×1024 grids, the proposed method is more than 10 times faster. It is worth mentioning that the binomial approximation can be regarded as an explicit FDM so that its converging property is similar to those of the CN-FDM and ABC. Thus, the relative error is only used to show the computational time for an accurate enough numerical value.

The corresponding early exercise boundary offers an alternative approach to examining the computational performance. Figure 2.5 plots the early exercise boundaries obtained from different numerical schemes for the case of $\sigma_0 = 0.3$. It can be seen that the early exercise boundaries produced by the traditional CN scheme and the ABC method are smoother with larger number of grid points and converge to the one obtained from the Laplace-Carson transform approach. In other words, the Laplace-Carson transform is more efficient in producing a smooth early exercise boundary which, in turn, facilitates the computation of hedging parameters based on Proposition 2.2.3. It is an indirect evidence that the option value produced by the Laplace-Carson transform may be even more accurate than the binomial approximation or other alternative competitor approaches.

2.4 Conclusion and Discussion

We study the valuation of American options under the CEV model by taking Laplace-Carson transforms in this chapter. The determination of the optimal early exercise boundary is separated from the valuation procedure. The LCTs of the optimal early exercise boundary, the American option price, and the Greeks are also obtained. Although it focuses on vanilla options, the method is generally applicable to many exotic derivatives with continuous earlier exercise rights.

Table 2.1: American put option prices under the CEV model

	ABC: 256 × 256			ABC: 512 × 512			ABC: 1024 × 1024		
$\beta = -1$	$\sigma_0 = 0.2$	$\sigma_0 = 0.3$	$\sigma_0 = 0.4$	$\sigma_0 = 0.2$	$\sigma_0 = 0.3$	$\sigma_0 = 0.4$	$\sigma_0 = 0.2$	$\sigma_0 = 0.3$	$\sigma_0 = 0.4$
K=35	1.8588	4.04	6.4009	1.8592	4.04	6.3968	1.8595	4.0404	6.3972
(RE)	(0.09%)	(0.00%)	(0.04%)	(0.06%)	(0.00%)	(0.03%)	(0.05%)	(0.01%)	(0.02%)
K=40	3.395	5.7911	8.2628	3.396	5.7909	8.2568	3.3965	5.7915	8.2574
(RE)	(0.03%)	(0.01%)	(0.08%)	(0.00%)	(0.00%)	(0.01%)	(0.01%)	(0.01%)	(0.02%)
K=45	5.9178	8.1127	10.5246	5.9195	8.1121	10.5159	5.9205	8.1129	10.5167
(RE)	(0.06%)	(0.00%)	(0.06%)	(0.03%)	(0.01%)	(0.02%)	(0.02%)	(0.00%)	(0.02%)
		CPU(s): 0.0698			CPU(s): 0.9225			CPU(s): 6.6956	
	FDM: 256 × 256			FDM: 1024 × 1024			Laplace-Carson transform		
$\beta = -1$	$\sigma_0 = 0.2$	$\sigma_0 = 0.3$	$\sigma_0 = 0.4$	$\sigma_0 = 0.2$	$\sigma_0 = 0.3$	$\sigma_0 = 0.4$	$\sigma_0 = 0.2$	$\sigma_0 = 0.3$	$\sigma_0 = 0.4$
K=35	1.8585	4.0394	6.3961	1.8595	4.0404	6.3973	1.8645	4.0388	6.391
(RE)	(0.10%)	(0.01%)	(0.04%)	(0.05%)	(0.01%)	(0.02%)	(0.22%)	(0.03%)	(0.12%)
K=40	3.3948	5.7899	8.2558	3.3965	5.7915	8.2574	3.378	5.7536	8.211
(RE)	(0.04%)	(0.01%)	(0.00%)	(0.01%)	(0.01%)	(0.02%)	(0.56%)	(0.64%)	(0.55%)
K=45	5.9178	8.1127	10.5246	5.9204	8.1129	10.5167	5.8952	8.1163	10.5111
(RE)	(0.06%)	(0.00%)	(0.06%)	(0.02%)	(0.00%)	(0.02%)	(0.44%)	(0.05%)	(0.07%)
		CPU(s): 0.0622			CPU(s): 6.8684			CPU(s): 0.609	

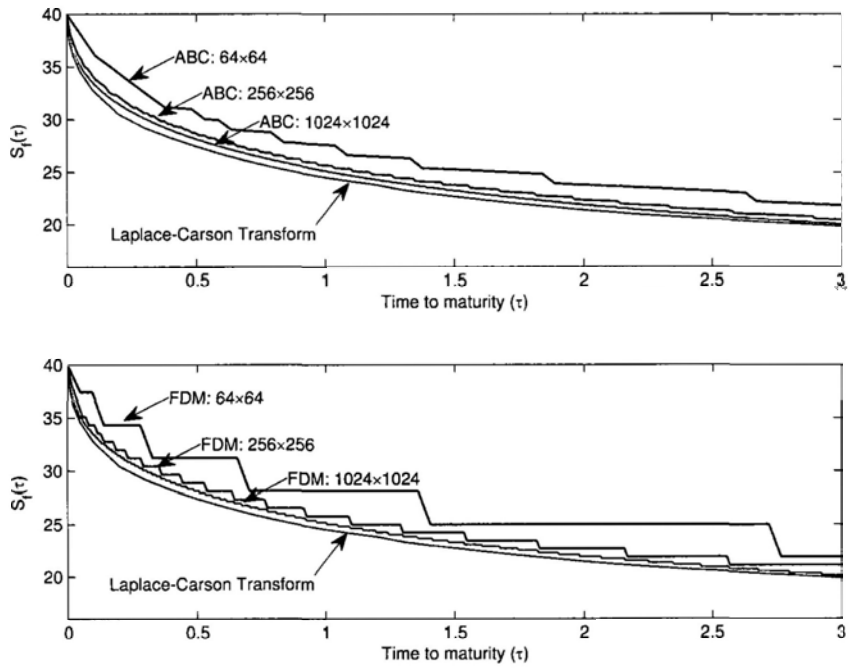

Figure 2.5: Early exercise boundaries based on different numerical schemes.

Chapter 3

American Options under General Diffusion Processes

This chapter considers a one-factor general diffusion process for the underlying asset price under a risk-neutral measure. Specifically, the underlying asset price is assumed to follow the diffusion process

$$\mathrm{d}S_t = (r - D(S_t, t))S_t\mathrm{d}t + \sigma(S_t, t)S_t\mathrm{d}W_t^Q, \tag{3.1}$$

where r is the constant interest rate, W_t^Q is the Wiener process, the deterministic function $D(S_t, t)$ is the dividend yield, and the deterministic function $\sigma(S_t, t)$ represents the local volatility. It is assumed that $D(S_t, t)$ and $\sigma(S_t, t)$ are continuously differentiable with bounded derivatives and positive almost everywhere.

This general diffusion model nests several asset price processes as special cases. For instance, it incorporates the CEV model if the volatility function $\sigma(S_t, t) = \delta S_t^{\beta}$. The hyperbolic sine model (Bibby and Sorensen 1996, Carr et al. 1999) is also a particular case of (3.1), in which the volatility function takes the form

$$\sigma(S_t, t) = \alpha\sqrt{1 + \left(\frac{\beta}{S_t e^{\mu(T-t)}}\right)^2}, \tag{3.2}$$

where β is given in $\beta = S_0 e^{\mu T}\mathrm{csch}(-\alpha L)$. The volatility smile implied by this model is approximately hyperbolic in S (normal volatility) for S near zero and asymptotically approaches a constant α (lognormal volatility) for a high value of S. As S increases from 0 to ∞, the volatility smile slopes downward in a convex fashion.

Therefore, the proposed general diffusion process incorporates an interesting and the most general one-factor model in the financial markets. In addition, our consideration allows the dividend yield to be a function of time and the underlying asset price. The main virtue of this general model is market completeness so that every derivative contract can be replicated by a dynamic trading strategy.

3.1 The Valuation of American Options

Similar to (2.2)–(2.6), the valuation of American put option can be formulated as a free boundary problem defined on $S \in [S_f(\tau), \infty)$ and $\tau \in [0, T]$. Specifically,

$$\frac{\partial P_A}{\partial \tau} = \frac{1}{2}\sigma^2(S, T-\tau)S^2\frac{\partial^2 P_A}{\partial S^2} + (r - D(S, T-\tau))S\frac{\partial P_A}{\partial S} - rP_A, \tag{3.3}$$

$$P_A(S, 0) = \max(K - S, 0), \tag{3.4}$$

$$P_A(S_f(\tau), \tau) = K - S_f(\tau), \tag{3.5}$$

$$\frac{\partial P_A(S_f(\tau), \tau)}{\partial S} = -1, \tag{3.6}$$

$$\lim_{S\to\infty} P_A(S, \tau) = 0. \tag{3.7}$$

Since $P_A(S, \tau + \triangle\tau) > P_A(S, \tau)$ for any positive $\Delta\tau$ in the continuation region, it is easily seen that the following inequality holds: $S_f(\tau) > S_f(\tau + \triangle\tau)$, implying that $S_f(\tau)$ is decreasing function of τ. It is known that $S_f(\infty) \leq S_f(\tau) \leq S_f(0^+)$. Appendix B shows that $S_f(0^+)$ can be obtained by solving the following equation:

$$S_f(0^+) = \min\left(\frac{r}{D(S_f(0^+), T^-)}K, K\right). \tag{3.8}$$

In addition, the Markov property of the generalized diffusion model enables us to consider the put option value alone because of the put-call symmetry of American options.

Remark 3.1.1. When the volatility is a function of time and asset price, Laplace-Carson transforms do not work any more in valuing American options. In addition, Dupire (1994) has shown that, if no-arbitrage market prices for European vanilla options are available for all strikes K and maturities T, $\sigma(S_t, t)$ can be extracted analytically from

market prices. Dupire's equation is a general non-parametric approach, which motivates us to establish a unified framework for American option pricing under general diffusion processes.

3.1.1 The Front-fixing Transformation

The major difficulty of accurately computing American options lies in the unknown free boundaries associated with the early exercise feature. Wu and Kwok (1997) suggest that this difficulty can be resolved by the front-fixing transformation proposed by Landau (1950). After rescaling the variables

$$S = K\widetilde{S}, \quad P_A(S,\tau) = K\widetilde{P}_A(\widetilde{S},\tau), \quad \text{and} \quad S_f(\tau) = K\widetilde{S}_f(\tau),$$

the following transformation of the state variable is applied for equations (3.3)–(3.7):

$$x = \ln(\widetilde{S}/\widetilde{S}_f(\tau)) \quad \text{or} \quad \widetilde{S} = \widetilde{S}_f(\tau)e^x. \tag{3.9}$$

Define $\widetilde{P}_A(\widetilde{S},\tau) = V(x,\tau)$. The valuation problem can then be expressed as

$$\frac{\partial V}{\partial \tau} - \frac{1}{\widetilde{S}_f(\tau)}\frac{\mathrm{d}\widetilde{S}_f(\tau)}{\mathrm{d}\tau}\frac{\partial V}{\partial x} = \frac{1}{2}a^2(*)\left[\frac{\partial^2 V}{\partial x^2} - \frac{\partial V}{\partial x}\right] + (r - d(*))\frac{\partial V}{\partial x} - rV, \tag{3.10}$$

$$V(x,0) = \max(1 - \widetilde{S}_f(0)e^x, 0), \tag{3.11}$$

$$V(0,\tau) = 1 - \widetilde{S}_f(\tau), \tag{3.12}$$

$$\frac{\partial V(0,\tau)}{\partial x} = -\widetilde{S}_f(\tau), \tag{3.13}$$

$$\lim_{x\to\infty} V(x,\tau) = 0, \tag{3.14}$$

where $a^2(*) = \sigma^2(K\widetilde{S}_f(\tau)e^x, T-\tau)$, $d(*) = D(K\widetilde{S}_f(\tau)e^x, T-\tau)$, and $x \in [0,\infty)$. Combining equations (3.12) and (3.13) yields

$$1 + \frac{\partial V(0,\tau)}{\partial x} = V(0,\tau) \quad \text{and} \quad \widetilde{S}_f(\tau) = 1 - V(0,\tau). \tag{3.15}$$

Consequently, the front-fixing transformation converts the linear partial differential equation (PDE) with a free boundary into a nonlinear PDE defined on a fixed domain.

The nonlinear operator is given by

$$\mathcal{N}[V(x,\tau),\widetilde{S}_f(\tau)] = \frac{\partial V}{\partial \tau} - \frac{1}{\widetilde{S}_f(\tau)}\frac{\mathrm{d}\widetilde{S}_f(\tau)}{\mathrm{d}\tau}\frac{\partial V}{\partial x} - \frac{1}{2}a^2(*)\left[\frac{\partial^2 V}{\partial x^2} - \frac{\partial V}{\partial x}\right] - (r - d(*))\frac{\partial V}{\partial x} + rV. \tag{3.16}$$

To simplify matters, the governing equation is written as

$$\mathcal{N}[V(x,\tau),\widetilde{S}_f(\tau)] = 0. \tag{3.17}$$

3.2 A Generalized Homotopy Analysis Method

The front-fixing transformation makes the American option pricing problem become a nonlinear PDE problem defined on a fixed domain. This section generalizes the homotopy analysis method by introducing a shape parameter and kernel function, and then solves the nonlinear problem.

A homotopy between two continuous functions f and g from a topological space X to a topological space Y is a continuous mapping $\mathcal{H} : X \times [0,1] \to Y$ such that $\mathcal{H}(x,0) = f(x)$ and $\mathcal{H}(x,1) = g(x)$ for all $x \in X$. The notion of homotopy is a very useful tool in topology. Applications of homotopy can be found in Patty (1993) and Liao (1997, 2004). The essence of the homotopy analysis method is that the solution of a nonlinear PDE problem can be transformed into an infinite sum of solutions of many linear subproblems. Each subproblem is associated with a deformation equation. The solution of the original problem can then be approximated by truncating the series into a partial sum, provided that the infinite sum is convergent.

3.2.1 Deformation

The homotopy analysis method is based on a continuous variation from an initial trial to the exact solution. We construct the homotopic mapping $V(x,\tau) \longrightarrow \Phi(x,\tau;p)$, $\widetilde{S}_f(\tau) \longrightarrow \eta(\tau;p)$ such that as the embedding parameter p increases from 0 to 1, $\Phi(x,\tau;p)$ and $\eta(\tau;p)$ vary continuously from the initial guesses to their exact solutions, $V(x,\tau)$ and $\widetilde{S}_f(\tau)$, respectively. Let $V_0(x,\tau)$ denote an initial guess of the exact solution $V(x,\tau)$ and

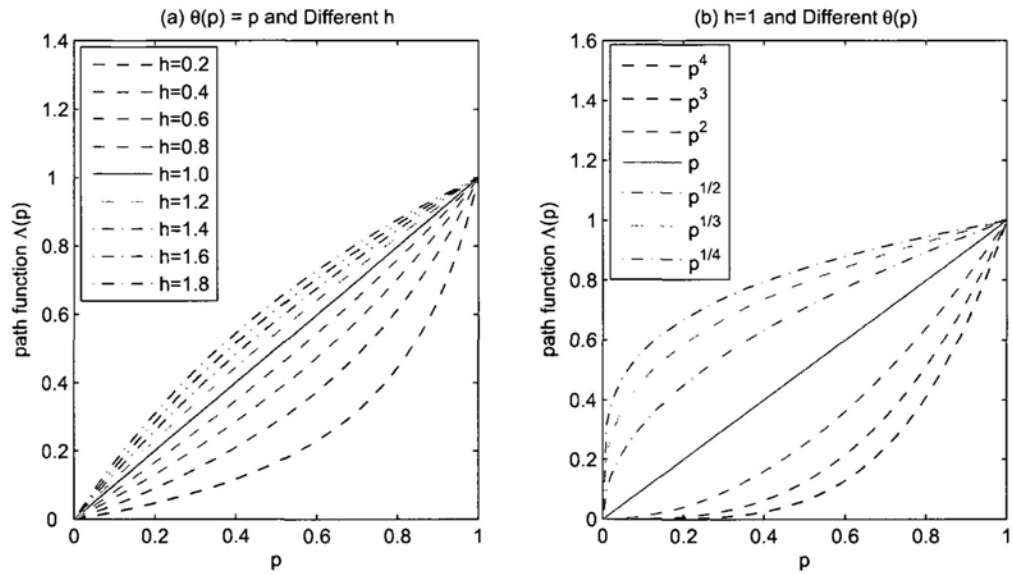

Figure 3.1: Path functions with different shape parameters and kernel functions.

$\mathcal{L}$ be an auxiliary linear operator with the property

$$\mathcal{L}[f(x,\tau)] = 0 \quad \text{when } f(x,\tau) = 0. \tag{3.18}$$

Using the embedding parameter $p \in [0,1]$, a generalized homotopy is constructed with a path function $\Lambda(p)$:

$$\begin{aligned}\mathcal{H}[\Phi(x,\tau;p),\eta(\tau;p);V_0(x,\tau),\Lambda(p)] &= (1-\Lambda(p))\{\mathcal{L}[\Phi(x,\tau;p)-V_0(x,\tau)]\} \\ &\quad +\Lambda(p)\mathcal{N}[\Phi(x,\tau;p),\eta(\tau;p)],\end{aligned}$$

where

$$\Lambda(p) = \frac{h\theta(p)}{1-\theta(p)+h\theta(p)}, \quad h \neq 0, \quad \theta(0) = 0, \quad \theta(1) = 1, \tag{3.19}$$

h is the shape parameter of the generalized homotopy, and $\theta(p)$ is the continuous kernel function. Thus, we have $\Lambda(0) = 0$ and $\Lambda(1) = 1$.

Figure 3.1(a) shows the path functions associated with different values of the shape parameter h and the identity kernel function. The kernel function has a substantial influence on the shape of the deformation. For example, Figure 3.1(b) presents the path functions in which different power functions are chosen as the kernel function. When $h = 1$ and $\theta(p) = p$, the generalized homotopy is reduced to the traditional homotopy

in which the path function is a straight line. This traditional homotopy is used by Zhu (2006).

Being homotopic is an equivalence relation on the set of all continuous functions from one topological space, X, to another one, Y. The paths in Figure 3.1 are homotopic relative to their endpoints and form isocontours of possible homotopies.

3.2.2 Zero-order Deformation Equation

The homotopy analysis method of Liao (2004) is a general approach for solving nonlinear differential equations. There is a great degree of freedom to choose the initial guess, the auxiliary linear operator, the shape parameter and the kernel function, but different choices result in different computational efficiency. However, there are no rigorous theoretical results on the optimal choice. Thus, the application of the homotopy analysis method usually relies on prior knowledge of a specific application, which is option pricing theory in our case, for a good balance between analytical tractability and practical usage.

Under the Black-Scholes model, the nonlinearity of the PDE solely comes from the unknown early-exercise boundary. Therefore, it is very natural for Zhu (2006) to consider the Black-Scholes formula for European option as the initial guess and the Black-Scholes linear operator within traditional homotopy analysis. Under general diffusion processes and generalized homotopy analysis, the situation is rather different and we have to consider an appropriate choice of the ingredients for the homotopic formulation. In practice, option investors always use the at-the-money (ATM) Black-Scholes implied volatility as the benchmark. This motivates us to use the Black-Scholes operator with a constant ATM implied volatility as the auxiliary linear operator to solve the American option pricing problem under general diffusion processes. The following gives the detail of our approach.

Enforcing the homotopy (3.19) to be zero, i.e.

$$\mathcal{H}[\Phi(x,\tau;p),\eta(\tau;p);V_0(x,\tau),\Lambda(p)]=0, \tag{3.20}$$

the zero-order deformation equation is obtained as

$$(1-\theta(p))\{\mathcal{L}[\Phi(x,\tau;p)-V_0(x,\tau)]\}=-h\theta(p)\mathcal{N}[\Phi(x,\tau;p),\eta(\tau;p)], \tag{3.21}$$

where $\Phi(x,\tau;p),\eta(\tau;p)$ is a solution that depends upon not only the initial guess $V_0(x,\tau)$ and the auxiliary linear operator $\mathcal{L}$ but also the embedding parameter $p\in[0,1]$, the shape parameter h, and the kernel function $\theta(p)$. When $p=0$, the zero-order deformation equation (3.21) becomes

$$\mathcal{L}[\Phi(x,\tau;0)-V_0(x,\tau)]=0. \tag{3.22}$$

According to the property of the auxiliary linear operator (3.18),

$$\Phi(x,\tau;0)=V_0(x,\tau) \tag{3.23}$$

satisfies the zero-order deformation equation (3.22).

To make a reasonable initial guess, $\Phi(x,\tau;p)$ and $\eta(\tau;p)$ are enforced to satisfy the following initial and boundary conditions corresponding to (3.11), (3.15), (3.14), and (3.12):

$$\Phi(x,0;p)=(1-p)V_0(x,0)+p\max(1-\widetilde{S}_f(0)e^x,0), \tag{3.24}$$

$$\frac{\partial\Phi(0,\tau;p)}{\partial x}-\Phi(0,\tau;p)+1=(1-p)\left(\frac{\partial V_0(0,\tau)}{\partial x}-V_0(0,\tau)+1\right), \tag{3.25}$$

$$\lim_{x\to\infty}\Phi(x,\tau;p)=0, \tag{3.26}$$

$$\eta(\tau;p)=1-\Phi(0,\tau;p). \tag{3.27}$$

When $p=0$, $V_0(x,\tau)$ satisfies the initial and boundary conditions (3.24)–(3.25) automatically.[1]

The choice of the auxiliary linear operator reflects the set of basis functions used to span the solution of the nonlinear problem. As a square-integrable real-value function can be spanned by any set of basis functions, the choice of $\mathcal{L}$ is important for the efficiency of approximating a nonlinear problem. In the Black-Scholes model, all coefficients of the nonlinear operator are constant values so that it is straightforward to choose its linear part

[1]Based on equation (3.23) and the fact that the derivative with respect to x is independent of p.

as the auxiliary linear operator. In our case, the coefficients are deterministic functions of time and asset value. It is believed that the Black-Scholes dynamics could partially explain the evolution of the underlying asset price. Based on the (constant) implied volatility of the ATM options observed in the market, we consider the Black-Scholes operator with the ATM-volatility on a non-dividend paying stock as the auxiliary linear operator. Specifically,

$$\mathcal{L}[V(x,\tau)] = \frac{\partial V}{\partial \tau} - \frac{1}{2}\sigma_0^2 \frac{\partial^2 V}{\partial x^2} - \left(r - \frac{1}{2}\sigma_0^2\right)\frac{\partial V}{\partial x} + rV, \tag{3.28}$$

where σ_0 is the ATM-volatility.

When $p = 0$, the initial guess should respect the Black-Scholes operator (3.28) and vanish at infinity as specified in equation (3.26). This enables us to use the closed-form solution for European options under the Black-Scholes model.

Defining $\zeta_0(\tau) = \eta(\tau; 0)$ as an initial guess of the optimal early exercise boundary, we obtain the relationship between the two initial guesses: $\zeta_0(\tau) = 1 - V_0(0,\tau)$ corresponding to equation (3.27).

When $p = 1$, the zero-order deformation equation (3.21) reduces to

$$\mathcal{N}[\Phi(x,\tau;1), \eta(\tau;1)] = 0. \tag{3.29}$$

Based on the original governing equation (3.17), we have

$$\Phi(x,\tau;1) = V(x,\tau) \text{ and } \eta(\tau;1) = \widetilde{S}_f(\tau), \tag{3.30}$$

satisfying equation (3.29). According to equations (3.23) and (3.30), as the embedding parameter p increases from 0 to 1, $\Phi(x,\tau;p)$ and $\eta(\tau;p)$ deform continuously from their initial approximations $V_0(x,\tau)$ and $\zeta_0(\tau)$ to exact solutions $V(x,\tau)$ and $\widetilde{S}_f(\tau)$ of the original problem (3.10)–(3.14). Such a continuous variation is called deformation in homotopy and hence equation (3.21) is called the zero-order deformation equation.

Define the mth-order deformation derivatives as

$$V_0^{[m]}(x,\tau) = \left.\frac{\partial^m \Phi(x,\tau;p)}{\partial p^m}\right|_{p=0} \text{ and } \zeta_0^{[m]}(\tau) = \left.\frac{\partial^m \eta(\tau;p)}{\partial p^m}\right|_{p=0}. \tag{3.31}$$

Consider the Taylor expansions of $\Phi(x,\tau;p)$ and $\eta(\tau;p)$ with respect to p,

$$\Phi(x,\tau;p) = \Phi(x,\tau;0) + \sum_{m=1}^{+\infty} \frac{V_0^{[m]}(x,\tau)}{m!} p^m, \tag{3.32}$$

and

$$\eta(\tau;p) = \eta(\tau;0) + \sum_{m=1}^{+\infty} \frac{\zeta_0^{[m]}(\tau)}{m!} p^m. \tag{3.33}$$

Let

$$V_m(x,\tau) = \frac{V_0^{[m]}(x,\tau)}{m!} \quad \text{and} \quad \zeta_m(\tau) = \frac{\zeta_0^{[m]}(\tau)}{m!}. \tag{3.34}$$

The power series (3.32) and (3.33) become, respectively,

$$\Phi(x,\tau;p) = \Phi(x,\tau;0) + \sum_{m=1}^{+\infty} V_m(x,\tau) p^m \tag{3.35}$$

and

$$\eta(\tau;p) = \eta(\tau;0) + \sum_{m=1}^{+\infty} \zeta_m(\tau) p^m, \tag{3.36}$$

where $V_m(x,\tau)$ and $\zeta_m(\tau)$ are determined by the high-order deformation equations described in the following section.

3.2.3 High-order Deformation Equations

Define the vectors

$$\overrightarrow{V}_n = \{V_0(x,\tau), V_1(x,\tau), V_2(x,\tau), \cdots, V_n(x,\tau)\}, \tag{3.37}$$

$$\overrightarrow{\zeta}_n = \{\zeta_0(\tau), \zeta_1(\tau), \zeta_2(\tau), \cdots, \zeta_n(\tau)\}. \tag{3.38}$$

From equation (3.34), the homotopy analysis method enables us to obtain the relation between $V_m(x,\tau)$ and $\zeta_m(\tau)$ by differentiating (3.27) m times with respect to the embedding parameter p, dividing it by $m!$, and setting $p = 0$. The result is given by

$$\zeta_m(\tau) = -V_m(0,\tau), \quad m \geq 1. \tag{3.39}$$

The governing equation, the initial and boundary conditions of $V_m(x,\tau)$, and $\zeta_m(\tau)$ can also be derived from the zero-order deformation equation (3.21) and conditions (3.24)–(3.26). Specifically, the following series of linear subproblems in a general form defined

on the semi-infinite domain $[0, \infty]$ are obtained:

$$\mathcal{L}[V_m(x,\tau)] = f_m(x,\tau), \tag{3.40}$$

$$V_m(x,0) = \psi_m(x), \tag{3.41}$$

$$\frac{\partial V_m(0,\tau)}{\partial x} - V_m(0,\tau) = \phi_m(\tau), \tag{3.42}$$

$$\lim_{x\to\infty} V_m(x,\tau) = 0, \tag{3.43}$$

where $f_m(x,\tau)$, $\psi_m(x)$ and $\phi_m(\tau)$ are expressed as follows.

(1) When $m = 1$,

$$f_m(x,\tau) = \left[-h\frac{\partial\theta}{\partial p}R_0(\overrightarrow{V}_0, \overrightarrow{\zeta}_0, x, \tau)\right]\Big|_{p=0}, \tag{3.44}$$

$$\psi_m(x) = -V_0(x,0) + \max(1 - \hat{S}_f(0)e^x, 0), \tag{3.45}$$

$$\phi_m(\tau) = V_0(0,\tau) - \frac{\partial V_0(0,\tau)}{\partial x} - 1. \tag{3.46}$$

(2) When $m \geq 2$,

$$f_m(x,\tau) = \left[\sum_{k=1}^{m-1}\frac{1}{k!}\frac{\partial^k\theta}{\partial p^k}\mathcal{L}[V_{m-k}(x,\tau)] - h\sum_{k=1}^{m}\frac{1}{k!}\frac{\partial^k\theta}{\partial p^k}R_{m-k}(\overrightarrow{V}_{m-k}, \overrightarrow{\zeta}_{m-k}, x, \tau)\right]\Big|_{p=0}, \tag{3.47}$$

$$\psi_m(x) = 0, \tag{3.48}$$

$$\phi_m(\tau) = 0. \tag{3.49}$$

For $m \geq 0$, the remainder function R_m is defined as

$$R_m(\overrightarrow{V}_m, \overrightarrow{\zeta}_m, x, \tau) = \frac{1}{m!}\frac{\partial^m\mathcal{N}[\Phi(x,\tau;p), \eta(\tau,p)]}{\partial p^m}\Big|_{p=0}. \tag{3.50}$$

The linear PDE (3.40)–(3.43) can be split into three problems. The first one is a homogeneous linear PDE with an arbitrary initial condition and a homogeneous boundary condition at $x = 0$. The second one is a homogeneous linear PDE with a nonhomogeneous boundary condition at $x = 0$ and zero initial condition. The third one is a nonhomogeneous linear PDE but both the boundary condition at $x = 0$ and the initial

condition are homogeneous. All three problems can be solved in explicit forms. The closed-form solution of the linear PDE (3.40)–(3.43) is presented as follows.

(1) When $m = 1$,

$$V_1(x,\tau) = \int_0^\infty G(x,\xi,\tau)\psi_1(\xi)d\xi - a\int_0^\tau \phi_1(\lambda)G(x,0,\tau-\lambda)d\lambda + \int_0^\tau\int_0^\infty f_1(\xi,\lambda)G(x,\xi,\tau-\lambda)d\xi d\lambda. \tag{3.51}$$

(2) When $m \geq 2$,

$$V_m(x,\tau) = \int_0^\tau\int_0^\infty f_m(\xi,\lambda)G(x,\xi,\tau-\lambda)d\xi d\lambda, \tag{3.52}$$

where

$$G(x,\xi,\tau) = \frac{1}{2\sqrt{\pi a\tau}}\exp\left[\frac{b(\xi-x)}{2a} + \left(c - \frac{b^2}{4a}\right)\tau\right]\left\{\exp\left[-\frac{(x-\xi)^2}{4a\tau}\right] + \exp\left[-\frac{(x+\xi)^2}{4a\tau}\right] - 2s\sqrt{\pi a\tau}\exp[s(x+\xi+as\tau)]\mathrm{Erfc}\left[\frac{x+\xi+2as\tau}{\sqrt{4a\tau}}\right]\right\}, \tag{3.53}$$

$$s = 1 + \frac{b}{2a}, \quad a = \frac{1}{2}\sigma^2, \quad b = r - \frac{1}{2}\sigma^2, \quad c = -r. \tag{3.54}$$

The homotopy analysis method enables us to solve a series of linear partial differential equations with constant coefficients instead of handling the nonlinear partial differential equation with variable coefficients directly. In essence, our solution takes a similar form as that of Zhu (2006) because we both use the Black-Scholes operator as the auxiliary linear operator. However, our solution is more general and flexible as it accommodates general diffusion processes and generalized homotopy with a shape parameter and kernel function.

The initial guess is defined through the Black-Scholes formula by setting the strike price to one. Thus,

$$V_0(x,\tau) = e^{-r\tau}\varphi(-d_2) - e^x\varphi(-d_1), \tag{3.55}$$

where $\varphi(*)$ is the standard normal cumulative distribution function and

$$d_1 = \frac{\mathrm{In}(e^x) + (r+\sigma^2/2)\tau}{\sigma\sqrt{\tau}} \quad \text{and} \quad d_2 = d_1 - \sigma\sqrt{\tau}.$$

Based on the relationship between V_m and ζ_m, we obtain

$$\zeta_m(\tau) = \begin{cases} 1 - V_0(0,\tau) & \text{when } m = 0, \\ -V_m(0,\tau) & \text{when } m \geq 1. \end{cases} \tag{3.56}$$

Consequently, an exact and explicit solution for the nonlinear problem (3.10)–(3.14) is derived as a Maclaurin series:

$$V(x,\tau) = \Phi(x,\tau;1) = \Phi(x,\tau;0) + \sum_{m=1}^{+\infty} V_m(x,\tau) = \sum_{m=0}^{+\infty} V_m(x,\tau), \tag{3.57}$$

$$\widetilde{S}_f(\tau) = \eta(\tau;1) = \eta(\tau;0) + \sum_{m=1}^{+\infty} \zeta_m(\tau) = \sum_{m=0}^{+\infty} \zeta_m(\tau). \tag{3.58}$$

The corresponding k-th order approximations are given by

$$V(x,\tau) \approx \sum_{m=0}^{k} V_m(x,\tau), \quad \widetilde{S}_f(\tau) \approx \sum_{m=0}^{k} \zeta_m(\tau). \tag{3.59}$$

The following proposition shows that the series solutions of the option price and early exercise boundary are the exact solutions of the original problem once the series expansion converges.

Proposition 3.2.1. If the series $V_0(x,\tau) + \sum_{m=1}^{+\infty} V_m(x,\tau)$ is convergent, it must be the exact solution to the nonlinear problem (3.10)–(3.14).

Proof. The convergence of the series $\sum_{m=0}^{+\infty} V_m(x,\tau)$ yields

$$\lim_{m \to +\infty} V_m(x,\tau) = 0. \tag{3.60}$$

According to equation (3.40), when $m \geq 1$,

$$\begin{aligned} &\mathcal{L}\left[V_m(x,\tau) - \sum_{k=1}^{m-1} \frac{1}{k!} \frac{\partial^k \theta}{\partial p^k} V_{m-k}(x,\tau)\right]\Bigg|_{p=0} \\ &= \left[-h \sum_{k=1}^{m} \frac{1}{k!} \frac{\partial^k \theta}{\partial p^k} R_{m-k}(\overrightarrow{V}_{m-k}, \overrightarrow{\zeta}_{m-k}, x, \tau)\right]\Bigg|_{p=0}. \end{aligned} \tag{3.61}$$

Thus, we obtain

$$\begin{aligned}
&\sum_{m=1}^{n}\left[V_m(x,\tau)-\sum_{k=1}^{m-1}\frac{1}{k!}\frac{\partial^k\theta}{\partial p^k}V_{m-k}(x,\tau)\right]\Bigg|_{p=0}\\
=\;& V_1(x,\tau)+\left[V_2(x,\tau)-\frac{\partial\theta}{\partial p}V_1(x,\tau)\right]\Bigg|_{p=0}+\left[V_3(x,\tau)-\frac{\partial\theta}{\partial p}V_2(x,\tau)-\frac{1}{2!}\frac{\partial^2\theta}{\partial p^2}V_1(x,\tau)\right]\Bigg|_{p=0}\\
&+\cdots+\left[V_n(x,\tau)-\frac{\partial\theta}{\partial p}V_{n-1}(x,\tau)-\cdots-\frac{1}{(n-1)!}\frac{\partial^{n-1}\theta}{\partial p^{n-1}}V_1(x,\tau)\right]\Bigg|_{p=0}\\
=\;& V_n(x,\tau)+\left(1-\frac{\partial\theta}{\partial p}\right)\Bigg|_{p=0}V_{n-1}(x,\tau)+\left(1-\frac{\partial\theta}{\partial p}-\frac{1}{2!}\frac{\partial^2\theta}{\partial p^2}\right)\Bigg|_{p=0}V_{n-2}(x,\tau)\\
&+\cdots+\left(1-\frac{\partial\theta}{\partial p}-\frac{1}{2!}\frac{\partial^2\theta}{\partial p^2}-\cdots-\frac{1}{(n-1)!}\frac{\partial^{n-1}\theta}{\partial p^{n-1}}\right)\Bigg|_{p=0}V_1(x,\tau).
\end{aligned}$$

As $\theta(0)=0$ and $\theta(1)=1$,

$$\lim_{i\to+\infty}\left(1-\frac{\partial\theta}{\partial p}-\frac{1}{2!}\frac{\partial^2\theta}{\partial p^2}-\cdots-\frac{1}{i!}\frac{\partial^i\theta}{\partial p^i}\right)\Bigg|_{p=0}=1-\sum_{i=0}^{+\infty}\frac{1}{i!}\frac{\partial^i\theta}{\partial p^i}\Bigg|_{p=0}=1-\theta(1)=0. \quad (3.62)$$

When $n\to+\infty$, combining equations (3.60) and (3.62) yields

$$\sum_{m=1}^{+\infty}\left[V_m(x,\tau)-\sum_{k=1}^{m-1}\frac{1}{k!}\frac{\partial^k\theta}{\partial p^k}V_{m-k}(x,\tau)\right]\Bigg|_{p=0}=0. \quad (3.63)$$

By equation (3.61) and the linear property of $\mathcal{L}$, we have

$$\begin{aligned}
&\sum_{m=1}^{+\infty}\left[\sum_{k=1}^{m}\frac{1}{k!}\frac{\partial^k\theta}{\partial p^k}R_{m-k}(\overrightarrow{V}_{m-k},\overrightarrow{\zeta}_{m-k},x,\tau)\right]\Bigg|_{p=0}\\
=\;&\left[\frac{\partial\theta}{\partial p}R_0+\frac{\partial\theta}{\partial p}R_1+\frac{1}{2!}\frac{\partial^2\theta}{\partial p^2}R_0+\frac{\partial\theta}{\partial p}R_2+\frac{1}{2!}\frac{\partial^2\theta}{\partial p^2}R_1+\frac{1}{3!}\frac{\partial^3\theta}{\partial p^3}R_0+\cdots\right]\Bigg|_{p=0}\\
=\;&\left[\sum_{i=1}^{+\infty}\frac{1}{i!}\frac{\partial^i\theta}{\partial p^i}\Bigg|_{p=0}\right]R_0+\left[\sum_{i=1}^{+\infty}\frac{1}{i!}\frac{\partial^i\theta}{\partial p^i}\Bigg|_{p=0}\right]R_1+\cdots=0.
\end{aligned}$$

As

$$\sum_{i=1}^{+\infty}\left[\frac{1}{i!}\frac{\partial^i\theta}{\partial p^i}\right]\Bigg|_{p=0}=\sum_{i=0}^{+\infty}\left[\frac{1}{i!}\frac{\partial^i\theta}{\partial p^i}\right]\Bigg|_{p=0}-\theta(0)=\theta(1)-\theta(0)=1,$$

it is given that

$$\sum_{m=0}^{+\infty}R_m(\overrightarrow{V}_m,\overrightarrow{\zeta}_m,x,\tau)=0. \quad (3.64)$$

Based on the definition of R_m in equation (3.50), we have

$$\sum_{m=0}^{+\infty}\frac{1}{m!}\frac{\partial^m\mathcal{N}[\Phi(x,\tau;p),\eta(\tau;p)]}{\partial p^m}\Bigg|_{p=0}=0. \quad (3.65)$$

Let $\varepsilon(x,\tau;p) = \mathcal{N}[\Phi(x,\tau;p),\eta(\tau;p)]$ be the residual error of the governing nonlinear equation. Clearly, $\varepsilon(x,\tau;p) = 0$ corresponds to the exact solution that satisfies the nonlinear operator.

Therefore, the Maclaurin series of the residual error $\varepsilon(x,\tau;p)$ with respect to the embedding parameter p is

$$\sum_{m=0}^{+\infty} \frac{p^m}{m!} \left.\frac{\partial^m \varepsilon[\Phi(x,\tau;p),\eta(\tau;p)]}{\partial p^m}\right|_{p=0} = \sum_{m=0}^{+\infty} \frac{p^m}{m!} \left.\frac{\partial^m \mathcal{N}[\Phi(x,\tau;p),\eta(\tau;p)]}{\partial p^m}\right|_{p=0}. \tag{3.66}$$

When $p = 1$, using equation (3.65), we obtain

$$\varepsilon(x,\tau;1) = \sum_{m=0}^{+\infty} \frac{1}{m!} \left.\frac{\partial^m \mathcal{N}[\Phi(x,\tau;p),\eta(\tau;p)]}{\partial p^m}\right|_{p=0} = 0. \tag{3.67}$$

This means (see the definition of $\varepsilon(x,\tau;p)$) that the obtained solution satisfies the nonlinear governing equation when $p = 1$. Based on (3.24)–(3.25), setting $\theta(p) = p$ and $h = 1$, a similar procedure verifies that the initial and boundary conditions are satisfied. The boundary condition at infinity (3.14) is also forced to hold by using equation (3.26). This completes the proof. □

Remark 3.2.1. Proposition 3.2.1 ensures that the homotopic series tends to the true value once it converges. However, the convergence of the series solution remains open. Thus, we follow Zhu (2006) to use numerical experiments to demonstrate the convergence of specific problems in the next section.

As important as computing the prices of an option is computing the standard hedge sensitivities: Δ, Γ, ν, Θ, and ρ. In financial markets, the aim of a trader is to manage the Greeks so that all risks are acceptable. Provided the resulting series of $V(x,\tau)$ and $\widetilde{S}_f(\tau)$ converge uniformly, we can derive the Greeks in explicit forms as follows:

$$\begin{aligned} \Delta = \frac{\partial P_A}{\partial S} = \frac{K}{S}\frac{\partial V}{\partial x}, \quad \Gamma = \frac{K^2}{S^2}\frac{\partial^2 V}{\partial x^2} - \frac{K^2}{S^2}\frac{\partial V}{\partial x}, \\ \nu = \frac{\partial P_A}{\partial \sigma} = K\frac{\partial V}{\partial \sigma}, \quad \Theta = \frac{\partial P_A}{\partial t} = -K\frac{\partial V}{\partial \tau}, \quad \text{and} \quad \rho = K\frac{\partial V}{\partial r}. \end{aligned} \tag{3.68}$$

3.2.4 Sequence Transformations: The Padé Technique

Let $\tilde{P}_m(S,\tau)$ denote the m-th order homotopic approximation of the American put option price determined by the m-th order approximations (3.59) of the nonlinear problem

(3.10)–(3.14) in the framework of homotopy analysis. Thus, it presents the partial sum of the series with the corresponding elements

$$a_m(S,\tau) = \begin{cases} \tilde{P}_0(S,\tau) & \text{when } m = 0, \\ \tilde{P}_m(S,\tau) - \tilde{P}_{m-1}(S,\tau) & \text{when } m \geq 1. \end{cases} \tag{3.69}$$

As $\{\tilde{P}_m(S,\tau) : m = 0,1,2,\cdots\}$ forms a sequence, various acceleration techniques can be used to improve the rate of convergence. Sequence transformation is a resummation of a series, which is commonly used for series acceleration in conjunction with extrapolation methods. It can be divided into two categories: linear sequence transformations and nonlinear sequence transformations. Nonlinear sequence transformations often provide powerful numerical methods for the summation of asymptotic series that arise, for instance, in perturbation theory, and may be regarded as highly effective extrapolation methods.

We advocate a nonlinear sequence transformation to improve homotopic approximations. For a given order of a partial sum, the Padé technique is the best way to approximate the function by a rational function (Sidi 2003). This method often provides superior approximation to truncating its Taylor series, and may still work when the Taylor series diverges.

To apply the Padé technique to the embedding parameter p, a homotopic power series is constructed:

$$\Omega_m(S,\tau;p) = \sum_{i=0}^{m} a_i(S,\tau)p^i, \tag{3.70}$$

where $\Omega_m(S,\tau;0) = \tilde{P}_0(S,\tau)$ and $\Omega_m(S,\tau;1) = \tilde{P}_m(S,\tau)$. Thus, for fixed m, as the embedding parameter p increases from 0 to 1, the mapping (3.70) deforms continuously from the zero-order homotopic approximation to the m-th-order homotopic approximation of the American put option price. In fact, $\{\Omega_m(S,\tau;1) : m = 0,1,2,\cdots\}$ is equivalent to $\{\tilde{P}_m(S,\tau) : m = 0,1,2,\cdots\}$.

When the traditional Padé technique is applied to $\{\Omega_m(S,\tau;p) : m = 0,1,2,\cdots\}$

with respect to p, the $[k,n]$ Padé approximation gives

$$\Omega_{k,n}(S,\tau;p) = \frac{W^U_{k,n}(S,\tau;p)}{W^D_{k,n}(S,\tau;p)} = \frac{\sum_{j=0}^{k} W^U_j(S,\tau)p^j}{1+\sum_{j=1}^{n} W^D_j(S,\tau)p^j}, \tag{3.71}$$

where $W^U_j(S,\tau)$ and $W^D_j(S,\tau)$ are functions determined by the elements

$$a_i(S,\tau), \quad i = 0,1,2,3,\cdots,k+n. \tag{3.72}$$

See Appendix C for details.

Setting $p = 1$ provides the $[k,n]$ homotopy-Padé approximation

$$\tilde{P}_{k,n}(S,\tau) = \Omega_{k,n}(S,\tau;1) = \frac{W^U_{k,n}(S,\tau;1)}{W^D_{k,n}(S,\tau;1)} = \frac{\sum_{j=0}^{k} W^U_j(S,\tau)}{1+\sum_{j=1}^{n} W^D_j(S,\tau)}, \tag{3.73}$$

which accelerates the convergence rate and enlarges the convergence region. Numerical examples demonstrate the efficiency of this approximation in the next section.

3.3 Numerical Examples

Using the homotopy analysis method, closed-form solutions of the option price and early exercise boundary are expressed in infinite series in which each individual term contains an integration over an infinite domain. In addition, the recursive computation of $f_m(x,\tau)$ is necessary at the endpoints of all sub-intervals in the numerical integration. All these imply an expensive computational cost if the exact solution is put into practical use.

What is the use of the homotopic closed-form solutions beyond mathematical satisfaction? The answer is twofold. The first application is to examine some qualitative properties of American options. For instance, the convexity of the early exercise boundary of the American put option under general diffusion can be examined by differentiating the closed-form solution of the early exercise boundary. For the Black-Scholes model, the convexity has been shown by Ekström and Johnson (2004) and Chen et. al (2008). This application may (or may not) be regarded as not practical enough. The second application is to construct a more stable and efficient numerical scheme to compute American option prices and their optimal exercise policy under general diffusion processes.

Traditional numerical methods, such as the explicit finite difference method and binomial tree, are conditionally stable in computing American options under general diffusion processes. The main reason is that the coefficients of the governing PDE are functions of S and t instead of constant. Thus, a varying grid or additional treatment is needed to guarantee stability and convergence of the numerical scheme. For instance, Wong and Zhao (2008) show that an artificial boundary approach is required to secure unconditional stability when American option prices under the CEV model are computed using numerical PDE methods. The CEV model is only an example of general diffusion processes. In fact, it is the simplest one. The homotopy analysis approach is not restricted to CEV but is widely applicable to almost all general diffusion models.

It is worth recalling that the mth-order deformation satisfies a linear PDE with constant coefficients over a fixed domain (3.40)–(3.43) for all m. Therefore, all of the deformations can be easily computed using standard numerical PDE methods, such as the finite difference method (FDM) or finite element method. The advantages of homotopy analysis are that all the required deformations can be computed from the same grid over the same domain and all governing deformation equations share the same linear operator, the Black-Scholes operator. Therefore, the discretization requires a negligible additional computational burden even though a large number of terms are used in the homotopic approximation. For a linear PDE with constant coefficients, the numerical method can be easily constructed to be unconditionally stable. The homotopic closed-form solution can then be accelerated by sequence transformations. If the order of the homotopic approximation is fixed in advance, the shape parameter h provides an alternative way to reduce the error further. To demonstrate the practical use of the proposed approach, this section employs the Crank-Nicolson FDM to solve the mth-order deformation and then combines the approaches to produce homotopic approximations. The CEV model and the hyperbolic sine model are taken as illustrative examples.

Example 3.3.1. Consider the pricing of American put options under the CEV model with a constant dividend yield q, in which the underlying asset price evolves according

Table 3.1: m-th Order homotopic approximations (CEV)

Order	4th	8th	12th	16th	20th	24th	28th	32th	36th
K=90	2.3446	1.7877	1.6020	1.5402	1.5010	1.4854	1.4743	1.4647	1.4557
(RE)	(61.59%)	(23.73%)	(10.88%)	(6.60%)	(3.89%)	(2.81%)	(2.04%)	(1.38%)	(0.75%)
K=100	6.2243	5.4872	5.2247	5.1197	5.0494	4.9933	4.9400	4.8832	4.8256
(RE)	(29.39%)	(14.07%)	(8.61%)	(6.43%)	(4.97%)	(3.80%)	(2.70%)	(1.52%)	(0.32%)
K=110	12.2618	11.6818	11.4570	11.3480	11.2778	11.2207	11.1682	11.1173	11.1003
(RE)	(10.65%)	(5.41%)	(3.38%)	(2.40%)	(1.77%)	(1.25%)	(0.78%)	(0.32%)	(0.16%)

to the stochastic differential equation

$$\mathrm{d}S_t = (r-q)S_t\mathrm{d}t + \delta S_t^{\beta+1}\mathrm{d}W_t^Q. \tag{3.74}$$

The parameters are: elasticity factor $\beta = -0.25$, stock price $S = 100$, risk-free interest rate $r = 5\%$, dividend yield $q = 1\%$, at-the-money volatility $\sigma = 0.2$, and time to expiration $T = 0.5$ year.

Without loss of generality, we use the identity kernel function and unity shape parameter for the constructed homotopy. Numerical experiments show that when m increases, the magnitude of $V_0^{[m]}(x,\tau)$ decreases monotonically and uniformly. Therefore, the convergence condition

$$\lim_{m\longrightarrow\infty}\left|\frac{V_0^{[m+1]}}{V_0^{[m]}}\right| < 1, \tag{3.75}$$

which is also used by Zhu (2006), is satisfied as evidenced by the numerical result. In the following examples, the condition (3.75) is tested for the convergence of the results.

Based on 50×50 grid points, Table 3.1 shows the results of the m-th order homotopic approximations (P_A^{HA}) with different strike prices, i.e., $K = 90$, $K = 100$, and $K = 110$. These strike prices correspond to out-of-the-money (OTM), at-the-money (ATM), and in-the-money (ITM) options, respectively. We use the binomial approximation (P_A^{Bin}) of the diffusion process proposed by Nelson and Ramaswamy (1990) with large time steps (3000) as the benchmark because the convergence of binomial methods for American options are well established by Amin and Khanna (1994), Jiang and Dai (1999) and others. The results from binomial method are 1.4462, 4.8103, and 11.0820 for OTM, ATM and ITM options, respectively. Thus, the relative error (RE)

$$RE = \frac{|P_A^{HA} - P_A^{Bin}|}{|P_A^{Bin}|}, \tag{3.76}$$

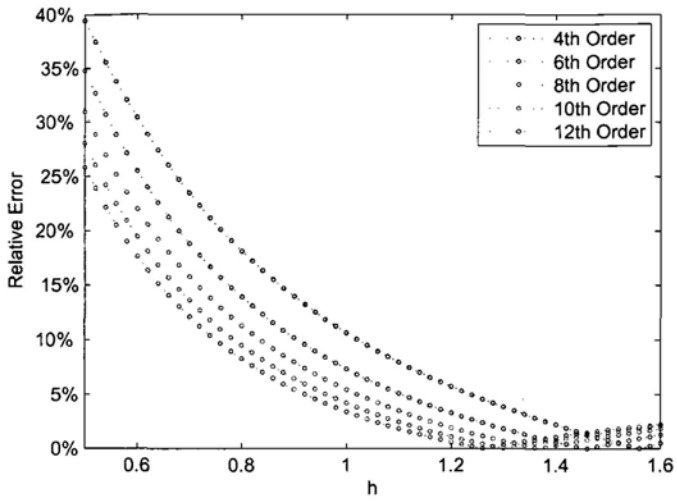

Figure 3.2: RE of m-th-order approximations with different h (CEV).

decreases as the order of approximation increases.

To investigate the influence of the shape parameter h on the constructed homotopy, the relative error (RE) of the m-th order homotopic approximations with different h are shown in Figure 3.2. We can see that for a fixed order, a non-unity shape parameter may provide better results than the original Maclaurin series for $h = 1$. As the path of the constructed homotopy is determined through the shape parameter and kernel function, they have substantial impacts on the obtained Maclaurin series. We can obtain an approximation of the nonlinear problem with sufficient accuracy by a small number of terms if the shape parameter and kernel function are properly chosen.

Example 3.3.2. We use another example to demonstrate the usage of homotopy analysis incorporating the Padé technique as a nonlinear sequence transformation. Under the hyperbolic sine model, the local volatility function is defined by

$$\sigma(S_t, t) = \alpha\sqrt{1 + \left(\frac{\beta}{S_t e^{\mu(T-t)}}\right)^2}, \tag{3.77}$$

where $\beta = S_0 e^{\mu T}\mathrm{csch}(-\alpha L)$.

The parameters are: $L = -4$, $S = 100$, $r = 1\%$, $q = 0$, $\alpha = 0.3$, and $T = 1$. Compared with the binomial approximation with large time steps, it can be seen from Table 3.2 that the relative error decreases as the order of homotopic approximation increases.

Table 3.2: m-th Order homotopic approximations (hyperbolic sine)

Order	4th	8th	12th	16th	20th	24th	28th	Bino3000
K=90	5.0556	5.8319	6.2368	6.4327	6.5158	6.5569	6.5790	6.5822
(RE)	(23.19%)	(11.40%)	(5.25%)	(2.27%)	(1.01%)	(0.38%)	(0.05%)	
K=100	9.0918	9.9682	10.3443	10.4988	10.5503	10.5775	10.5865	10.5887
(RE)	(14.14%)	(5.86%)	(2.31%)	(0.85%)	(0.36%)	(0.11%)	(0.02%)	
K=110	14.6286	15.4469	15.7431	15.8463	15.8797	15.8905	15.8941	15.8916
(RE)	(7.95%)	(2.79%)	(0.93%)	(0.29%)	(0.07%)	(0.01%)	(0.01%)	

In Table 3.3, the Padé technique is employed to accelerate the rate of convergence for $h = 1$. The $[m, m]$ homotopy-Padé approximation is determined by the first $2m$ terms of the original homotopic approximations. For the different strike prices, all the homotopy-Padé approximations outperform their pure homotopy counterparts with a negligible additional computational burden. The computational time of the binomial approximation with large time steps (3000) is about 1147 seconds for each output. In contrast, [4,4] homotopy-Padé approximation takes about seven seconds to obtain a result with relative error less than the bid-ask spread. As shown in Figure 3.3, the Padé technique effectively accelerates the convergence of the sequence and provides us with an efficient way to obtain an accurate result for a small number of terms.

3.4 Conclusion and Discussion

In this chapter, closed-form solutions for American options and their early exercise boundary are investigated under general diffusion models. Based on generalized homotopy analysis, an exact and explicit solution for American options on dividend-paying stocks is derived in Maclaurin series. The corresponding optimal early exercise boundary and the Greeks are also obtained. Since the mth-order deformation satisfies a linear PDE with constant coefficients over a fixed domain for all m, we directly solve the deformations by Crank-Nicolson scheme with unconditional stability. The Padé technique, a nonlinear sequence transformation, is proposed to accelerate the convergence of the homotopic solution. Numerical examples showed that, for a fixed order of the homotopic approximation, an accurate result can be obtained if an appropriate value of the shape parameter h is chosen. Future research may consider how h can be chosen so as to reach

Table 3.3: $[m, m]$ Homotopy-Padé approximations (hyperbolic sine)

$\tilde{P}_{m,m}$	K=90	K=100	K=110	CPU(s)
[1,1]	5.3939	8.5487	13.8814	0.3819
(RE)	(18.05%)	(19.25%)	(12.65%)	
[2,2]	6.1061	10.0720	15.2328	0.4750
(RE)	(7.23%)	(4.87%)	(4.15%)	
[3,3]	6.3599	10.8797	15.9687	0.7976
(RE)	(3.37%)	(2.74%)	(0.48%)	
[4,4]	6.6298	10.6469	15.9259	7.0972
(RE)	(0.72%)	(0.54%)	(0.20%)	

an optimal homotopic approximation by a small number of terms.

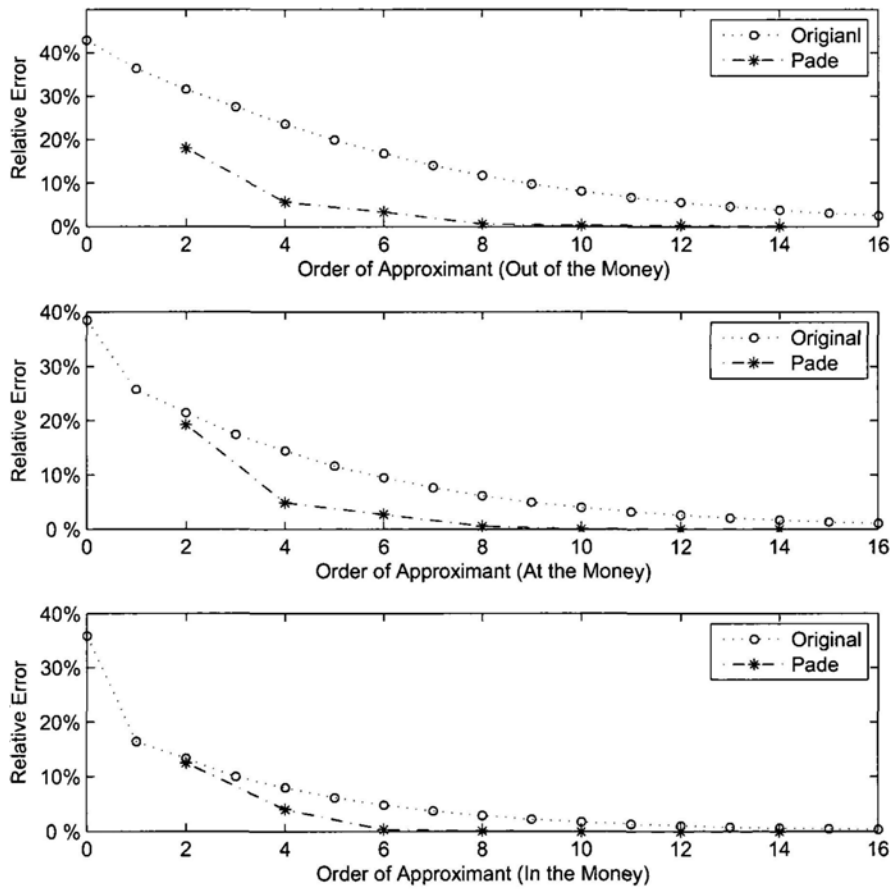

Figure 3.3: Original homotopic and homotopy-Padé approximations (hyperbolic sine).

Chapter 4

Optimal Dividends with Bankruptcy Procedures

For the convenience of derivative pricing, the dividend yield of the asset price dynamics is assumed to be constant in Chapter 2 and is extended to the case of deterministic function of time and the underlying asset price in Chapter 3. What is the suitable dividend-value function? This question is yet to be addressed. By employing firm-surplus approach, this chapter investigates the impact of bankruptcy procedures on optimal dividend barrier policies. Specifically, we focus on the Chapter 11 of the US Bankruptcy Code, which allows a firm in default to continue its business for a period. The model is based on the surplus of a firm that earns investment income at a constant rate of credit interest when it is in a creditworthy condition. The firm pays a debit interest rate that depends on the deficit level when it is in financial distress. Thus, the surplus follows an Ornstein-Uhlenbeck (OU) process with a negative surplus-dependent mean-reverting rate, which is a special case of general diffusions.

4.1 The Model

Let X_t be the surplus of a firm if no dividends are paid. We assume that the surplus earns interest at the constant force $\alpha_0 > 0$. When the surplus is negative, a debit interest is charged at a rate related to the deficit position of the firm rather than the constant debit interest used in Cai et al. (2006). In particular, define a step function $\rho(X_t) : \mathbb{R} \longrightarrow \mathbb{R}$ through the following quantities.

1. A sequence of interval margins

$$\{x_n < x_{n-1} < \cdots < x_1 = 0\} \subset \mathbb{R}, n \in \mathbb{N};$$

2. A sequence of intervals

$$A_n := (-\infty, x_n); \quad A_i := [x_{i+1}, x_i) \text{ for } i = 1, \cdots, n-1; \quad A_0 := [x_1, \infty);$$

3. A sequence of constant interest rates

$$\{\alpha_n, \alpha_{n-1}, \cdots, \alpha_0\} \subset \mathbb{R} \quad \text{satisfying} \quad \alpha_n > \alpha_{n-1} > \cdots > \alpha_1 > \alpha_0 > 0.$$

When the surplus is negative, i.e. $x_1 = 0$, the firm should borrow money to continue its operation. A debit interest rate which is greater than that from the normal investment income, α_0, should be charged to the firm under financial distress. The larger the deficit, the higher the debit interest rate the lenders use.

Given the notation above, we define the surplus-dependent credit/debit interest rate $\rho(X_t)$ as

$$\rho(X_t) = \sum_{i=0}^{n} \alpha_i \mathbf{1}_{A_i}(X_t), \quad \text{for all } X_t \in \mathbb{R}, \tag{4.1}$$

where $\mathbf{1}_A$ is the indicator function for the event A. In other words, $\rho(X_t) = \alpha_i$ if $X_t \in A_i$ for $i = 1, 2, \cdots, n$.

Using the arguments of Cai et al. (2006), the surplus process follows the stochastic differential equation (SDE),

$$\mathrm{d}X_t = (\mu + \rho(X_t)X_t)\mathrm{d}t + \sigma \mathrm{d}W_t^P, \quad t \geq 0, \tag{4.2}$$

where W_t^P is a Wiener process under the physical probability measure, $(\mu + \rho(X_t)X_t)$ is the drift, σ^2 is the variance per unit time, and X_t is the current surplus. It is clear that $(\mu + \rho(X_t)X_t)$ and σ are Lipschitz-continuous functions.

In the time interval $[t, t + \mathrm{d}t)$, the firm pays a nonnegative amount $\mathrm{d}D_t$ in dividends such that the dividend aggregated up to time t, D_t, is a nondecreasing function of time that is adapted to the filtration $\{\mathcal{F}_t\}$, the smallest filtration satisfying the usual conditions

where $\mathcal{F}_t$ contains $\sigma\{W_s : s \leq t\}$. Although we assume that $\rho(X_t) > 0$, the results below can automatically be applied to both the case of $\rho(X_t) < 0$, which corresponds to the traditional mean-reverting process, and the case of $\rho(X_t) = 0$, the Brownian motion.

The dividend barrier strategy proposed by Gerber and Shiu (2003, 2004) is as follows. If the surplus goes above an upside barrier level b, the overflow will be immediately paid to shareholders as dividends so that the surplus is brought back to b. A formal definition can be given in terms of the running maximum

$$M_t = \max_{0 \leq s \leq t} X_s. \tag{4.3}$$

Then, the dividends aggregated up to time t is determined by the formula:

$$D_t = \max(M_t - b, 0), \tag{4.4}$$

and the modified surplus at time t is $X_t - D_t$.

4.1.1 The Bankruptcy Procedure

It is often assumed that bankruptcy immediately occurs when the surplus hits a downside default barrier. We, however, consider a more realistic situation in which default and bankruptcy are two distinguishable events. Suppose that a regulatory authority takes its bankruptcy filing actions according to a hypothetical default clock, which can be modeled by two kinds of frameworks: excursion time framework and occupation time framework.

Excursion Time Framework

In the case of excursion time framework, the hypothetical default clock, counting an excursion time, starts ticking when the modified surplus process breaches the default threshold L and is reset to zero if the firm recovers from the default. The liquidation of the firm is declared at the first time that the modified surplus stays below the default threshold longer than a prescribed amount of time in a single excursion. This bankruptcy procedure calls for the use of excursion time associated with the default threshold. The excursion time t_L is simply the period during which the modified surplus remains below

the default threshold L in the current excursion. Mathematically, let

$$\tau_t^L := \sup\{u \leq t | X_u - D_u \geq L\} \tag{4.5}$$

be the last time that the modified surplus was above the default threshold L. Define the random quantity, called the excursion time,

$$t_L(t) := t - \tau_t^L = t - \sup\{u \leq t | X_u - D_u \geq L\}. \tag{4.6}$$

As a hypothetical default clock, $t_L(t)$ measures the length of time the modified surplus has spent below the default threshold L in the current excursion. Note that, $t_L(t) = 0$ if the modified surplus is above the default threshold.

The dynamics of $t_L(t)$ are described by the expression

$$\mathrm{d}t_L(t) = \begin{cases} \mathrm{d}t & \text{if } X_t - D_t < L, \\ -t_L(t-) & \text{if } X_t - D_t = L, \\ 0 & \text{if } X_t - D_t > L, \end{cases} \tag{4.7}$$

where $t_L(t-)$ is the left limit of $t_L(t)$. The hypothetical default clock $t_L(t)$ is reset to zero when the default threshold is reached from below, and does not change when the modified surplus is above the default threshold. Denote

$$\mathrm{d}t_L(t) = H(L - [X_t - D_t])\mathrm{d}t, \tag{4.8}$$

we have

$$H(x) = \begin{cases} 0 & \text{when } x < 0, \\ 1 & \text{when } x > 0. \end{cases} \tag{4.9}$$

To illustrate the idea, we assume that $L = 0$ throughout this chapter but the extension to other values of L is trivial.

With the bankruptcy procedure just mentioned (see Chen and Suchaneki 2007 and others), the bankruptcy time becomes

$$T := \inf\{t \geq 0 | t_L(t) = T_L\}, \tag{4.10}$$

where T_L can be interpreted as the "grace" period granted to a defaulted firm.

Occupation Time Framework

In the case of occupation time framework, the hypothetical default clock, corresponding to an occupation time, is not reset to zero when a firm emerges from default, but it is only halted and restarted when the modified surplus goes below the default threshold again. As a result, the past defaults are never forgiven and affects further defaults by shortening the maximum allowed length of time that the company can spend in default without being liquidated. The occupation time $\widetilde{t}_L(t)$ is simply the length of period spent by the modified surplus below the default threshold L between 0 and t. Mathematically,

$$\widetilde{t}_L(t) := \int_0^t \mathbf{1}_{\{X_u - D_u \leq L\}} \mathrm{d}u \tag{4.11}$$

which leads to a differential form

$$\mathrm{d}\widetilde{t}_L = \widetilde{H}(L - [X_t - D_t])\mathrm{d}t. \tag{4.12}$$

with

$$\widetilde{H}(x) = \begin{cases} 0 & \text{when } x < 0, \\ 1 & \text{when } x \geq 0. \end{cases} \tag{4.13}$$

The hypothetical default clock based on occupation time does not reset at the default threshold L and the corresponding bankruptcy time becomes:

$$\widetilde{T} := \inf\{t \geq 0 | \widetilde{t}_L(t) = T_L\}, \tag{4.14}$$

4.1.2 Dividend Barrier Strategy

Although both excursion time framework and occupation time framework are possible choices for modeling bankruptcy procedure, we primarily concentrate on the former approach for a smooth presentation. The latter framework will be established and analyzed with a very similar procedure and less details. In the case of excursion time framework, the discounted total dividends with an interest rate of r and bankruptcy procedure becomes

$$\mathbf{D} = \int_0^T e^{-rt} \mathrm{d}D_t. \tag{4.15}$$

One of our objectives is to determine the optimal dividend barrier level b^* such that the expectation of the discounted total dividends in (4.15) is maximized. When the dividend value function is denoted as

$$V(X_t, t_L(t); b, T_L) = \mathbb{E}\left[\mathbf{D} | \mathcal{F}_t\right],$$

our goal is to determine,

$$b^* = \arg \max_{b \in (0,\infty)} V(X_0, t_L(0); b, T_L).$$

In the case of occupation time framework, we also have the associated optimal dividend barrier level $\widetilde{b}^*$ determined by

$$\widetilde{b}^* = \arg \max_{b \in (0,\infty)} \widetilde{V}(X_0, \widetilde{t}_L(0); b, T_L) = \arg \max_{b \in (0,\infty)} \mathbb{E}\left[\int_0^{\widetilde{T}} e^{-rt} \mathrm{d}D_t\right].$$

4.2 The Dividend Value Function

To determine the optimal dividend barrier, the derivation can start by obtaining a closed-form solution for the dividend value function, $V(X_0, t_L(0); b, T_L)$. The optimal dividend barrier is thus determined by maximizing the function $V(X_0, t_L(0); b, T_L)$ with the initial surplus $X_0 = x$ over all possible values of b. This section is devoted to deriving the dividend value function.

4.2.1 Differential Equations

With the derivation process in mind, we concentrate on the dividend value function $V(x, t_L(0); b, T_L)$. The following proposition plays a key role in the analysis.

Proposition 4.2.1. The dividend value function, $V(x, t_L(0); b, T_L)$, satisfies the homogeneous partial differential equation (PDE):

$$\frac{\sigma^2}{2}\frac{\partial^2 V}{\partial x^2} + (\mu + \rho(x)x)\frac{\partial V}{\partial x} + H(L - x)\frac{\partial V}{\partial t_L} - rV = 0, \tag{4.16}$$

for $-\infty < x \leq b$ and $0 \leq t_L < T_L$.

Proof. This proposition is actually a consequence of the classical Feynman-Kac formula. Hugonnier (1999) and Karatzas and Shreve (1991) provide useful comments and a rigorous proof for the case of general diffusion, respectively. For our case, in the infinitesimal time interval from 0 to $\mathrm{d}t$, it is required that

$$e^{-r\mathrm{d}t}\mathbb{E}[V(X_{\mathrm{d}t}, t_L(\mathrm{d}t); b, T_L)] = V(X_0 = x, t_L(0); b, T_L). \tag{4.17}$$

We recognize that

$$\begin{aligned} e^{r\mathrm{d}t}V(x, t_L(0); b, T_L) &= (1 + r\mathrm{d}t)V(x, t_L(0); b, T_L) \\ &= V(x, t_L(0); b, T_L) + rV(x, t_L(0); b, T_L)\mathrm{d}t, \end{aligned}$$

and the initial dividend $D_0 = 0$ as $x \in (-\infty, b]$. Applying Itô's Lemma on V with respect to the differential forms of (4.2) and (4.8), we arrive at

$$\begin{aligned} & \mathbb{E}[V(X_{\mathrm{d}t}, t_L(\mathrm{d}t); b, T_L)] \\ = \; & V(x, t_L(0); b, T_L) + (\mu + \rho(x)x)\frac{\partial V(x, t_L(0); b, T_L)}{\partial x}\mathrm{d}t \\ & + \frac{1}{2}\sigma^2\frac{\partial^2 V(x, t_L(0); b, T_L)}{\partial x^2}\mathrm{d}t + H(L - x)\frac{\partial V(x, t_L(0); b, T_L)}{\partial t_L}\mathrm{d}t. \end{aligned}$$

Substituting the above into (4.17) produces the desired PDE (4.16). □

To obtain a closed-form solution for $V(x, t_L(0); b, T_L)$, appropriate boundary conditions for the dividend value function are required. When the default threshold is set at zero, i.e. $L = 0$, three sets of boundary conditions are defined based on the initial values of x and $t_L(0)$. Figure 4.1 illustrates three possible regions for the surplus.

1. Region One (R1): For $x \in (-\infty, 0)$ and $t_L(0) \in [0, T_L]$,

$$\begin{cases} \frac{1}{2}\sigma^2\frac{\partial^2 V}{\partial x^2} + (\mu + \rho(x)x)\frac{\partial V}{\partial x} + \frac{\partial V}{\partial t_L} - rV = 0, \\ V(x, t_L(0) = T_L; b, T_L) = 0, \\ V(-\infty, t_L(0); b, T_L) = 0, \\ V(0-, t_L(0); b, T_L) = V(0+, 0; b, T_L), \\ \left.\frac{\partial V(x, t_L(0); b, T_L)}{\partial x}\right|_{x=0-} = \left.\frac{\partial V(x, 0; b, T_L)}{\partial x}\right|_{x=0+}. \end{cases} \tag{4.18}$$

When the current surplus x falls below the default threshold, the hypothetical default clock is switched on for counting the grace period. It is natural to see

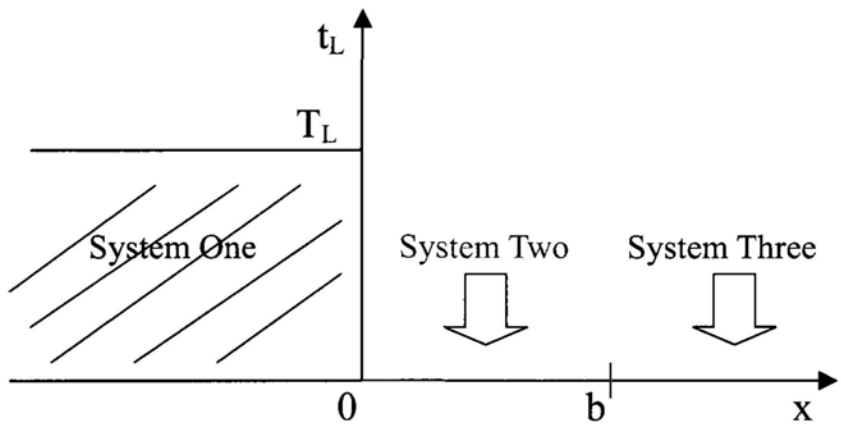

Figure 4.1: Three possible regions for $V(x, t_L; b, T_L)$.

that the governing equation involves t_L, according to Proposition 4.2.1. Since the initial surplus is below the default threshold, the firm may have already filed for bankruptcy with some initial timing $t_L(0) \geq 0$. By the end of the grace period, shareholders should be unable to receive dividends, and hence we have the first boundary condition: $V(x, T_L; b, T_L) = 0$. When the surplus tends to negative infinity, the probability of reaching the dividend barrier is zero. Thus, we have the second boundary condition for $x \to -\infty$. The continuity of the dividend value function across the default threshold yields the last two boundary conditions.

2. Region Two (R2): For $x \in (0, b]$ and $t_L(0) = 0$,

$$\begin{cases} \frac{1}{2}\sigma^2 \frac{\partial^2 V}{\partial^2 x^2} + (\mu + \alpha_0 x)\frac{\partial V}{\partial x} - rV = 0, \\ V'(x, 0; b, T_L)|_{x=b} = 1, \\ V(0+, 0; b, T_L) = V(0-, t_L(0); b, T_L), \\ \frac{\partial V(x,0;b,T_L)}{\partial x}\Big|_{x=0+} = \frac{\partial V(x,t_L(0);b,T_L)}{\partial x}\Big|_{x=0-}. \end{cases} \tag{4.19}$$

When the surplus is above the default threshold, the hypothetical default clock is reset to zero and does not change. According to Proposition 4.2.1, the governing equation is reduced to an ordinary differential equation of x. In this region, it is possible for the surplus to hit the upside dividend barrier on which a reflecting boundary condition is applied according to Gerber and Shiu (2003, 2004). This gives the first boundary condition. The remaining boundary conditions account for

the continuity of the dividend value function.

3. Region Three (R3): For $x \in (b, \infty)$ and $t_L(0) = 0$,

$$V(x, 0; b, T_L) = x - b + V(b, 0; b, T_L). \tag{4.20}$$

When the initial surplus rises above the dividend barrier, a dividend equivalent to $x - b$ is paid to shareholders at once. Thus, the change in the dividend value function should be the payment received by the shareholders.

Remark 4.2.1. In the case of occupation time framework, similar procedures could show that $\widetilde{V}(x, \widetilde{t}_L(0); b, T_L)$ also satisfies the homogeneous PDE (4.16) with $H(L-x)$ replaced with $\widetilde{H}(L-x)$. However, $\widetilde{V}$ does not jump at the default threshold $L = 0$. This means that we need to solve and calculate the values of $\widetilde{V}$ for all possible values of $\widetilde{t}_L(0)$ even if x is above the default threshold. In Figure 4.1, system two and system three will then be defined in the rectangle $x \in (0, b], \widetilde{t}_L(0) \in [0, T_L]$ and $x \in (b, +\infty), \widetilde{t}_L(0) \in [0, T_L]$, respectively.

In the case of excursion time framework, to separate the influence of the barrier level from the dividend value function, we present the solution in R1 and R2 in factorization form as follows.

(R1): For $x \in (-\infty, 0)$ and $t_L(0) \in [0, T_L]$,

$$V(x, t_L(0); b, T_L) = \frac{g(x, t_L(0))}{g_0'(b)}. \tag{4.21}$$

(R2): For $x \in (0, b]$ and $t_L(0) = 0$,

$$V(x, 0; b, T_L) = \frac{g_0(x)}{g_0'(b)}. \tag{4.22}$$

Here $g(x, t_L(0))$ and $g_0(x)$ are independent of the barrier level b. The boundary condition at $x = b$ in (4.19) is satisfied automatically. For a fixed parameter set $\Theta = \{\mu; n; \alpha_i (i = 0, \cdots, n); \sigma; r; b; T_L\}$, $g_0(0+)$ and $g_0'(b)$ are constant. Based on (4.18) and (4.19), we obtain the corresponding system for $g(x, t_L(0))$ in R1 and $g_0(x)$ in R2, respectively.

1. Region One (R1): For $x \in (-\infty, 0)$ and $t_L(0) \in [0, T_L]$,

$$\begin{cases} \frac{1}{2}\sigma^2 \frac{\partial^2 g}{\partial x^2} + (\mu + \rho(x)x)\frac{\partial g}{\partial x} + \frac{\partial g}{\partial t_L} - rg = 0, \\ g(x, t_L(0) = T_L) = 0, \\ g(-\infty, t_L(0)) = 0, \\ g(0-, t_L(0)) = g_0(0+), \\ \left.\frac{\partial g(x, t_L(0))}{\partial x}\right|_{x=0-} = \left.\frac{\partial g_0(x)}{\partial x}\right|_{x=0+}. \end{cases} \tag{4.23}$$

2. Region Two (R2): For $x \in (0, b]$ and $t_L(0) = 0$,

$$\begin{cases} \frac{1}{2}\sigma^2 \frac{\partial^2 g_0}{\partial^2 x^2} + (\mu + \alpha_0 x)\frac{\partial g_0}{\partial x} - r g_0 = 0, \\ g_0(0+) = g(0-, t_L(0)), \\ \left.\frac{\partial g_0(x)}{\partial x}\right|_{x=0+} = \left.\frac{\partial g(x, t_L(0))}{\partial x}\right|_{x=0-}. \end{cases} \tag{4.24}$$

4.2.2 Solving the PDE in R1

To solve the PDE of $g(x, t_L(0))$ in R1, we reverse the excursion time by setting $t_L^* = T_L - t_L(0)$ and substitute it into (4.23) to obtain an initial boundary value problem on a fixed domain with a zero initial condition. As R1 can be decomposed into subregions corresponding to $A_i \times [0, T_L]$, the notation $g_i(x, t_L^*) = g(x, t_L^*)$ is used to indicate that $x \in A_i$ for all $i = 1, \cdots, n$.

Consider the Laplace transform,

$$\hat{g}_i(x) = \int_0^\infty g_i(x, t_L^*) e^{-st_L^*} \mathrm{d}t_L^* := \mathcal{L}_s(g_i(x, t_L^*)), \tag{4.25}$$

where $s > 0$ is the parameter of the Laplace transform. The subsidiary equation for (4.23) with zero initial condition is then given by

$$\frac{1}{2}\sigma^2 \frac{\mathrm{d}^2 \hat{g}_i}{\mathrm{d}x^2} + (\mu + \alpha_i x)\frac{\mathrm{d}\hat{g}_i}{\mathrm{d}x} - r\hat{g}_i = s\hat{g}_i, \tag{4.26}$$

and the corresponding boundary conditions are:

$$\hat{g}_n(-\infty) = 0, \quad \hat{g}_1(0-) = \frac{g_0(0+)}{s}. \tag{4.27}$$

The solution of (4.26) is classic (Zwillinger 1992):

$$\hat{g}_i(x) = C_{i,1}\Phi_{i,r+s}(x) + C_{i,2}\Psi_{i,r+s}(x), \tag{4.28}$$

where

$$\begin{aligned}\Phi_{i,r+s}(x) &= {}_1F_1\left(a_i, \frac{1}{2}, z_i(x)\right), \quad \Psi_{i,r+s}(x) = z_i(x)^{\frac{1}{2}}\ {}_1F_1\left(a_i + \frac{1}{2}, \frac{3}{2}, z_i(x)\right), \\ a_i &= -\frac{r+s}{2\alpha_i}, \quad z_i(x) = -\frac{1}{\alpha_i\sigma^2}(\mu + \alpha_i x)^2, \end{aligned} \tag{4.29}$$

$C_{i,1}$ and $C_{i,2}$ are constants with respect to the fixed parameter set Θ. The function ${}_1F_1(y_1, y_2, y_3)$ is the Kummer confluent hypergeometric function.

Using an asymptotic property of the confluent hypergeometric function:

$${}_1F_1(y_1, y_2, y_3) = \frac{\Gamma(y_2)}{\Gamma(y_2 - y_1)}(-y_3)^{-y_1}[1 + O(|y_3|^{-1})], \quad (\Re(y_3) < 0), \tag{4.30}$$

where $\Gamma(\cdot)$ is the gamma function, the boundary conditions (4.27) are reduced to

$$\begin{cases} d_{n,1}C_{n,1} + d_{n,2}C_{n,2} = 0 \\ u_{1,1}C_{1,1} + u_{1,2}C_{1,2} = g_0(0+)/s, \end{cases} \tag{4.31}$$

where

$$d_{n,1} = (-1)^{\frac{1}{2}}\frac{\Gamma\left(\frac{1}{2}\right)}{\Gamma\left(\frac{1}{2} - a_n\right)}, d_{n,2} = \frac{\Gamma\left(\frac{3}{2}\right)}{\Gamma(1 - a_n)}, u_{1,1} = \Phi_{1,r+s}(0-), u_{1,2} = \Psi_{1,r+s}(0-). \tag{4.32}$$

Using the continuity of the functions $\hat{g}(x)$ and $\frac{\partial \hat{g}}{\partial x}$ at $x = x_i$ for $i = 2, \cdots, n$, we obtain

$$\begin{cases} u_{i,1}C_{i,1} + u_{i,2}C_{i,2} - d_{i-1,1}C_{i-1,1} - d_{i-1,2}C_{i-1,2} = 0 \\ u^*_{i,1}C_{i,1} + u^*_{i,2}C_{i,2} - d^*_{i-1,1}C_{i-1,1} - d^*_{i-1,2}C_{i-1,2} = 0, \end{cases} \tag{4.33}$$

where

$$\begin{aligned} u_{i,1} = \Phi_{i,r+s}(x_i-), u_{i,2} = \Psi_{i,r+s}(x_i-), d_{i-1,1} = \Phi_{i-1,r+s}(x_i), d_{i-1,2} = \Psi_{i-1,r+s}(x_i), \\ u^*_{i,1} = \left.\frac{\partial \Phi_{i,r+s}}{\partial x}\right|_{x=x_i-}, u^*_{i,2} = \left.\frac{\partial \Psi_{i,r+s}}{\partial x}\right|_{x=x_i-}, \\ d^*_{i-1,1} = \left.\frac{\partial \Phi_{i-1,r+s}}{\partial x}\right|_{x=x_i}, d^*_{i-1,2} = \left.\frac{\partial \Psi_{i-1,r+s}}{\partial x}\right|_{x=x_i}. \end{aligned} \tag{4.34}$$

Combining (4.31) with (4.33) yields a system of linear equations,

$$\mathbf{A}\mathbf{C}^{\mathbf{T}} = g_0(0+)\mathbf{G}^{\mathbf{T}} \tag{4.35}$$

where $\mathbf{C} = [C_{n,1}, C_{n,2}, C_{n-1,1}, C_{n-1,2}, \cdots, C_{1,1}, C_{1,2}]$ is a vector of $2n$ unknowns, $\mathbf{G}_{1\times 2n} = [\mathbf{0}_{1\times 2n-1}, 1/s]$ is a vector of $2n$ given elements, and $\mathbf{A}$ is a block tridiagonal matrix with

entries $u_{i,1}, u^*_{i,1}, d_{i,1}$ and $d^*_{i,1}$. Classical LU factorization methods, such as the Thomas algorithm, can be used to efficiently solve the system of linear equations in (4.35). As $\mathbf{A}$ is a full-rank square matrix, $\mathbf{C^T}$ can be uniquely determined as

$$\mathbf{C^T} = g_0(0+)\mathbf{A^{-1}G^T}. \tag{4.36}$$

By inverting the Laplace transform, the solution of $g(x, t^*_L)$ in R1 (4.23) takes the form,

$$g(x, t^*_L) = \sum_{i=1}^{n} g_i(x, t^*_L)\mathbf{1}_{A_i}(x) \tag{4.37}$$

where

$$g_i(x, t^*_L) = \mathcal{L}_s^{-1}[\hat{g}_i(x)]|_{\tau=t^*_L} = \mathcal{L}_s^{-1}[C_{i,1}\Phi_{i,r+s}(x) + C_{i,2}\Psi_{i,r+s}(x)]|_{\tau=t^*_L}. \tag{4.38}$$

We then obtain the Neumann boundary condition at $x = 0-$ and $t^*_L = T_L$ ($t_L(0) = 0$) from (4.38):

$$\left.\frac{\partial g_1}{\partial x}\right|_{x=0-,\tau=T_L} = \mathcal{L}_s^{-1}\left[\left.\frac{\partial \hat{g}_1}{\partial x}\right|_{x=0-}\right]\Bigg|_{\tau=T_L} = g_0(0+)\gamma, \tag{4.39}$$

where

$$\gamma = \mathcal{L}_s^{-1}\left[C^*_{1,1}\left.\frac{\partial \Phi_{1,r+s}(x)}{\partial x}\right|_{x=0-} + C^*_{1,2}\left.\frac{\partial \Psi_{1,r+s}(x)}{\partial x}\right|_{x=0-}\right]\Bigg|_{\tau=T_L},$$

$$C^*_{1,1} = \frac{C_{1,1}}{g_0(0+)}, \quad C^*_{1,2} = \frac{C_{1,2}}{g_0(0+)}. \tag{4.40}$$

The constant γ can be efficiently evaluated by numerical Laplace inversion with high accuracy.

4.2.3 Solving the ODE in R2

The differential equation of $g_0(x)$ in R2 (4.24) is an ordinary differential equation with respect to x, the solution of which can be easily obtained as (Zwillinger 1992)

$$g_0(x) = C_{0,1}\Phi_{0,r}(x) + C_{0,2}\Psi_{0,r}(x), \tag{4.41}$$

where

$$\Phi_{0,r}(x) = M\left(a_0, \frac{1}{2}, z_0(x)\right), \quad \Psi_{0,r}(x) = z_0(x)^{\frac{1}{2}} M\left(a_0 + \frac{1}{2}, \frac{3}{2}, z_0(x)\right),$$

$$a_0 = -\frac{r}{2\alpha_0}, \quad z_0(x) = -\frac{1}{\alpha_0\sigma^2}(\mu + \alpha_0 x)^2. \tag{4.42}$$

The ratio between $C_{0,1}$ and $C_{0,2}$ is constant for a given parameter set Θ. Moreover, the Dirichlet and Neumann boundary conditions at $x = 0+$ can be obtained as follows:

$$g_0(0+) = d_{0,1}C_{0,1} + d_{0,2}C_{0,2}, \quad \left.\frac{\partial g_0}{\partial x}\right|_{x=0+} = d^*_{0,1}C_{0,1} + d^*_{0,2}C_{0,2} \tag{4.43}$$

where

$$d_{0,1} = \Phi_{0,r}(0+), d_{0,2} = \Psi_{0,r}(0+), d^*_{0,1} = \left.\frac{\partial \Phi_{0,r}}{\partial x}\right|_{x=0+}, d^*_{0,2} = \left.\frac{\partial \Psi_{0,r}}{\partial x}\right|_{x=0+}. \tag{4.44}$$

Using the pathwise continuity of the solution, i.e. (4.39) and (4.43), we have

$$d^*_{0,1}C_{0,1} + d^*_{0,2}C_{0,2} = g_0(0+)\gamma = (d_{0,1}C_{0,1} + d_{0,2}C_{0,2})\gamma. \tag{4.45}$$

Thus, we can set

$$C_{0,1} = d_{0,2}\gamma - d^*_{0,2}, \quad C_{0,2} = d^*_{0,1} - d_{0,1}\gamma. \tag{4.46}$$

According to (4.36), (4.43), and (4.46), $C_{0,1}$, $C_{0,2}$, $g_0(0)$ and $\mathbf{C^T}$ are obtained. Moreover, by recognizing the denominator of the factorization form (4.21)–(4.22) satisfying

$$g_0'(b) = C_{0,1}\left.\frac{\partial \Phi_{0,r}}{\partial x}\right|_{x=b} + C_{0,2}\left.\frac{\partial \Psi_{0,r}}{\partial x}\right|_{x=b}, \tag{4.47}$$

we arrive at the dividend value function $V(x, t_L(0); b, T_L)$.

4.2.4 The Solution and Examples

The solutions for the differential equations in three regions are summarized in the following proposition.

Proposition 4.2.2. In the case of excursion time framework, under the dividend barrier strategy, the dividend value function satisfies

1. Region One (R1): For $x \in (-\infty, 0)$ and $t_L(0) \in [0, T_L]$,

$$V(x, t^*_L; b, T_L) = \sum_{i=1}^{n} \mathcal{L}_s^{-1}[C_{i,1}\Phi_{i,r+s}(x) + C_{i,2}\Psi_{i,r+s}(x)]|_{\tau=t^*_L}\mathbf{1}_{A_i}(x)/g_0'(b). \tag{4.48}$$

2. Region Two (R2): For $x \in (0, b]$ and $t_L(0) = 0$,

$$V(x, 0; b, T_L) = (C_{0,1}\Phi_{0,r}(x) + C_{0,2}\Psi_{0,r}(x))/g_0'(b). \tag{4.49}$$

3. Region Three (R3): For $x \in (b, \infty)$ and $t_L(0) = 0$,

$$V(x, 0; b, T_L) = x - b + V(b, 0; b, T_L). \tag{4.50}$$

Remark 4.2.2. Although the derivation above assumes $\rho(x) > 0$, the results generally hold for the case that $\rho(x) \neq 0$, which includes the traditional mean-reverting process. When $\rho(x) = 0$, the surplus process (4.2) becomes the Brownian motion with constant drift considered by Gerber and Shiu (2004). With the underlying bankruptcy procedure, the dividend value function still satisfies the differential equations corresponding to the three different regions (4.18)–(4.20) but the fundamental solutions are simpler:

$$\Phi_r^*(x) = \exp\left(-\frac{(\mu - \sqrt{\mu^2 + 2\sigma^2 r})}{\sigma^2}x\right), \quad \Psi_r^*(x) = \exp\left(-\frac{(\mu + \sqrt{\mu^2 + 2\sigma^2 r})}{\sigma^2}x\right). \tag{4.51}$$

$\mathbb{E}[\mathbf{D}]$ can then be obtained by the same technique.

In the case of occupation time framework, by performing similar techniques the solutions for $\widetilde{V}(x, \widetilde{t}_L(0); b, T_L)$ are characterized in the following proposition.

Proposition 4.2.3. In the case of occupation time framework, under the dividend barrier strategy, the dividend value function satisfies

1. Region One (R1): For $x \in (-\infty, 0)$ and $\widetilde{t}_L(0) \in [0, T_L]$,

$$\widetilde{V}(x, \widetilde{t}_L^*; b, T_L) = \frac{\sum_{i=1}^{n} \mathcal{L}_s^{-1}\left[\widetilde{C}_{i,1}^R \Phi_{i,r+s}(x) + \widetilde{C}_{i,2}^R \Psi_{i,r+s}(x)\right]\Big|_{\tau=\widetilde{t}_L^*} \mathbf{1}_{A_i}(x)}{\mathcal{L}_s^{-1}\left[\widetilde{C}_{0,1}^R \frac{\partial \Phi_{0,r}}{\partial x}\Big|_{x=b} + \frac{\partial \Psi_{0,r}}{\partial x}\Big|_{x=b}\right]\Big|_{\tau=\widetilde{t}_L^*}}. \tag{4.52}$$

2. Region Two (R2): For $x \in (0, b]$ and $\widetilde{t}_L(0) \in [0, T_L]$,

$$\widetilde{V}(x, \widetilde{t}_L^*; b, T_L) = \frac{\mathcal{L}_s^{-1}\left[\widetilde{C}_{0,1}^R \Phi_{0,r}(x) + \Psi_{0,r}(x)\right]\Big|_{\tau=\widetilde{t}_L^*}}{\mathcal{L}_s^{-1}\left[\widetilde{C}_{0,1}^R \frac{\partial \Phi_{0,r}}{\partial x}\Big|_{x=b} + \frac{\partial \Psi_{0,r}}{\partial x}\Big|_{x=b}\right]\Big|_{\tau=\widetilde{t}_L^*}}. \tag{4.53}$$

3. Region Three (R3): For $x \in (b, \infty)$ and $\widetilde{t}_L(0) \in [0, T_L]$,

$$\widetilde{V}(x, \widetilde{t}_L^*; b, T_L) = x - b + \widetilde{V}(b, \widetilde{t}_L^*; b, T_L). \tag{4.54}$$

Please refer to Appendix D for the details of the derivation and the definitions of the notations.

Remark 4.2.3. Although we assume that the grace period T_L is a predetermined constant, with the aid of the analytical solution of the dividend value function in the form of Laplace inversion, the extension to the stochastic T_L is straightforward based on the tower rule of expectation:

$$\mathbb{E}[\mathbf{D}] = \mathbb{E}[\mathbb{E}[\mathbf{D}|T_L]] = \mathbb{E}[V(x, t_L(0); b, T_L)] = \int_0^\infty V(x, t_L(0); b, T_L) f(T_L) dT_L, \tag{4.55}$$

where the probability distribution of T_L admits a probability density function $f(T_L)$.

Example 4.2.1. In the case of excursion time framework and occupation time framework, consider the expectation of the discounted dividends under barrier strategy with parameter $b = 10$, which corresponds to bankruptcy procedures with different grace periods T_L. We assume that the parameter set is taken as $\Theta = \{\mu = 1; n = 1; \alpha_0 = 3\%; \alpha_1 = 5\%; \sigma = 5; r = 4\%; b = 10; T_L = 0, 1/24, 1/12, 1/6, 1/4, 1/2, 3/4, 1\}$.

Table 4.1 shows how the dividend value function changes with the grace period T_L and the initial surplus x in the case of excursion time framework and occupation time framework, respectively. It can be seen that, for a fixed T_L, the dividend value function is increasing with the initial surplus x for different frameworks. It is natural that the higher the initial surplus value, the higher the probability of hitting the dividend barrier. Other things being fixed, the bankruptcy procedures substantially influence the dividend value function. The effect is particularly pronounced for small values of initial surplus. For example, in the case of excursion time framework, when $x = 0.2$ the dividend value with $T_L = 1/24$ (or $1/2$ months) will be seven times larger than that it would be with the immediate bankruptcy rule. With same initial surplus and grace period, the dividend value function in the case of excursion time framework is larger than that in the case

Table 4.1: Dividend value function against the grace period

Excursion Time Framework								
x	$T_L = 0$	$T_L = 1/24$	$T_L = 1/12$	$T_L = 1/6$	$T_L = 1/4$	$T_L = 1/2$	$T_L = 3/4$	$T_L = 1$
0.2	0.4050	2.9711	4.0137	5.4586	6.5389	8.8690	10.5401	11.8621
0.4	0.8037	3.3480	4.3817	5.8143	6.8854	9.1957	10.8525	12.1633
0.6	1.1960	3.7191	4.7443	6.1649	7.2272	9.5183	11.1613	12.4612
0.8	1.5822	4.0848	5.1016	6.5108	7.5644	9.8369	11.4666	12.7559
1.0	1.9622	4.4451	5.4538	6.8518	7.8971	10.1515	11.7683	13.0475
2.0	3.7753	6.1683	7.1406	8.4880	9.4956	11.6685	13.2268	14.4597
4.0	7.0065	9.2627	10.1793	11.4496	12.3995	14.4481	15.9173	17.0796
6.0	9.7901	11.9582	12.8391	14.0598	14.9726	16.9413	18.3531	19.4701
8.0	12.2093	14.3297	15.1912	16.3852	17.2779	19.2033	20.5842	21.6766
10.0	14.3351	16.4411	17.2967	18.4825	19.3692	21.2815	22.6529	23.7379
Occupation Time Framework								
x	$T_L = 0$	$T_L = 1/24$	$T_L = 1/12$	$T_L = 1/6$	$T_L = 1/4$	$T_L = 1/2$	$T_L = 3/4$	$T_L = 1$
0.2	0.4050	2.1486	2.8611	3.8544	4.6028	6.2388	7.4363	8.4082
0.4	0.8037	2.5324	3.2389	4.2237	4.9658	6.5879	7.7751	8.7388
0.6	1.1960	2.9104	3.6110	4.5876	5.3235	6.9322	8.1095	9.0651
0.8	1.5822	3.2826	3.9775	4.9463	5.6762	7.2717	8.4396	9.3874
1.0	1.9622	3.6492	4.3386	5.2997	6.0238	7.6067	8.7653	9.7056
2.0	3.7753	5.4013	6.0658	6.9921	7.6899	9.2157	10.3324	11.2387
4.0	7.0065	8.5395	9.1659	10.0392	10.6972	12.1357	13.1884	14.0429
6.0	9.7901	11.2633	11.8652	12.7045	13.3368	14.7191	15.7308	16.5519
8.0	12.2093	13.6500	14.2388	15.0596	15.6780	17.0299	18.0194	18.8225
10.0	14.3351	15.7660	16.3508	17.1660	17.7802	19.1229	20.1056	20.9032

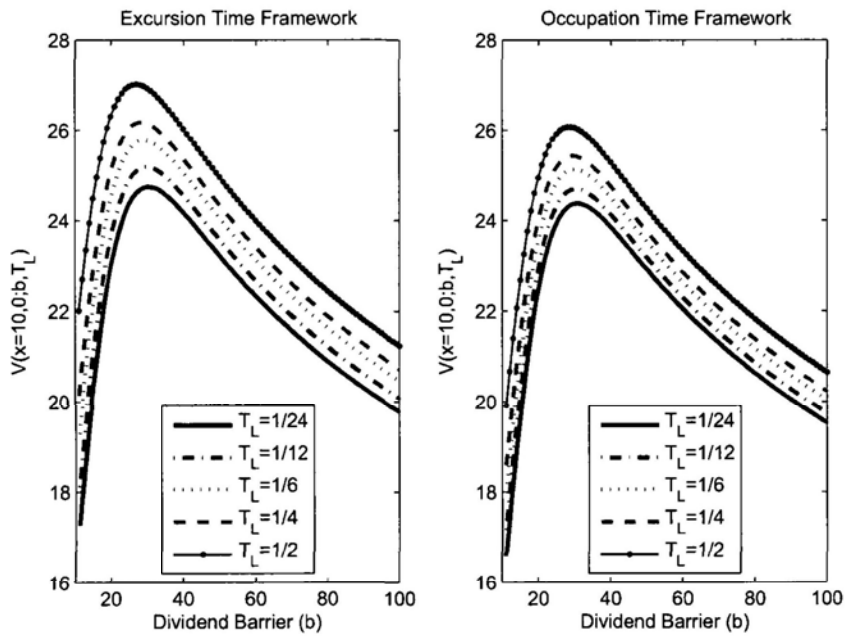

Figure 4.2: $V(x, t_L(0); b, T_L)$ against b with different T_L

of occupation time framework, since the past defaults are never forgiven in the case of occupation time framework such that it is more likely for the firm to be liquidated after which no more dividends will be paid out.

Figure 4.2 plots the dividend value function against the dividend barrier for $x = 10$ for different frameworks. The graph further illustrates that the larger the T_L the greater the dividends paid to shareholders for a given b. By fixing the bankruptcy procedure, the dividend value function increases with b, attains the maximum value, and then decreases to 0 if $b \to \infty$. Hence, Figure 4.2 shows numerically that the optimal dividend barrier is finite and exists. A deeper analysis is made in the next section.

4.3 The Optimal Dividends

In the case of excursion time framework, let b^* be the optimal dividend barrier that maximizes the dividend value function, $V(x, t_L(0); b, T_L)$. The following proposition gives the condition of the optimal dividend barrier through the denominator of the factorization forms.

Proposition 4.3.1. Suppose that the uncontrolled surplus process follows the stochastic differential equation (4.2). The dividend value function under the bankruptcy procedure, $V(x, t_L(0); b, T_L)$, attains its maximum by setting the dividend barrier to b^* if the optimal dividend barrier b^* exists and satisfies,

$$\left.\frac{\partial^2 g_0(x)}{\partial x^2}\right|_{x=b^*} = 0. \tag{4.56}$$

Proof. The proof is based on Shreve et al. (1984) but extends to the case of bankruptcy procedure. As

$$V(x, t_L(0); b, T_L) = \begin{cases} g(x, t_L(0))/g_0'(b), & \text{if } x \in (-\infty, 0),\ t_L(0) \in [0, T_L], \\ g_0(x)/g_0'(b), & \text{if } x \in (0, b],\ t_L(0) = 0, \\ x - b + g_0(b)/g_0'(b), & \text{if } x \in (b, \infty),\ t_L(0) = 0, \end{cases} \tag{4.57}$$

we obtain

$$\frac{\partial V(x, t_L(0); b, T_L)}{\partial b} = \begin{cases} -g(x, t_L(0))g_0''(b)/(g_0'(b))^2, & \text{if } x \in (-\infty, 0),\ t_L(0) \in [0, T_L], \\ -g_0(x)g_0''(b)/(g_0'(b))^2, & \text{if } x \in (0, b],\ t_L(0) = 0, \\ -g_0(b)g_0''(b)/(g_0'(b))^2, & \text{if } x \in (b, \infty),\ t_L(0) = 0. \end{cases} \tag{4.58}$$

If $V(x, t_L(0); b, T_L)$ attains its maximum at b^*, the corresponding first-order condition is

$$g_0''(b^*) = \left.\frac{\partial^2 g_0(x)}{\partial x^2}\right|_{x=b^*} = 0. \tag{4.59}$$

The proof is completed. □

According to (4.41), we have

$$\left.\frac{\partial^2 g_0(x)}{\partial x^2}\right|_{x=b^*} = C_{0,1} \left.\frac{\partial^2 \Phi_{0,r}}{\cdot \partial x^2}\right|_{x=b^*} + C_{0,2} \left.\frac{\partial^2 \Psi_{0,r}}{\partial x^2}\right|_{x=b^*} = 0. \tag{4.60}$$

This enables us to define the set of all optimal dividend barriers, which is independent of the initial surplus, as

$$\mathcal{B}_\xi = \{0 < y < \xi : f(y) = 0\}, \tag{4.61}$$

where

$$f(y) = C_{0,1} \left.\frac{\partial^2 \Phi_{0,r}}{\partial x^2}\right|_{x=y} + C_{0,2} \left.\frac{\partial^2 \Psi_{0,r}}{\partial x^2}\right|_{x=y}. \tag{4.62}$$

Clearly, $\mathcal{B}_\xi$ is nonempty if the following conditions hold,

$$\begin{cases} f(0) < 0, \\ f(\xi) > 0, \\ f'(y) > 0, \quad \text{for all} \quad y \in (0, \xi). \end{cases} \tag{4.63}$$

Moreover, there must be a unique $b^* \in \mathcal{B}_\xi$ such that $f(y) = 0$. It is straightforward to show that $f(y)$ does satisfy all conditions in (4.63).

Setting $x = b = b^*$ in (4.19) and utilizing the reflecting boundary condition at $x = b$ in (4.19) and the optimal barrier condition (4.56), we have

$$V(b^*, t_L(0) = 0; b^*, T_L) = \frac{\mu + \alpha_0 b^*}{r}. \tag{4.64}$$

Thus, $V(b^*, 0; b^*, T_L)$ is identical to the present value of a perpetuity, where the payment rate is the sum of the drift and the interest on the initial capital. The relation (4.64) also holds for both the models considered by Gerber and Shiu (2004) and Cai et al. (2006). It is worth mentioning that the value of b^* is, however different, because it depends on T_L and $\rho(x)$ in our case.

Table 4.2: Optimal barrier with different bankruptcy procedures

	$T_L = 0$	$T_L = 0.05$	$T_L = 0.10$	$T_L = 0.15$	$T_L = 0.20$	$T_L = 0.25$	$T_L = 0.30$
b^*	31.7496	30.2534	29.6263	29.1422	28.7320	28.3691	28.0397
$\widetilde{b}^*$	31.7496	30.7395	30.3193	29.9966	29.7245	29.4848	29.2682
	$T_L = 0.35$	$T_L = 0.40$	$T_L = 0.45$	$T_L = 0.50$	$T_L = 0.55$	$T_L = 0.60$	$T_L = 0.65$
b^*	27.7357	27.4519	27.1845	26.9309	26.6890	26.4572	26.2344
$\widetilde{b}^*$	29.0691	28.8840	28.7102	28.5461	28.3901	28.2412	28.0986
	$T_L = 0.70$	$T_L = 0.75$	$T_L = 0.80$	$T_L = 0.85$	$T_L = 0.90$	$T_L = 0.95$	$T_L = 1.00$
b^*	26.0195	25.8116	25.6101	25.4143	25.2239	25.0382	24.8571
$\widetilde{b}^*$	27.9616	27.8295	27.7019	27.5783	27.4583	27.3412	27.2254

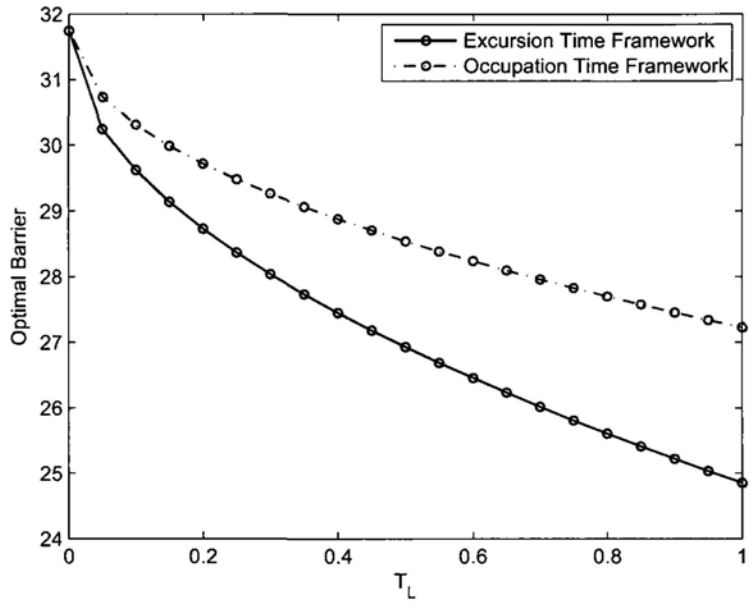

Figure 4.3: Optimal barrier with different "grace" period T_L

Remark 4.3.1. In the case of occupation time framework, similar procedures could be performed to find the optimal dividend barrier $\widetilde{b}^*$ satisfying

$$\left.\frac{\partial^2 \widetilde{g}_0(x,0)}{\partial x^2}\right|_{x=\widetilde{b}^*} = 0, \tag{4.65}$$

where the initial occupation time has be reset to 0 by shortening the grace period $T_L^* = T_L - \widetilde{t}_L(0)$.

Example 4.3.1. We look at the optimal dividend barrier b^* corresponding to different T_L using parameters $\Theta = \{\mu = 1; n = 1; \alpha_0 = 3\%; \alpha_1 = 5\%; \sigma = 5; r = 4\%; b = 10; T_L\}$ in the case of excursion time framework and occupation time framework, respectively.

It can be seen from Table 4.2 that the bankruptcy procedure has a significant impact on the optimal dividend barrier. If renegotiation time is granted to a defaulted firm, a

lower optimal barrier level can be set because the bankruptcy procedure lowers the firm's bankruptcy risk. Shareholders could enjoy a more aggressive dividend policy. As the grace period is closely related to the negotiation power of the management of the firm, a reputable management team benefits shareholders by decreasing the bankruptcy risk and hence improving the total amount of dividends. With the same length of "grace period", the optimal barrier in the case of excursion time framework is lower than that in the case of occupation time framework because of the memoryless feature of the hypothetical default clock in the case of excursion time framework so that a more aggressive dividend policy could be applied.

Figure 4.3 shows the decreasing trend of the optimal dividend barrier against T_L. When $T_L \to \infty$, the optimal dividend barrier reaches 0. In other words, if T_L is large enough, it takes a very long time for the firm to declare bankruptcy. Consequently, shareholders can receive dividends whenever the surplus is positive and the risk remains with debt holders. This implies that the grace period should not be too long for protecting debt holders. In addition, the optimal barrier in the case of excursion time framework is beneath that in the case of occupation time framework.

Shareholders are interested in the dividend value function. Table 4.3 and Figure 4.4 show the dividend value function with different initial surplus under the optimal dividend strategy for different bankruptcy procedures. Several observations could be highlighted. Firstly, although the optimal dividend level b^* is independent of the initial surplus, the dividend value function increases with the initial surplus for a fixed bankruptcy procedure with the corresponding optimal dividend strategy. Secondly, the dividend value function under the excursion time framework is the largest among the three. By allowing a defaulted firm to continue its business, the bankruptcy procedures do benefit the shareholders by increasing their expected dividend payments. The effect is particularly pronounced for firms with small initial surplus. Thirdly, when the initial surplus rises above the optimal dividend barrier, the dividend value is a linear function of the initial surplus for all of the three cases. It is natural because the immediate dividend payment

Table 4.3: Dividend value function under the optimal dividend strategy

initial surplus (x)	0.5	1.0	1.5	2.0	2.5	3.0	3.5	(b^*)
$T_L = 0$	1.6441	3.22407	4.7428	6.20308	7.6076	8.95896	10.2597	(31.7496)
Occupation $T_L = 1$	11.4409	12.4731	13.4734	14.4433	15.3842	16.2976	17.1848	(27.2554)
Excursion $T_L = 1$	14.5396	15.4073	16.252	17.0749	17.877	18.6593	19.4229	(24.8571)
initial surplus (x)	5	10	15	20	25	30	35	(b^*)
$T_L = 0$	13.8819	23.5534	30.7843	36.7095	42.0086	47.0618	52.0626	(31.7496)
Occupation $T_L = 1$	19.7019	26.8635	32.8044	38.1276	43.192	48.1936	53.1936	(27.2554)
Excursion $T_L = 1$	21.6104	28.0312	33.6031	38.7676	43.7857	48.7857	53.7857	(24.8571)

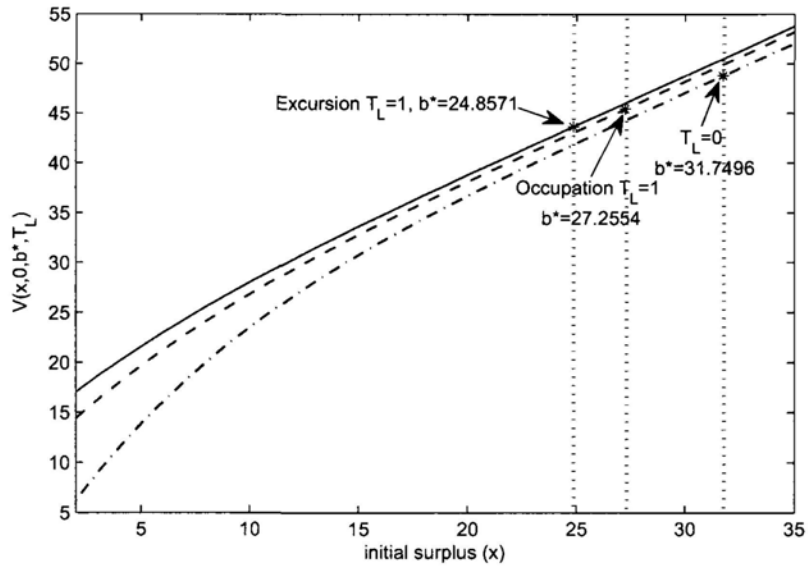

Figure 4.4: Dividend value function under the optimal dividend strategy

brings the surplus back to the optimal barrier level.

4.4 Distribution of the Bankruptcy Time

Consider the dividends are paid according to a barrier strategy with parameter b, which may be different from the optimal value b^*. Under the excursion time framework, we would like to know the distribution of the bankruptcy time T. Consider

$$L(x, t_L(0); b, T_L) = \mathbb{E}[e^{-rT}], \tag{4.66}$$

where x is the initial surplus. This can be interpreted as the expected present value of \$1 paid at the bankruptcy time, or the Laplace transform of the probability density function of T, or the moment generating function of T. Thus, the expected bankruptcy time can

be determined by

$$\mathbb{E}[T] = -\left.\frac{\mathrm{d}L(x, t_L(0); b, T_L)}{\mathrm{d}r}\right|_{r=0}. \tag{4.67}$$

Using the framework established in Section 4.2, the differential equations for $L(x, t_L(0); b, T_L)$ in three different regions can be formulated as follows.

1. Region One (R1): For $x \in (-\infty, 0)$ and $t_L(0) \in [0, T_L]$,

$$\begin{cases} \frac{1}{2}\sigma^2 \frac{\partial^2 L}{\partial x^2} + (\mu + \rho(x)x)\frac{\partial L}{\partial x} + \frac{\partial L}{\partial t_L} - rL = 0, \\ L(x, T_L; b, T_L) = 1, \\ \lim\limits_{x \to -\infty} \frac{\partial L(x, t_L(0); b, T_L)}{\partial x} = 0, \\ L(0-, t_L(0); b, T_L) = L(0+, 0; b, T_L), \\ \left.\frac{\partial L(x, t_L(0); b, T_L)}{\partial x}\right|_{x=0-} = \left.\frac{\partial L(x, 0; b, T_L)}{\partial x}\right|_{x=0+}. \end{cases} \tag{4.68}$$

2. Region Two (R2): For $x \in (0, b]$ and $t_L(0) = 0$,

$$\begin{cases} \frac{1}{2}\sigma^2 \frac{\partial^2 L}{\partial x^2} + (\mu + \alpha_0 x)\frac{\partial L}{\partial x} - rL = 0, \\ \left.\frac{\partial L}{\partial x}\right|_{x=b} = 0, \\ L(0+, 0; b, T_L) = L(0-, t_L(0); b, T_L), \\ \left.\frac{\partial L(x, 0; b, T_L)}{\partial x}\right|_{x=0+} = \left.\frac{\partial L(x, t_L(0); b, T_L)}{\partial x}\right|_{x=0-}. \end{cases} \tag{4.69}$$

3. Region Three (R3): For $x \in (b, \infty)$ and $t_L(0) = 0$,

$$L(x, 0; b, T_L) = L(b, 0; b, T_L). \tag{4.70}$$

In the case of occupation time framework, we need to solve and calculate $\widetilde{L}(x, \widetilde{t}_L(0); b, T_L)$ for all possible values of $\widetilde{t}_L(0)$ even if x is above the default threshold. Region Two and Three should then be defined in the rectangle $x \in (0, b]$, $\widetilde{t}_L(0) \in [0, T_L]$ and $x \in (b, +\infty)$, $\widetilde{t}_L(0) \in [0, T_L]$, respectively.

Using techniques similar to those introduced in Section 4.3 and Appendix D, the analytical solution of L and $\widetilde{L}$ could be obtained in the form of Laplace inversion.

Proposition 4.4.1. For the same initial surplus x, barrier level b and grace period $T_L \geq 0$,

$$\mathbb{E}[T] \geq \mathbb{E}[\widetilde{T}] \geq \mathbb{E}[T^*], \tag{4.71}$$

where T^* is the default time or the bankruptcy time with $T_L = 0$.

Proof. The process of the modified surplus is independent of the bankruptcy procedure with the same initial surplus and barrier level. The bankruptcy procedure influences the dividend value function only be the hypothetical default clock counting the lifespan of the company.

For any path of the modified surplus, on the one hand, let

$$\widetilde{T} = \Theta_x(T_L) := \inf\left\{t \geq 0 \middle| \int_0^t \mathbf{1}_{\{X_u - D_u \leq L\}} \mathrm{d}u \geq T_L, X_0 - D_0 = x\right\} \tag{4.72}$$

denote the bankruptcy time in the case of occupation time framework with grace period T_L and initial surplus x. Since the past defaults affect further defaults by shortening the maximum allowed length of time that the company can spend in default without being liquidated, we have $\widetilde{L}(x, \widetilde{t}_L(0); b, T_L) = \widetilde{L}(x, 0; b, T_L - \widetilde{t}_L(0))$. Without loss of generality, it is assumed that $\widetilde{t}_L(0) = 0$ and consequently

$$\widetilde{T} = \Theta_x(T_L) = T_0 + \Theta_0(T_L), \tag{4.73}$$

where T_0 is the first hitting time of zero by the modified surplus and $\Theta_0(T_L)$ is the bankruptcy time with zero initial surplus and grace period of T_L. Based on the linearity of the expectation operator,

$$\mathbb{E}[\widetilde{T}] = \mathbb{E}[T_0] + \mathbb{E}[\Theta_0(T_L)].$$

Since $\mathbb{E}[T_0] = \mathbb{E}[T^*]$ is the default time with $T_L = 0$ and $\Theta_0(T_L) \geq 0$, we have

$$\mathbb{E}[\widetilde{T}] \geq \mathbb{E}[T^*]. \tag{4.74}$$

On the other hand, based on the dynamics of $\mathrm{d}t_L(t)$ and $\mathrm{d}\widetilde{t}_L(t)$ as shown in (4.7) and (4.12),

$$\widetilde{t}_L(t) - t_L(t) = \sum_{u \in S} t_L(u-), \quad \text{where} \quad S = \{u \geq 0 | X_u - D_u = L\}. \tag{4.75}$$

Since $t_L(u-) \geq 0$ for any $u \geq 0$, $\widetilde{t}_L(t) \geq t_L(t)$. By the definition of the bankruptcy time, we have $\widetilde{T} \leq T$ for any path of the modified surplus. Based on the monotonicity of the expectation operator,

$$\mathbb{E}[\widetilde{T}] \leq \mathbb{E}[T]. \tag{4.76}$$

The proof is completed. □

Table 4.4: Expectation of bankruptcy time with different initial surplus

x	0.5	1.0	1.5	2.0	2.5	3.0	3.5	(b^*)
$T_L = 0$	15.268	29.907	43.929	57.350	70.184	82.446	94.152	(31.7496)
Occupation	64.938	70.964	76.727	82.234	87.494	92.513	97.297	(27.2554)
Excursion	227.657	223.120	238.338	243.318	248.067	252.592	256.899	(24.8571)
x	4	7	10	13	16	19	22	(b^*)
$T_L = 0$	105.316	161.812	202.779	231.470	250.807	263.272	270.867	(31.7496)
Occupation	**101.856**	**124.849**	**141.433**	**152.963**	**160.617**	**165.382**	**168.055**	(27.2554)
Excursion	260.995	281.525	296.112	306.025	312.369	316.066	317.857	(24.8571)

Remark 4.4.1. The expected bankruptcy time $\mathbb{E}[T]$ can be determined by (4.67). According to the fundamental theorem of calculus, the differentiation with respect to r and the Laplace inversion can be interchanged. Thus, the analytical solution of $\mathbb{E}[T]$ is obtained in the form of Laplace inversion.

Remark 4.4.2. As the Laplace transform of the probability density function of T is obtained, the density function can be calculated using numerical Laplace inversion. Let

$$m(y) = \mathbb{E}[e^{yT}]$$

denote the moment generating function of T, $m(-r) = L(x, t_L(0); b, T_L)$, which has been determined in this section. Hence, moments of T can be obtained by differentiation.

For the same initial surplus x and dividend barrier level b, we have the relationship between the expected bankruptcy time under different bankruptcy procedures according to Proposition 4.4.1. However, the firm optimized its dividend strategy by setting b^* to maximize the dividend value function as described in Section 4.3.

Example 4.4.1. We look at the expectation of bankruptcy time under the optimal dividend strategy using parameters $\Theta = \{\mu = 1; n = 1; \alpha_0 = 3\%; \alpha_1 = 5\%; \sigma = 5; r = 4\%; b = 10; T_L = 1\}$ in the case of excursion time framework and occupation time framework, respectively.

The optimal dividend level b^* is independent of the initial surplus as shown in Section 4.3. It can be seen from Table 4.4 and Figure 4.5 that under the optimal dividend strategy the initial surplus has an influence on the expected bankruptcy time for different bankruptcy procedures. Firstly, for any initial surplus, the expected bankruptcy time in

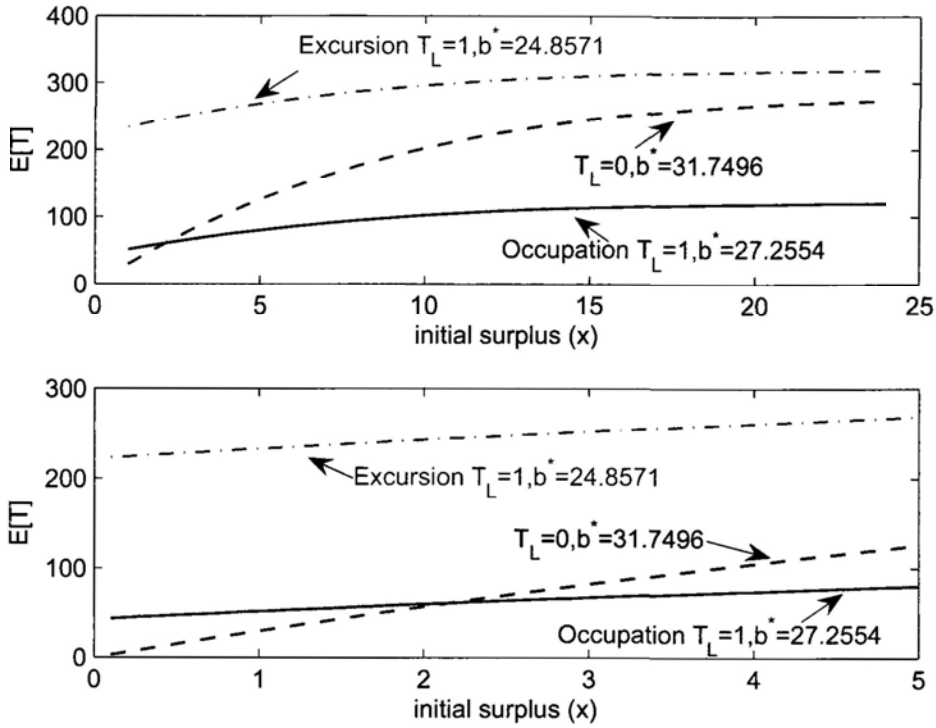

Figure 4.5: Expectation of bankruptcy time under optimal dividend strategy

the case of excursion time framework is the longest among the three. It is due to the resetting feature of the hypothetical default clock so that the liquidation of the firm is only triggered by a consecutive stay below the default threshold. Secondly, for the firm with low initial surplus, the bankruptcy procedure in the case of occupation time do prolong the expected lifespan of the firm. Under such situation, the impact of the barrier level on the modified surplus is mild. Although a more aggressive dividend policy is employed in the case of occupation time framework, the firm could still enjoy a longer life with little probability to pay dividends. Thirdly, for the firm with relatively large initial surplus, the bankruptcy procedure in the case of occupation time framework surprisingly shortens the expected bankruptcy time. Under such situation, the barrier level plays the key role and past defaults are never forgiven. Granted the grace period, the firm will adopt an aggressive barrier level, which makes it more likely to be liquidated. Fourthly, there exists some critical value of initial surplus, with which the expected bankruptcy time in the case of occupation time framework is equal to that in the case of zero grace period.

4.5 Generalized Barrier Strategies

If a barrier strategy is applied, the ultimate ruin of the company is certain. In some circumstances this is not desirable. This consideration leads to the idea of imposing restrictions on the nature of the dividend stream, resulting in optimization problems with additional constraints. When $\rho = 0$, Jeanblanc-Picqué and Shiryaev (1995) and Asmussen and Taksar (1997) postulate a generalized barrier strategy, called a threshold strategy. Under this strategy, dividends are paid at a constant rate κ whenever the surplus rises above threshold b. Gerber and Shiu (2006) carry out some elementary and down-to-earth calculations on this model. Threshold b plays the role of a break-point or a regime-switching boundary. The discounted value of dividends takes the form,

$$\mathbf{D} = \kappa \int_0^T e^{-rt} \mathbf{1}_{\{X_t - D_t > b\}} \mathrm{d}t. \tag{4.77}$$

The excursion time framework is now applied to this barrier strategy with the surplus following the OU process. The dividend value function $\mathbb{E}[\mathbf{D}] = V(x, t_L(0); b, T_L)$ still satisfies the differential equations in three different regions (4.18)–(4.20), except that the following modification is required.

1. The boundary condition in R2 at $x = b$ is replaced by

$$V(b, t_L(0) = 0; b, T_L) = \zeta, \tag{4.78}$$

   where ζ is a constant with respect to the fixed parameter set Θ.

2. In R3, the dividend value function is no longer a direct formula but should be solved from a differential equation. For $x \in (b, \infty)$ and $t_L(0) = 0$,

$$\begin{cases} \frac{1}{2}\sigma^2 \frac{\partial^2 V}{\partial^2 x^2} + (\mu + \alpha_0 x - \kappa)\frac{\partial V}{\partial x} - rV + \kappa = 0, \\ V(b+, 0; b, T_L) = \zeta, \\ V(x, 0; b, T_L) \to \frac{\kappa}{r}, \quad \text{for} \quad x \to \infty. \end{cases} \tag{4.79}$$

When $x > b$, the modified surplus behaves with an extra drift of $-\kappa$. If there is infinite surplus, then the dividends are a continuous perpetuity of amount κ per unit time. Thus, we have the last boundary condition in (4.79).

Using techniques similar to those introduced in Section 4.2 and the continuity of the dividend value function at $x = b$, a system of equations with a larger number of unknown coefficients can be obtained. Simple calculation can yield the result. Once the formula of the dividend value function is derived, the optimal dividend barrier and the expected bankruptcy time can be obtained by mimicking the analysis in the earlier sections. The detailed calculation is omitted here.

4.6 Conclusion

This chapter extends the optimal dividend barrier strategy of Gerber and Shiu (2003, 2004) to incorporate bankruptcy procedures consistent with Chapter 11 of the US Bankruptcy Code. More precisely, bankruptcy occurs if a firm is in financial distress over a period of time. This is realized by using an excursion time that measures the total time spent below the default threshold in a single excursion or an occupation time variable that measures the cumulative length of period instead. To allow general discussion, we consider a general Ornstein-Uhlenbeck process in which the mean-reverting rate can take any real number. Moreover, we assume that the debit rate is dependent on the deficit position of the firm. A general framework is then formulated to study the problem. Consequently, the closed-form solution for the dividend value function is derived in the case of excursion time framework and occupation time framework, respectively. By maximizing the dividend value function, the optimal dividend barrier is obtained numerically. Our result shows that the underlying bankruptcy procedure can significantly affect the optimal dividend policy. We sketch possible extensions of our framework to related problems, such as generalized dividend barrier strategies.

Chapter 5

Multi-Dimensional GDP: Application in Currency Option Pricing

The analysis so far focuses on a one-factor general diffusion processes. In order to capture the evidence of mean reversion and multi-scale stochastic volatility in currency market, this chapter considers a multi-dimensional general diffusion process for currency option pricing.

5.1 The Model

Let S_t be the underlying currency for which the risk-neutral process is postulated as

$$\begin{aligned} S_t &= \exp(X_t), \\ \mathrm{d}X_t &= (\theta(t) - \kappa X_t - v_{1,t}/2 - v_{2,t}/2)\mathrm{d}t + \sqrt{v_{1,t}}\mathrm{d}W_t^{0,1} + \sqrt{v_{2,t}}\mathrm{d}W_t^{0,2}, \\ \mathrm{d}v_{1,t} &= (a_1(t) - b_1 v_{1,t})\mathrm{d}t + \sigma_1\sqrt{v_{1,t}}\mathrm{d}W_t^1 \\ \mathrm{d}v_{2,t} &= (a_2(t) - b_2 v_{2,t})\mathrm{d}t + \sigma_2\sqrt{v_{2,t}}\mathrm{d}W_t^2 \end{aligned} \tag{5.1}$$

where the constant κ is the mean reversion speed for the log-currency-value; the deterministic function $\theta(t)$ represents the equilibrium mean level of the log-currency-value against time; $v_{1,t}$ and $v_{2,t}$ are stochastic variances on different time scales with the mean reversion speed b_1 and b_2; $a_1(t)$ and $a_2(t)$ are equilibrium mean levels of the two stochastic variances against time; σ_1 and σ_2 are the volatility coefficients of the volatility processes;

$W_t^{0,1}$, $W_t^{0,2}$, W_t^1 and W_t^2 are Wiener processes. In fact, the empirical study of Alizadeh et al. (2002) documented that there were two dominated stochastic factors that governed the evolution of currency volatility, with one highly persistent factor and one quickly mean-reverting factor. Based on the suggestion of Alizadeh et al. (2002), the proposed model specified in (5.1) considers a two-scale stochastic volatility. Following Fatone et al. (2009), we further assume that

$$\begin{aligned} \langle \mathrm{d}W_t^1 \mathrm{d}W_t^2 \rangle = 0, \quad \langle \mathrm{d}W_t^{0,1} \mathrm{d}W_t^1 \rangle = \rho_1 \mathrm{d}t, \quad \langle \mathrm{d}W_t^{0,1} \mathrm{d}W_t^2 \rangle = 0, \\ \langle \mathrm{d}W_t^{0,2} \mathrm{d}W_t^1 \rangle = 0, \quad \langle \mathrm{d}W_t^{0,2} \mathrm{d}W_t^2 \rangle = \rho_2 \mathrm{d}t, \quad \langle \mathrm{d}W_t^{0,1} \mathrm{d}W_t^{0,2} \rangle = 0, \end{aligned} \tag{5.2}$$

where $\langle \cdot \rangle$ denotes the expectation operator, and ρ_1, $\rho_2 \in [-1, 1]$ are constant correlation coefficients.

Our proposed model is a multi-dimensional general diffusion process, see (1.9), with $\mathbf{X}_t = (X_t, v_{1,t}, v_{2,t})^{\mathbf{T}}$ and is reduced to the model of Fatone et al. (2009) if $\kappa = 0$ and $\theta(t) = r$, the risk-free interest rate, for an equity option. As long as currency option is concerned, the domestic interest rate, r_d, and the foreign interest rate, r_f, are embedded into the risk-neutral parameter $\theta(t)$. We will see shortly that the effects of r_d and r_f are fully reflected in and captured by the currency future prices, which will be regarded as observations that are "super-calibrated" to the model.

5.1.1 The Characteristic Function

Given the currency dynamic, it is possible to obtain the characteristic function for the log-currency-value X_t. Denote the characteristic function as

$$f(x, v_1, v_2, t; \phi) = \mathbb{E}[e^{i\phi X_T} | X_t = x, v_{1,t} = v_1, v_{2,t} = v_2], \tag{5.3}$$

where $T \geq t$ and $i = \sqrt{-1}$. The following lemma holds.

Lemma 5.1.1. If X_t follows the dynamics in (5.1), then the characteristic function for X_T defined in (5.3) is given by

$$f(x, v_1, v_2, t; \phi) = \exp\left[A_1(\tau; \phi)v_1 + A_2(\tau; \phi)v_2 + B(\tau; \phi) + i\phi x e^{-\kappa\tau}\right], \tag{5.4}$$

where $\tau = T - t$,

$$B(\tau;\phi) = \int_0^\tau ie^{-\kappa s}\phi\theta(T-s)\mathrm{d}s + \int_0^\tau a_1(T-s)A_1(s;\phi)\mathrm{d}s + \int_0^\tau a_2(T-s)A_2(s;\phi)\mathrm{d}s,$$

$$\begin{aligned}
A_j(\tau;\phi) &= \frac{U_{j1}(\tau)+U_{j2}(\tau)+U_{j3}(\tau)}{D_j(\tau)}, \qquad \text{for } j=1,2, \qquad (5.5)\\
U_{j1}(\tau) &= -e^{-\kappa\tau}C_{j1}[M_{a_j^*,b_j^*}(c_j^*e^{-\kappa\tau}) + F_jW_{a_j^*,b_j^*}(c_j^*e^{-\kappa\tau})],\\
U_{j2}(\tau) &= -C_{j2}M_{a_j^*+1,b_j^*}(c_j^*e^{-\kappa\tau}),\\
U_{j3}(\tau) &= -C_{j3}[M_{a_j^*,b_j^*}(c_j^*e^{-\kappa\tau}) + F_jW_{a_j^*,b_j^*}(c_j^*e^{-\kappa\tau})] - 4\rho_j^*\kappa F_jW_{a_j^*+1,b_j^*}(c_j^*e^{-\kappa\tau}),\\
D_j(\tau) &= 2\rho_j^*\sigma_j^2[F_jW_{a_j^*,b_j^*}(c_j^*e^{-\kappa\tau}) + M_{a_j^*,b_j^*}(c_j^*e^{-\kappa\tau})],\\
a_j^* &= \frac{-i(2\rho_j(\kappa-b_j)+\sigma_j)}{4\kappa\rho_j^*},\ b_j^* = \frac{b_j}{2\kappa},\ c_j^* = \frac{\phi\sigma_j\rho_j^*}{\kappa},\ \rho_j^* = \sqrt{1-\rho_j^2},\\
C_{j1} &= 2\phi\sigma_j(\rho_j^2 - 1 + i\rho_j^*\rho_j),\\
C_{j2} &= -2\rho_j^*(\kappa+b_j) + i(2\kappa\rho_j - 2b_j\rho_j + \sigma_j),\\
C_{j3} &= 2\rho_j^*(\kappa-b_j) - i(2\kappa\rho_j - 2b_j\rho_j + \sigma_j),\\
C_{j4} &= 2\rho_j^*(\kappa - b_j + i\rho_j\sigma_j\phi) + \sigma_j(2\phi\rho_j^2 - 2\phi - i) + 2i\rho_j(b_j-\kappa),\\
F_j &= \frac{C_{j4}M_{a_j^*,b_j^*}(c_j^*) + C_{j2}M_{a_j^*+1,b_j^*}(c_j^*)}{C_{j4}W_{a_j^*,b_j^*}(c_j^*) + 4\rho_j^*\kappa W_{a_j^*+1,b_j^*}(c_j^*)}, \qquad (5.6)
\end{aligned}$$

and $M_{k,m}(x)$ and $W_{k,m}(x)$ are the Whittaker functions.

Proof. The Feynman-Kac formula gives the following partial differential equation (PDE) for the characteristic function.

$$\begin{gathered}
\tfrac{v_1+v_2}{2}f_{xx} + \rho_1\sigma_1v_1f_{xv_1} + \tfrac{\sigma_1^2v_1}{2}f_{v_1v_1} + (a_1(t) - b_1v_1)f_{v_1} + \rho_2\sigma_2v_2f_{xv_2}\\
+\tfrac{\sigma_2^2v_2}{2}f_{v_2v_2} + (a_2(t) - b_2v_2)f_{v_2} + \left(\theta(t) - \kappa x - \tfrac{v_1}{2} - \tfrac{v_2}{2}\right)f_x + f_t = 0, \qquad (5.7)\\
f(x, v_1, v_2, T;\phi) = e^{i\phi x}.
\end{gathered}$$

To see this, we apply the Ito Lemma to $\{f(x,v,s;\phi)\}_{t\le s\le T}$, and obtain

$$\begin{aligned}
&f(x_T, v_{1,T}, v_{2,T}, T;\phi) = f(x_t, v_{1,t}, v_{2,t}, t;\phi)\\
&+\int_t^T \sqrt{v_1}f_x dW_s^{0,1} + \int_t^T \sqrt{v_2}f_x dW_s^{0,2} + \int_t^T \sigma_1\sqrt{v_1}f_{v_1}dW_s^1 + \int_t^T \sigma_2\sqrt{v_2}f_{v_2}dW_s^2\\
&+\int_t^T \left(\frac{v_1+v_2}{2}f_{xx} + \rho_1\sigma_1v_1f_{xv_1} + \frac{\sigma_1^2v_1}{2}f_{v_1v_1} + (a_1(t)-b_1v_1)f_{v_1} + \rho_2\sigma_2v_2f_{xv_2}\right.\\
&\left.+\frac{\sigma_2^2v_2}{2}f_{v_2v_2} + (a_2(t)-b_2v_2)f_{v_2} + \left(\theta(t) - \kappa x - \frac{v_1}{2} - \frac{v_2}{2}\right)f_x + f_t\right)ds
\end{aligned}$$

Taking the expectation on both sides and recognizing that $f(x_T, v_{1,T}, v_{2,T}, T;\phi) = e^{i\phi x_T}$ then gives the result. Consider an exponential affine form for the characteristic function:

$$f(x,v,t;\phi) = \exp\left(A_1(\tau;\phi)v_1 + A_2(\tau;\phi)v_2 + B(\tau;\phi) + C(\tau;\phi)x + i\phi x\right),$$

where $\tau = T - t$ and $A_1(\tau = 0; \phi) = A_2(\tau = 0; \phi) = B(\tau = 0; \phi) = C(\tau = 0; \phi) = 0$. Substituting it into (5.7) yields

$$\begin{aligned}
0 &= v_1 \left[\frac{1}{2}(C(\tau) + i\phi)^2 + \rho_1\sigma_1 A_1(\tau)(C(\tau) + i\phi) + \frac{1}{2}\sigma_1^2 A_1^2(\tau)\right. \\
&\quad \left. -\frac{1}{2}(C(\tau) + i\phi) - b_1 A_1(\tau) - A_1'\right] + x[-\kappa(C(\tau) + i\phi) - C'] \\
&\quad + v_2 \left[\frac{1}{2}(C(\tau) + i\phi)^2 + \rho_2\sigma_2 A_2(\tau)(C(\tau) + i\phi) + \frac{1}{2}\sigma_2^2 A_2^2(\tau)\right. \\
&\quad \left. -\frac{1}{2}(C(\tau) + i\phi) - b_2 A_2(\tau) - A_2'\right] + [\theta(T - \tau)(C(\tau) + i\phi) \\
&\quad + a_1(t)A_1(\tau) + a_2(t)A_2(\tau) - B'],
\end{aligned}$$

where the differentiations are taken with respect to τ. This leads to the following system of ordinary differential equations:

$$\begin{aligned}
0 &= \frac{1}{2}(C(\tau) + i\phi)^2 + \rho_1\sigma_1 A_1(\tau)(C(\tau) + i\phi) \\
&\quad + \frac{1}{2}\sigma_1^2 A_1^2(\tau) - \frac{1}{2}(C(\tau) + i\phi) - b_1 A_1(\tau) - A_1', && (5.8) \\
0 &= \frac{1}{2}(C(\tau) + i\phi)^2 + \rho_2\sigma_2 A_2(\tau)(C(\tau) + i\phi) \\
&\quad + \frac{1}{2}\sigma_2^2 A_2^2(\tau) - \frac{1}{2}(C(\tau) + i\phi) - b_2 A_2(\tau) - A_2', && (5.9) \\
0 &= -\kappa(C(\tau) + i\phi) - C', && (5.10) \\
0 &= \theta(t)(C(\tau) + i\phi) + a_1 A_1(\tau) + a_2 A_2(\tau) - B'. && (5.11)
\end{aligned}$$

It is clear from (5.10) and $C(0) = 0$ that

$$C(\tau) = i\phi e^{-\kappa\tau} - i\phi. \tag{5.12}$$

Substituting (5.12) into (5.8), we have

$$-A_1' = -\frac{1}{2}\sigma_1^2 A_1^2 + (b_1 - \rho_1\sigma_1 i\phi e^{-\kappa\tau})A_1 + \frac{1}{2}(i\phi e^{-\kappa\tau} + \phi^2 e^{-2\kappa\tau}), \tag{5.13}$$

whose solution is

$$A_1(\tau) = \frac{U_{11}(\tau) + U_{12}(\tau) + U_{13}(\tau)}{D_1(\tau)},$$

which is specified in (5.5) and involves the undetermined constant coefficient F_1 and the Whittaker functions $M_{k,m}(x)$ and $W_{k,m}(x)$. Imposing the initial condition that $A_1(\tau =$

$0) = 0$ gives the explicit form of F_1. Similar procedures can be applied to (5.9) for the solution of $A_2(\tau)$. With $A_1(\tau)$ and $A_2(\tau)$ available, from (5.11), we obtain

$$B(\tau;\phi) = \int_0^\tau ie^{-\kappa s}\phi\theta(T-s)\mathrm{d}s + \int_0^\tau a_1(T-s)A_1(s;\phi)\mathrm{d}s + \int_0^\tau a_2(T-s)A_2(s;\phi)\mathrm{d}s.$$

□

Although the closed-form solution of the characteristic function seems to be complicated, it is expressed in certain elementary functions. The computation of the Whittaker functions is also standard as these functions are available in the Mathematica and Matlab software packages. These mathematical functions are widely applied to mathematics, physics, engineering and finance (see the comments in Wong and Lau, 2008). As the Whittaker functions require a little more computational time than other elementary functions, such as sine, cosine and exponential, the Fourier inversion formulas for a function involving them should be implemented using a highly efficient numerical method. Our suggestion is to use the fractional FFT (FRFT), which detailed in section Fractional FFT.

The probability density function of the log-return can be obtained by inverting the Fourier transform on the characteristic function. Here, we examine the distributional properties of the proposed model. Figure 5.1 shows how the positive correlations of volatilities with the spot return create a fat-right-tail and thin-left-tail distribution of the log-return. Positive correlations result in a high variance when the spot asset rises, which fattens the right tail of the density function.

Figure 5.2 shows how the mean reversion rate of the underlying asset pushes the distribution toward the equilibrium mean level $\theta(t)$. If we interpret the underlying asset as an exchange rate, then the mean reversion rate can be regarded as an indicator of the magnitude of central bank intervention. An increase in the magnitude of such intervention on the exchange rate thus results in a decrease in the volatility of the exchange rate.

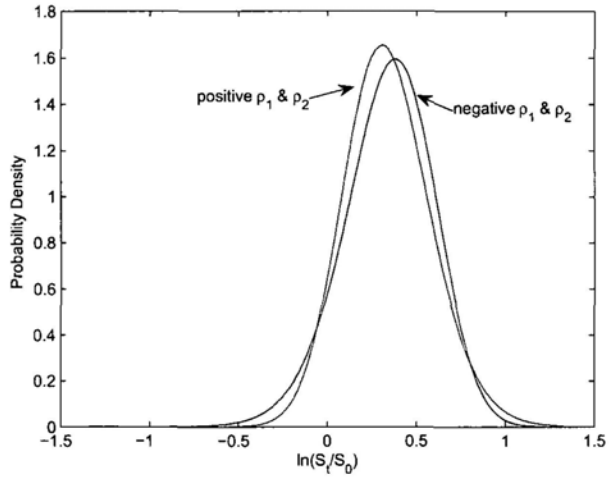

Figure 5.1: Probability density function of the log-return over a 1-year horizon with different correlations. The parameter values are: $\kappa = 10$, $\theta(t) = 4.0339$, $S_0 = 1.0$, $v_{1,0} = 0.5$, $a_1(t) = 0.5328$, $b_1 = 1.45$, $\sigma_1 = 0.4$, $\rho_1 = -0.4$ or 0.4, $v_{2,0} = 0.18$, $a_2(t) = 1.2$, $b_2 = 5.33$, $\sigma_2 = 0.2$, $\rho_2 = -0.6$ or 0.6.

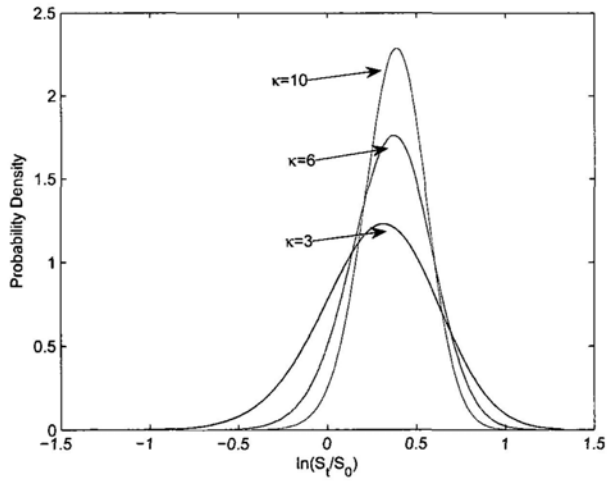

Figure 5.2: Probability density function for different values of κ. The parameter values are: $\theta(t) = \kappa \ln(1.5)$, $S_0 = 1.0$, $v_{1,0} = 0.5$, $a_1(t) = 0.5328$, $b_1 = 1.45$, $\sigma_1 = 0.4$, $\rho_1 = -0.4$, $v_{2,0} = 0.18$, $a_2(t) = 1.2$, $b_2 = 5.33$, $\sigma_2 = 0.2$, $\rho_2 = -0.6$.

5.2 Super-Calibration to Currency Futures

As pointed out by Heston (1993) and many others, the characteristic function is not only useful for examining distributional properties but also for deriving formulas for standard derivative products. An obvious application is to derive a closed-form solution for future prices. Under risk-neutral dynamics (5.1), the future price of underlying asset S_t with maturity T is given by

$$F_T(t) = \mathbb{E}_t[S_T] = f(x, v_1, v_2, t; -i), \tag{5.14}$$

where $f(x, v_1, v_2, t; \phi)$ is defined in (5.3). Lemma 5.1.1 immediately gives the following.

Corollary 5.2.1. The future price of an asset following the proposed mean reversion MSV model in (5.1) is given by

$$F_T(t) = \exp\left[A_1^F(\tau)v_1 + A_2^F(\tau)v_2 + B^F(\tau) + xe^{-\kappa\tau}\right], \tag{5.15}$$

where $\tau = T - t$, $A_1^F(\tau) = A_1(\tau; -i)$, $A_2^F(\tau) = A_2(\tau; -i)$, and $B^F(\tau) = B(\tau; -i)$ are defined in (5.4).

Let us imagine a situation in which the term structure of future prices is observed at time t. In practice, it is often useful to express the characteristic function in terms of the observed term structure of future prices. More precisely, we would like to calibrate the characteristic function to observed future prices. This is important to ensure that we can derive option pricing formulas that are consistent with the observed future prices. We now carry out the super-calibration by directly expressing the characteristic function in terms of observed market future prices in the following proposition.

Proposition 5.2.1. If the underlying asset follows the mean reversion MSV process in (5.1), then the characteristic function calibrated to the term structure of future prices is given by

$$f(x, v_1, v_2, t; \phi, F_T(t)) = F_T(t)^{i\phi} \exp[\Delta A_1(\tau; \phi)v_1 + \Delta A_2(\tau; \phi)v_2 + \Delta B(\tau; \phi)], \tag{5.16}$$

where

$$\Delta B(\tau; \phi) = \int_0^\tau a_1(T - s)\Delta A_1(s; \phi)\mathrm{d}s + \int_0^\tau a_2(T - s)\Delta A_2(s; \phi)\mathrm{d}s,$$

$$\Delta A_1(\tau;\phi) = A_1(\tau;\phi) - i\phi A_1^F(\tau), \Delta A_2(\tau;\phi) = A_2(\tau;\phi) - i\phi A_2^F(\tau),$$

with $\tau = T - t$, $A_1(\tau;\phi)$ and $A_2(\tau;\phi)$ defined in Lemma 5.1.1, $A_1^F(\tau)$ and $A_2^F(\tau)$ defined in Corollary 5.2.1.

Proof. Corollary 5.2.1 gives us

$$\begin{aligned} B^F(\tau) &= \ln F_T(t) - A_1^F(\tau)v_1 - A_2^F(\tau)v_2 + xe^{-\kappa\tau} = B(\tau;-i) \\ &= \int_0^\tau e^{-\kappa s}\theta(T-s)\mathrm{d}s + \int_0^\tau a_1(T-s)A_1^F(s)\mathrm{d}s + \int_0^\tau a_2(T-s)A_2^F(s)\mathrm{d}s. \end{aligned} \tag{5.17}$$

By Lemma 5.1.1,

$$\begin{aligned} B(\tau;\phi) &= i\phi\int_0^\tau e^{-\kappa s}\theta(T-s)\mathrm{d}s + \int_0^\tau a_1(T-s)A_1(s;\phi)\mathrm{d}s + \int_0^\tau a_2(T-s)A_2(s;\phi)\mathrm{d}s \\ &= i\phi B^F(\tau) + \int_0^\tau a_1(T-s)\Delta A_1(s;\phi)\mathrm{d}s + \int_0^\tau a_2(T-s)\Delta A_2(s;\phi)\mathrm{d}s, \end{aligned} \tag{5.18}$$

where

$$\Delta A_1(\tau;\phi) = A_1(\tau;\phi) - i\phi A_1^F(\tau), \Delta A_2(\tau;\phi) = A_2(\tau;\phi) - i\phi A_2^F(\tau).$$

Substituting (5.18) into (5.4) yields

$$f(x, v_1, v_2, t; \phi, F_T(t)) = F_T(t)^{i\phi}\exp[\Delta A_1(\tau;\phi)v_1 + \Delta A_2(\tau;\phi)v_2 + \Delta B(\tau;\phi)],$$

with

$$\Delta B(\tau;\phi) = \int_0^\tau a_1(T-s)\Delta A_1(s;\phi)\mathrm{d}s + \int_0^\tau a_2(T-s)\Delta A_2(s;\phi)\mathrm{d}s.$$

□

5.3 European Option Pricing

Using the characteristic function, European options can be valued through Fourier inversion. While Carr and Madan (1999) advocate the FFT to numerically implement the Fourier inversion, Chourdakis (2004) shows significant improvement using the FRFT, which is a linear transformation that generalized the Fourier transform. The FRFT algorithm has the advantage of using the characteristic function information in a more efficient way than the straight FFT by relaxing the restriction on grid sizes. Using several numerical examples, this section demonstrates how the FRFT can be applied to our case. The implied volatility surface generated by the proposed model is reported. We attempt to show numerically that this model not only fits the term structure of future prices, but is also able to produce a realistic volatility surface consistent with the market.

5.3.1 Vanilla Call Option

The plain vanilla call option has the following payoff:

$$\max(S_T - K, 0),$$

where K is the strike price and T is the option's maturity. Let k denote the log of the strike price K, $C_T(k)$ be the desired value of a T-maturity call option with strike $\exp(k)$, and $q_T(s)$ be the risk-neutral density of the log-asset price $s_T = \ln S_T$.

Following Carr and Madan (1999), the modified call price is defined by

$$c_T(k) = \exp(\alpha k) C_T(k), \quad \text{for some constant} \quad \alpha > 0,$$

where $C_T(k) = \int_k^\infty e^{-rT}(e^s - e^k) q_T(s) ds$. As $C_T(k)$ is not square integrable over $(-\infty, \infty)$, the introduction of a damping factor $\exp(\alpha k)$ aims to remove this problem. This makes the Fourier transform of $c_T(k)$ exist:

$$\psi_T(\xi) = \int_{-\infty}^{\infty} e^{i\xi k} c_T(k) dk = \frac{e^{-rT} f(x, v_1, v_2, t; \phi = \xi - (\alpha + 1)i)}{\alpha^2 + \alpha - \xi^2 + i(2\alpha + 1)\xi}, \tag{5.19}$$

where f is the characteristic function defined in Proposition 5.2.1.

The call option prices can then be numerically obtained using the inverse transform:

$$C_T(k) = \frac{e^{-\alpha k}}{2\pi} \int_{-\infty}^{\infty} e^{-i\xi k} \psi_T(\xi) d\xi = \frac{e^{-\alpha k}}{\pi} \int_0^{\infty} e^{-i\xi k} \psi_T(\xi) d\xi. \tag{5.20}$$

More precisely, the call price is determined by substituting (5.19) into (5.20) and performing the required integration.

5.3.2 Fractional FFT

Integration (5.20) is a direct Fourier transform and leads itself to an application of the FFT. The integration is first approximated using a numerical integration rule:

$$\frac{e^{-\alpha k}}{\pi} \int_0^{\infty} e^{-i\xi k} \psi_T(\xi) d\xi \approx \frac{e^{-\alpha k}}{\pi} \sum_{j=0}^{N_{FFT}-1} e^{-i\xi_j k} \psi_T(\xi_j) w_j \eta, \quad \xi_j = j\eta, \tag{5.21}$$

where N_{FFT} is the number of grid points and w_j is the weight of the j-th component in implementing the integration rule. For instance, $w_0 = w_{N_{FFT}-1} = 1/2$ and $w_j =$

$1, j = 1, \cdots, N_{FFT} - 2$, for the trapezoid rule, and $w_0 = w_{N_{FFT}-1} = 1/3$ and $w_j = (3 + (-1)^{j+1})/3, j = 1, \cdots, N_{FFT} - 2$, for Simpson's rule.

The standard FFT method simultaneously computes the values of the integral approximations (5.21) for the set of log strikes

$$\{k_u = -b + \lambda u, \quad u = 0, \cdots, N_{FFT} - 1\},$$

ranging from $-b$ to $b - \lambda$, where $b = \frac{\lambda N_{FFT}}{2}$. This FFT method suffers from a restriction that the grid spacing must satisfy the condition

$$\lambda\eta = \frac{2\pi}{N_{FFT}}. \tag{5.22}$$

The sum in (5.21) can then be expressed in the form

$$C_T(k_u) \approx \frac{e^{-\alpha k}}{\pi} \sum_{j=0}^{N_{FFT}-1} e^{-i\lambda\eta j u} e^{i\eta j b} \psi_T(\xi_j) w_j \eta = \frac{e^{-\alpha k}}{\pi} \sum_{j=0}^{N_{FFT}-1} e^{-i\frac{2\pi}{N_{FFT}} j u} h_j, \tag{5.23}$$

which allows the application of the FFT procedure invoked on the vector

$$\mathbf{h} = \{h_j = e^{i\pi j} \psi_T(\xi_j) w_j \eta, \quad j = 0, \cdots, N_{FFT} - 1\}.$$

As an inverse relationship exists between the grid sizes, η and λ, specified in (5.22), we must either increase η, thus rendering the grid across ξ_j coarser, or increase N_{FFT} with a larger length of input vector $\mathbf{h}$, thus leading to the substantial waste of computational time, to obtain a fine grid across the log strikes. In addition, the resulting series will extend beyond the range of required log strikes. For example in the case of the 4,096-point FFT employed in Carr and Madan (1999), only 66 of them correspond to the option prices of interest in the sense that the stike-to-spot ratio falls in between 0.80 and 1.20.

To facilitate the calibration to the implied volatilities quoted against the strike prices, the FRFT suggested by Chourdakis (2005) is considered to replace the standard FFT in this chapter. It rapidly computes the sum in the form

$$D_k(\mathbf{h}, \beta) = \sum_{j=0}^{N-1} e^{-i2\pi k j \beta} h_j, \tag{5.24}$$

for any value of β. When $\beta = \frac{1}{N}$, it is reduced to the FFT. Specifically, (5.21) gives us

$$C_T(k_u) \approx \frac{e^{-\alpha k}}{\pi} \sum_{j=0}^{N-1} e^{-ij\eta\lambda u} e^{i\eta j b} \psi_T(\xi_j) w_j \eta = \frac{e^{-\alpha k}}{\pi} \sum_{j=0}^{N-1} e^{-i2\pi j\beta u} \psi_T(\xi_j) w_j \eta e^{i\pi j}, \qquad (5.25)$$

where $2\pi\beta = \eta\lambda$. The sum in (5.25) can then be computed using the FRFT without imposing the restriction as in (5.22). In other words, the two grid spacings (those among the characteristic function support and the log-strikes) can be chosen independently within the FRFT parameter: $2\pi\beta = \eta\lambda$.

The sums in the FRFT are computed by invoking two normal and one inverse FFT procedures. To compute an N-point FRFT on the vector $\mathbf{h} = (h_j)_{j=0}^{N-1}$, the following $2N$-point vectors have to be defined

$$\mathbf{y} = ((h_j e^{-i\pi j^2\beta})_{j=0}^{N-1}, (0)_{j=0}^{N-1}),$$

$$\mathbf{z} = ((e^{-i\pi j^2\beta})_{j=0}^{N-1}, (e^{-i\pi(N-j)^2\beta})_{j=0}^{N-1}).$$

Then the FRFT is given by

$$D_k(\mathbf{h}, \beta) = (e^{-i\pi k^2\beta})_{k=0}^{N-1} \odot D_k^{-1}(D_j(\mathbf{y}) \odot D_j(\mathbf{z})), \qquad (5.26)$$

where $\odot$ denotes element-by-element vector multiplication, $D_k(\mathbf{h})$ denotes the FFT sum

$$D_k(\mathbf{h}) = \sum_{j=0}^{N-1} e^{-i\frac{2\pi}{N}kj} h_j,$$

and $D_k^{-1}(\mathbf{h})$ is the inverse FFT sum

$$D_k^{-1}(\mathbf{H}) = \frac{1}{N} \sum_{j=0}^{N-1} e^{i\frac{2\pi}{N}kj} H_j.$$

Note that the exponential quantities $(e^{-i\pi j^2\beta})_{k=0}^{N-1}$ do not depend on the actual function that is integrated and therefore can be precomputed and stored.

The major advantage of the FRFT is that both the grid sizes of η and λ are chosen independently. Although three FFTs are required instead of just one, the freedom to choose the grid sizes prevails and, in turns, considerably speeds up computation because the input vectors are typically much shorter. This approach has been proven to be useful

Table 5.1: Call option prices: FRFT vs. Monte Carlo (MC)

	T=0.5				T=1			
Strike Price	32-FRFT	64-FRFT	128-FRFT	MC	32-FRFT	64-FRFT	128-FRFT	MC
0.85	0.6035	0.6034	0.6034	0.6037	0.5933	0.5931	0.5931	0.5936
(%difference)	(-0.03%)	(-0.05%)	(-0.05%)		(-0.05%)	(-0.08%)	(-0.08%)	
0.9	0.5547	0.5548	0.5548	0.5552	0.5455	0.5457	0.5457	0.5462
(%difference)	(-0.09%)	(-0.07%)	(-0.07%)		(-0.13%)	(-0.09%)	(-0.09%)	
0.95	0.5062	0.5065	0.5065	0.5068	0.4982	0.4985	0.4985	0.499
(%difference)	(-0.12%)	(-0.06%)	(-0.06%)		(-0.16%)	(-0.10%)	(-0.10%)	
1	0.4584	0.4585	0.4585	0.4589	0.4514	0.4516	0.4516	0.4522
(%difference)	(-0.11%)	(-0.09%)	(-0.09%)		(-0.18%)	(-0.13%)	(-0.13%)	
1.05	0.4113	0.4113	0.4113	0.4116	0.4054	0.4053	0.4053	0.4059
(%difference)	(-0.07%)	(-0.07%)	(-0.07%)		(-0.12%)	(-0.15%)	(-0.15%)	
1.1	0.3652	0.3651	0.3651	0.3654	0.3602	0.36	0.36	0.3607
(%difference)	(-0.05%)	(-0.08%)	(-0.08%)		(-0.14%)	(-0.19%)	(-0.19%)	
1.15	0.3206	0.3204	0.3204	0.3208	0.3163	0.3161	0.3161	0.3167
(%difference)	(-0.06%)	(-0.12%)	(-0.12%)		(-0.13%)	(-0.19%)	(-0.19%)	
CPU Time	2.6915s	5.7033s	14.2695s	66.6635s	4.09s	8.4532s	19.5388s	70.7336s

when a large number of characteristic function evaluations are needed for calibration purpose. Chourdakis (2005) has already demonstrated that, to produce 64 option prices for the strike-to-spot ratio ranging from 0.80 to 1.20, only three 128-point FFTs are required, and the execution time is shorter by a factor of about 25 compared with the straight FFT used by Carr and Madan (1999).

5.3.3 Numerical Examples

It would also be interesting to determine the performance of the FRFT applied to vanilla options under the proposed mean reversion MSV model. Our numerical example uses $\eta = 0.5$, $b = 0.2$, and different N, i.e., $N = 32, 64, 128$ corresponding to the log strike price spacing of $\Delta k = \lambda = 1/40, 1/80, 1/160$, respectively. The damping coefficient is set at $\alpha = 3$. The other parameter values are $\kappa = 10$, $\theta(t) = 4.0339$, $S_0 = 1.3$, $v_{1,0} = 0.5$, $a_1(t) = 0.5328$, $b_1 = 1.45$, $\sigma_1 = 0.4$, $\rho_1 = -0.04$, $v_{2,0} = 0.18$, $a_2(t) = 1.2$, $b_2 = 5.33$, $\sigma_2 = 0.2$, and $\rho_2 = -0.06$. We compute the half-year and one-year maturity call options using the FRFT and contrast the results with the Monte Carlo simulation of $40,000$ sample paths and time-step of $1/500$. The numerical results are displayed in Table 5.1.

The 32-FRFT takes less than 5 seconds to produce 32 option prices corresponding to different strike prices with $\Delta k = 0.025$. If the Monte Carlo price is regarded as

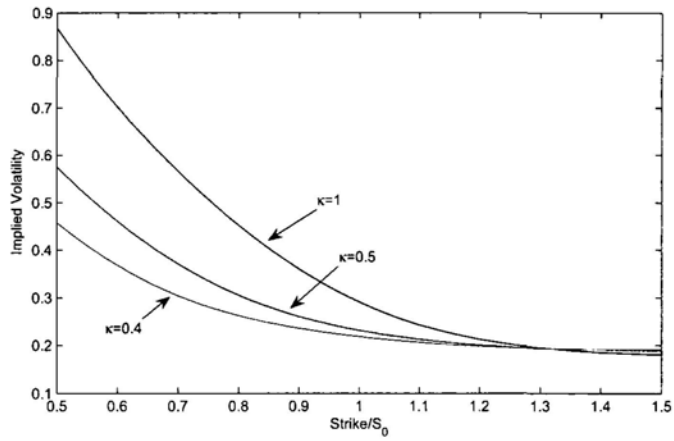

Figure 5.3: Implied volatility for different values of κ. The parameters are $\theta(t) = \kappa \ln(1.2)$, $S_0 = 1.0$, $v_{1,0} = 0.15^2$, $a_1(t) = 0.3328^2$, $b_1 = 1.45$, $\sigma_1 = 0.4$, $\rho_1 = -0.4$, $v_{2,0} = 0.08^2$, $a_2(t) = 0.2^2$, $b_2 = 2.33$, $\sigma_2 = 0.2$, and $\rho_2 = -0.6$.

the benchmark, then the absolute percentage difference in the prices obtained using 32-FRFT is less than 0.2% for all cases. The 64-FRFT and 128-FRFT generate even more option prices with slightly better level of accuracy at the cost of a longer computational time. The Monte Carlo simulation takes more than 60 seconds for each option price. This numerical example verifies that our analytical solution is correct and the FRFT is accurate and efficient. Although constant $\theta(t)$ is considered here, the proposed FRFT method can generally be applied to the case of the characteristic function calibrated to the term structure of futures, as demonstrated in the following subsection.

5.3.4 Implied Volatility

The accurate FRFT option pricing framework enables us to further investigate the volatility smile implied by the proposed model. Figure 5.3 shows that the left-tail skewness of the volatility smile increases with κ, the mean reversion speed for the asset. Consider the case of an exchange rate. If the mean reversion rate κ represents the force of central bank intervention, then the proposed model implies that the greater the left-tail skewness, the greater the market expectation that the central bank will intervene.

The proposed mean reversion MSV model enables the exact fit of the option prices to the term structure of currency futures. Consider the term structure of future contracts

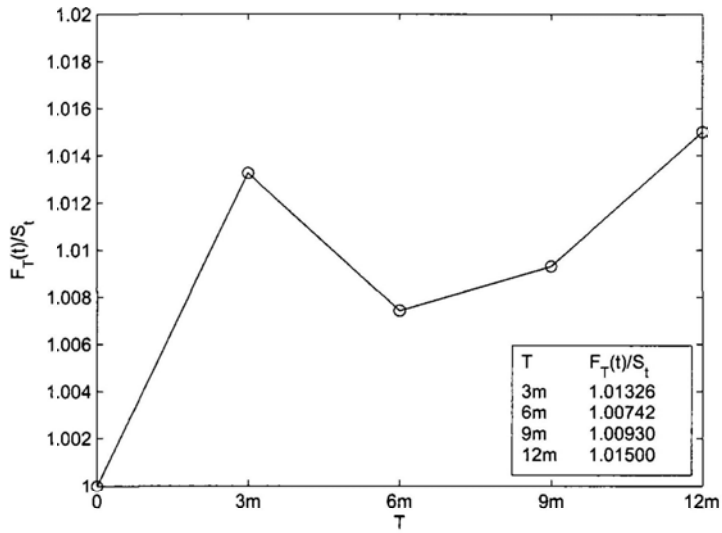

Figure 5.4: Observed future prices

shown in Figure 5.4 in which a linear interpolation is employed. We produce the implied volatility surface of European options in Figure 5.5. The graph is generated based on parameters: $\kappa = 0.3$, $S_0 = 1.0$, $v_{1,0} = 0.15^2$, $a_1(t) = 0.3328^2$, $b_1 = 1.45$, $\sigma_1 = 0.5$, $\rho_1 = 0.1$, $v_{2,0} = 0.08^2$, $a_2(t) = 0.2^2$, $b_2 = 2.33$, $\sigma_2 = 0.2$, $\rho_2 = 0.1$. It can be seen that the implied volatility surface that integrates the information from future contracts resembles the volatility surface used by currency option traders. The volatility is relatively low for at-the-money options. It becomes progressively higher as an option moves either in the money or out of the money. Two-scale stochastic volatility provides the model with greater flexibility to produce a rich set of volatility surfaces.

5.4 Conclusion

This chapter proposes a new option pricing model for currency options that allows mean reversion and multi-scale stochastic volatility to be captured within a unified framework. The model also allows the super-calibration of the observed term structure of currency futures. Analytical solutions are derived for the characteristic function and European options. The fractional FFT is adopted for implementation to ensure that the restriction

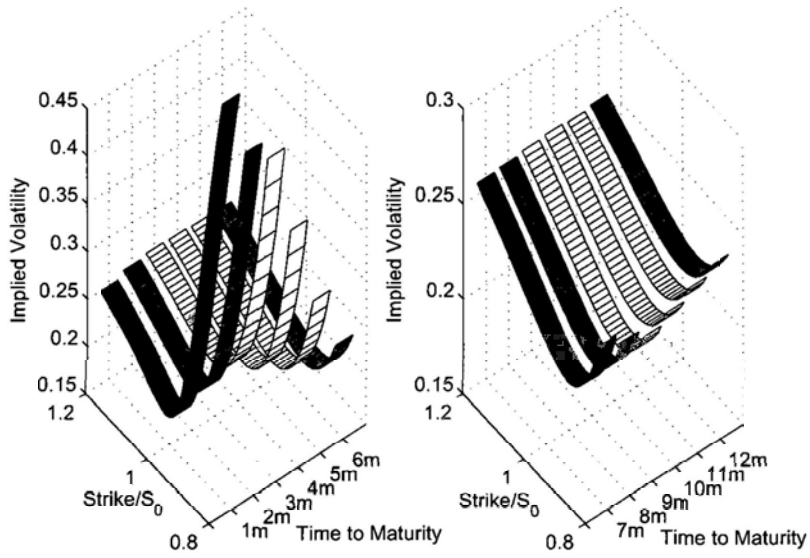

Figure 5.5: Implied volatility surface consistent with the future prices in Figure 5.4

on grid spacing in the standard FFT is relaxed and the information contained in the characteristic function is effectively used for calibration to the entire implied volatility surface. Although the model is applied to European options in this chapter, we recognize that it could also be applied to discrete barrier option pricing by slightly modifying the framework of Griebsch andWystup (2008) for the Heston model. Thus, the proposed model has rich potential application in practice.

Chapter 6

Conclusion

This thesis investigates the applications of general diffusion processes in the field of American option pricing, optimal dividend barrier policies, and currency option pricing to cope with empirical evidence. Different techniques are adopted to facilitate the corresponding analysis.

Firstly, with the aid of Laplace-Carson transform (LCT), we separate the determination of the optimal early exercise boundary from the valuation procedure of American options under the CEV model. Although, the analysis focuses on vanilla options, the method is generally applicable to other exotic derivatives with continuous earlier exercise rights and facilitates the analysis of optimal stopping strategy.

Secondly, the impact of bankruptcy procedures on optimal dividend barrier policies is investigated by assuming that liquidation is triggered by an excursion time or an occupation time and the surplus of a firm follows an Ornstein-Uhlenbeck (OU) process with a negative surplus-dependent mean-reverting rate. By using Laplace transform, we obtain the optimal dividend barrier, and further characterize the distributional property and the expectation of bankruptcy time subject to the bankruptcy procedure.

Thirdly, general diffusion processes are extended to a multi-dimensional setup to simultaneously capture the empirical evidences of mean reversion and multi-scale stochastic volatility for currencies. A closed-form solution is derived for the characteristic function of the log-asset price, which links up with vanilla option prices through Fourier transform. The proposed model enables us to calibrate simultaneously to the observed currency fu-

tures and the implied volatility surface of the currency within a unified framework. The fractional fast fourier transform (FRFT) is adopted for implementation to ensure that the restriction on grid spacing in the standard FFT is relaxed and the information contained in the characteristic function is effectively used for calibration procedure. The proposed model is thus flexible enough for a financial analyst to perform scenario analysis with it and also allows seasonal volatility within derivative pricing.

Laplace-Carson transform, Laplace transform, and Fourier transform are all widely used integral transforms. Although the problems considered are difficult to solve in their original representations, integral transforms provide possible mapping into a frequency domain and simplify the corresponding quantitative and qualitative analysis. However, the application of integral transforms is not without restriction as it highly depends on the parametric form of the model. Homotopy analysis method is an alternative powerful technique based on a continuous variation from an initial trail to the desired solution. Taking American option pricing under general diffusions as an example, we demonstrate the effectiveness, and the flexibility of homotopy analysis. A theoretical drawback is that a formal proof of convergence of the homotopic expansion still remains an open problem. Future research may consider the corresponding convergence analysis and how the ingredients of the generalized homotopy can be chosen so as to reach an optimal homotopic approximation by a small number of terms.

Appendix

A Fundamental Solutions in (2.13) and Their Properties

Use the notation of Davydov and Linetsky (2001):

$$\mu = r - q, \quad x = \frac{|\mu|}{\delta^2|\beta|} S^{-2\beta}, \quad z = \frac{1}{\delta|\beta|} S^{-\beta}, \quad \epsilon = \text{sign}(\mu\beta),$$

$$m = \frac{1}{4|\beta|}, \quad k = \epsilon\left(\frac{1}{2} + \frac{1}{4\beta}\right) - \frac{\lambda + r}{2|\mu\beta|}, \quad \nu = \frac{1}{2|\beta|}.$$

The fundamental increasing ($\psi_{\lambda+r}$) and decreasing ($\phi_{\lambda+r}$) solutions in (2.13) are

$$\begin{cases} \psi_{\lambda+r}(S) = S^{\beta+1/2} e^{\epsilon x/2} M_{k,m}(x), & \phi_{\lambda+r}(S) = S^{\beta+1/2} e^{\epsilon x/2} W_{k,m}(x), & \beta < 0, \mu \neq 0, \\ \psi_{\lambda+r}(S) = S^{\beta+1/2} e^{\epsilon x/2} W_{k,m}(x), & \phi_{\lambda+r}(S) = S^{\beta+1/2} e^{\epsilon x/2} M_{k,m}(x), & \beta > 0, \mu \neq 0, \\ \psi_{\lambda+r}(S) = S^{1/2} I_\nu(\sqrt{2(\lambda+r)}z), & \phi_{\lambda+r}(S) = S^{1/2} K_\nu(\sqrt{2(\lambda+r)}z), & \beta < 0, \mu = 0, \\ \psi_{\lambda+r}(S) = S^{1/2} K_\nu(\sqrt{2(\lambda+r)}z), & \phi_{\lambda+r}(S) = S^{1/2} I_\nu(\sqrt{2(\lambda+r)}z), & \beta > 0, \mu = 0, \end{cases}$$

where $M_{k,m}(x)$ and $W_{k,m}(x)$ are the Whittaker functions, and $I_\nu(x)$ and $K_\nu(x)$ are the modified Bessel functions. The corresponding Wronskian and its derivatives are given by

$$\Lambda(S) = \omega_{\lambda+r}\xi(S), \quad \frac{\mathrm{d}\Lambda(S)}{\mathrm{d}S} = \omega_{\lambda+r}\frac{\mathrm{d}\xi(S)}{\mathrm{d}S},$$

where

$$\xi(S) = \exp\left(\frac{\mu}{\delta^2\beta} S^{-2\beta}\right), \quad \frac{\mathrm{d}\xi(S)}{\mathrm{d}S} = -\frac{2\mu S^{-2\beta-1}\xi(S)}{\delta^2}, \quad \omega_{\lambda+r} = \begin{cases} \frac{2|\mu|\Gamma(2m+1)}{\delta^2\Gamma(m-k+1/2)}, & \mu \neq 0, \\ |\beta|, & \mu = 0. \end{cases}$$

The derivatives of the fundamental solutions are presented below:

1. When $\beta < 0$ and $\mu \neq 0$,

$$\begin{aligned} \frac{\mathrm{d}\psi_{\lambda+r}(S)}{\mathrm{d}S} &= \left(\frac{1+2\beta+4\beta k-2\beta(1+\epsilon)x}{2S} - \frac{\beta(1+2k+2m)M_{1+k,m}(x)}{SM_{k,m}(x)}\right)\psi_{\lambda+r}(S), \\ \frac{\mathrm{d}\phi_{\lambda+r}(S)}{\mathrm{d}S} &= \left(\frac{1+2\beta+4\beta k-2\beta(1+\epsilon)x}{2S} + \frac{2\beta W_{1+k,m}(x)}{SW_{k,m}(x)}\right)\phi_{\lambda+r}(S), \\ \frac{\mathrm{d}^2\psi_{\lambda+r}(S)}{\mathrm{d}S^2} &= \left[\frac{4(\beta+2\beta k)^2-1}{4S^2} - \frac{4\beta^2 k(1+\epsilon)x}{S^2} + \frac{\beta^2(1+\epsilon)^2x^2}{S^2} + \left(-\frac{4\beta^2(1+k)(1+2k+2m)}{S^2}\right.\right. \\ &\quad \left.\left. + \frac{2\beta^2(1+2k+2m)(1+\epsilon)x}{S^2}\right)\frac{M_{1+k,m}(x)}{M_{k,m}(x)} + \frac{\beta^2(1+2k+2m)(3+2k+2m)M_{2+k,m}(x)}{S^2M_{k,m}(x)}\right]\psi_{\lambda+r}(S), \\ \frac{\mathrm{d}^2\phi_{\lambda+r}(S)}{\mathrm{d}S^2} &= \left[\frac{4(\beta+2\beta k)^2-1}{4S^2} - \frac{4\beta^2 k(1+\epsilon)x}{S^2} + \frac{\beta^2(1+\epsilon)^2x^2}{S^2} + \left(\frac{8\beta^2(1+k)}{S^2} - \frac{4\beta^2(1+\epsilon)x}{S^2}\right)\frac{W_{1+k,m}(x)}{W_{k,m}(x)}\right. \\ &\quad \left. + \frac{4\beta^2 W_{2+k,m}(x)}{S^2W_{k,m}(x)}\right]\phi_{\lambda+r}(S). \end{aligned}$$

2. When $\beta > 0$ and $\mu \neq 0$,

$$\begin{aligned}
\frac{\mathrm{d}\psi_{\lambda+r}(S)}{\mathrm{d}S} &= \left(\frac{1+2\beta+4\beta k-2\beta(1+\epsilon)x}{2S} + \frac{2\beta W_{1+k,m}(x)}{SW_{k,m}(x)}\right)\psi_{\lambda+r}(S), \\
\frac{\mathrm{d}\phi_{\lambda+r}(S)}{\mathrm{d}S} &= \left(\frac{1+2\beta+4\beta k-2\beta(1+\epsilon)x}{2S} - \frac{\beta(1+2k+2m)M_{1+k,m}(x)}{SM_{k,m}(x)}\right)\phi_{\lambda+r}(S), \\
\frac{\mathrm{d}^2\psi_{\lambda+r}(S)}{\mathrm{d}S^2} &= \left[\frac{4(\beta+2\beta k)^2-1}{4S^2} - \frac{4\beta^2 k(1+\epsilon)x}{S^2} + \frac{\beta^2(1+\epsilon)^2x^2}{S^2} + \left(\frac{8\beta^2(1+k)}{S^2} - \frac{4\beta^2(1+\epsilon)x}{S^2}\right)\frac{W_{1+k,m}(x)}{W_{k,m}(x)}\right. \\
&\quad \left. + \frac{4\beta^2 W_{2+k,m}(x)}{S^2 W_{k,m}(x)}\right]\psi_{\lambda+r}(S), \\
\frac{\mathrm{d}^2\phi_{\lambda+r}(S)}{\mathrm{d}S^2} &= \left[\frac{4(\beta+2\beta k)^2-1}{4S^2} - \frac{4\beta^2 k(1+\epsilon)x}{S^2} + \frac{\beta^2(1+\epsilon)^2x^2}{S^2} + \left(-\frac{4\beta^2(1+k)(1+2k+2m)}{S^2}\right.\right. \\
&\quad \left.\left. + \frac{2\beta^2(1+2k+2m)(1+\epsilon)x}{S^2}\right)\frac{M_{1+k,m}(x)}{M_{k,m}(x)} + \frac{\beta^2(1+2k+2m)(3+2k+2m)M_{2+k,m}(x)}{S^2 M_{k,m}(x)}\right]\phi_{\lambda+r}(S).
\end{aligned}$$

3. When $\beta < 0$ and $\mu = 0$,

$$\begin{aligned}
\frac{\mathrm{d}\psi_{\lambda+r}(S)}{\mathrm{d}S} &= \left(\frac{1}{2S} - \frac{\beta\sqrt{\lambda+r}z(I_{\nu-1}(\sqrt{2(\lambda+r)}z)+I_{\nu+1}(\sqrt{2(\lambda+r)}z))}{\sqrt{2}SI_\nu(\sqrt{2(\lambda+r)}z)}\right)\psi_{\lambda+r}(S), \\
\frac{\mathrm{d}\phi_{\lambda+r}(S)}{\mathrm{d}S} &= \left(\frac{1}{2S} + \frac{\beta\sqrt{\lambda+r}z(K_{\nu-1}(\sqrt{2(\lambda+r)}z)+K_{\nu+1}(\sqrt{2(\lambda+r)}z))}{\sqrt{2}SK_\nu(\sqrt{2(\lambda+r)}z)}\right)\phi_{\lambda+r}(S), \\
\frac{\mathrm{d}^2\psi_{\lambda+r}(S)}{\mathrm{d}S^2} &= \left[-\frac{1}{4S^2} + \frac{\beta^2\sqrt{\lambda+r}z(I_{\nu-1}(\sqrt{2(\lambda+r)}z)+I_{\nu+1}(\sqrt{2(\lambda+r)}z))}{\sqrt{2}S^2I_\nu(\sqrt{2(\lambda+r)}z)}\right. \\
&\quad \left. + \frac{\beta^2(\lambda+r)z^2(I_{\nu-2}(\sqrt{2(\lambda+r)}z)+I_\nu(\sqrt{2(\lambda+r)}z)+I_{\nu+2}(\sqrt{2(\lambda+r)}z))}{2S^2I_\nu(\sqrt{2(\lambda+r)}z)}\right]\psi_{\lambda+r}(S), \\
\frac{\mathrm{d}^2\phi_{\lambda+r}(S)}{\mathrm{d}S^2} &= \left[-\frac{1}{4S^2} - \frac{\beta^2\sqrt{\lambda+r}z(K_{\nu-1}(\sqrt{2(\lambda+r)}z)+K_{\nu+1}(\sqrt{2(\lambda+r)}z))}{\sqrt{2}S^2K_\nu(\sqrt{2(\lambda+r)}z)}\right. \\
&\quad \left. + \frac{\beta^2(\lambda+r)z^2(K_{\nu-2}(\sqrt{2(\lambda+r)}z)+K_\nu(\sqrt{2(\lambda+r)}z)+K_{\nu+2}(\sqrt{2(\lambda+r)}z))}{2S^2K_\nu(\sqrt{2(\lambda+r)}z)}\right]\phi_{\lambda+r}(S).
\end{aligned}$$

4. When $\beta > 0$ and $\mu = 0$,

$$\begin{aligned}
\frac{\mathrm{d}\psi_{\lambda+r}(S)}{\mathrm{d}S} &= \left(\frac{1}{2S} + \frac{\beta\sqrt{\lambda+r}z(K_{\nu-1}(\sqrt{2(\lambda+r)}z)+K_{\nu+1}(\sqrt{2(\lambda+r)}z))}{\sqrt{2}SK_\nu(\sqrt{2(\lambda+r)}z)}\right)\psi_{\lambda+r}(S), \\
\frac{\mathrm{d}\phi_{\lambda+r}(S)}{\mathrm{d}S} &= \left(\frac{1}{2S} - \frac{\beta\sqrt{\lambda+r}z(I_{\nu-1}(\sqrt{2(\lambda+r)}z)+I_{\nu+1}(\sqrt{2(\lambda+r)}z))}{\sqrt{2}SI_\nu(\sqrt{2(\lambda+r)}z)}\right)\phi_{\lambda+r}(S), \\
\frac{\mathrm{d}^2\psi_{\lambda+r}(S)}{\mathrm{d}S^2} &= \left[-\frac{1}{4S^2} - \frac{\beta^2\sqrt{\lambda+r}z(K_{\nu-1}(\sqrt{2(\lambda+r)}z)+K_{\nu+1}(\sqrt{2(\lambda+r)}z))}{\sqrt{2}S^2K_\nu(\sqrt{2(\lambda+r)}z)}\right. \\
&\quad \left. + \frac{\beta^2(\lambda+r)z^2(K_{\nu-2}(\sqrt{2(\lambda+r)}z)+K_\nu(\sqrt{2(\lambda+r)}z)+K_{\nu+2}(\sqrt{2(\lambda+r)}z))}{2S^2K_\nu(\sqrt{2(\lambda+r)}z)}\right]\psi_{\lambda+r}(S), \\
\frac{\mathrm{d}^2\phi_{\lambda+r}(S)}{\mathrm{d}S^2} &= \left[-\frac{1}{4S^2} + \frac{\beta^2\sqrt{\lambda+r}z(I_{\nu-1}(\sqrt{2(\lambda+r)}z)+I_{\nu+1}(\sqrt{2(\lambda+r)}z))}{\sqrt{2}S^2I_\nu(\sqrt{2(\lambda+r)}z)}\right. \\
&\quad \left. + \frac{\beta^2(\lambda+r)z^2(I_{\nu-2}(\sqrt{2(\lambda+r)}z)+I_\nu(\sqrt{2(\lambda+r)}z)+I_{\nu+2}(\sqrt{2(\lambda+r)}z))}{2S^2I_\nu(\sqrt{2(\lambda+r)}z)}\right]\phi_{\lambda+r}(S).
\end{aligned}$$

B Asymptotic Behavior of $S_f(\tau)$ Close to Expiry

When $\tau \to 0^+$ and $S < K$, by the continuity of the put option,

$$P(S, 0^+) = K - S. \tag{1}$$

If the American put is alive, it satisfies the governing equation (3.3). By substituting (1) into (3.3), given that (S,τ) lies in the continuation region, we have

$$\begin{aligned}\left.\frac{\partial P_A}{\partial \tau}\right|_{\tau=0^+} &= \frac{1}{2}\sigma^2(S,T^-)S^2\left.\frac{\partial^2 P_A}{\partial S^2}\right|_{\tau=0^+} + (r - D(S,T^-))S\left.\frac{\partial P_A}{\partial S}\right|_{\tau=0^+} - rP_A|_{\tau=0^+} \\ &= -(r - D(S,T^-))S - r(K-S) \\ &= -rK + D(S,T^-)S.\end{aligned}$$

As in the continuation region, the American put $P(S,\tau)$ is always above the intrinsic value $P(S,\tau) = K - S$, to keep it alive until the time close to expiry, we have

$$\left.\frac{\partial P_A}{\partial \tau}\right|_{\tau=0^+} \geq 0. \tag{2}$$

The value of S at which $\frac{\partial P_A}{\partial \tau}\big|_{\tau=0^+}$ changes sign satisfies $S = \frac{r}{D(S,T^-)}K$. As $\frac{r}{D(S,T^-)}K$ lies in the interval $S < K$ only when $r < D(S,T^-)$, if $r \geq D(S,T^-)$, the changing sign point will become $S = K$.

The optimal exercise price $S_f(0^+)$ is given by the underlying asset value at which $\frac{\partial P_A}{\partial \tau}\big|_{\tau=0^+}$ changes sign. We then obtain $S_f(0^+)$ by solving the following equation:

$$S_f(0^+) = \min\left(\frac{r}{D(S_f(0^+),T^-)}K, K\right). \tag{3}$$

C The Determination of the Homotopy-Padé Approximation

As follows from (3.71), the polynomials on the embedding parameter p, $W^U_{k,n}(S,\tau;p)$ and $W^D_{k,n}(S,\tau;p)$, satisfy

$$W^D_{k,n}(S,\tau;p) \times \Omega_{k+n}(S,\tau;p) - W^U_{k,n}(S,\tau;p) = \mathbf{O}(p^{k+n+1}), \quad \text{as} \quad p \to 0. \tag{4}$$

Substituting $W^U_{k,n}(S,\tau;p) = \sum_{j=0}^{k} W^U_j(S,\tau)p^j$ and $W^D_{k,n}(S,\tau;p) = 1 + \sum_{j=1}^{n} W^D_j(S,\tau)p^j$ in (4) yields the linear system

$$a_i(S,\tau) + \sum_{j=1}^{\min(i,n)} a_{i-j}(S,\tau) \times W^D_j(S,\tau) = W^U_i(S,\tau), \quad i = 0,1,\cdots,k, \tag{5}$$

$$a_i(S,\tau) + \sum_{j=1}^{\min(i,n)} a_{i-j}(S,\tau) \times W_j^D(S,\tau) = 0, \quad i = k+1, \cdots, k+n. \tag{6}$$

Obviously, $W_j^D(S,\tau)$ can be obtained by solving the equations in (6). With these available, the determination of $W_j^U(S,\tau)$ from (5) is straightforward. Using Cramer's rule to express $W_j^D(S,\tau)$, it is easy to show that $\Omega_{k,n}(S,\tau;p)$ has the determinant representation

$$\Omega_{k,n}(S,\tau;p) = \frac{W_{k,n}^U(S,\tau;p)}{W_{k,n}^D(S,\tau;p)} = \frac{\begin{vmatrix} \Omega_{k-n}(*)p^n & \Omega_{k-n+1}(*)p^{n-1} & \cdots & \Omega_k(*)p^0 \\ a_{k-n+1}(S,\tau) & a_{k-n+2}(S,\tau) & \cdots & a_{k+1}(S,\tau) \\ a_{k-n+2}(S,\tau) & a_{k-n+3}(S,\tau) & \cdots & a_{k+2}(S,\tau) \\ \vdots & \vdots & \ddots & \vdots \\ a_k(S,\tau) & a_{k+1}(S,\tau) & \cdots & a_{k+n}(S,\tau) \end{vmatrix}}{\begin{vmatrix} p^n & p^{n-1} & \cdots & p^0 \\ a_{k-n+1}(S,\tau) & a_{k-n+2}(S,\tau) & \cdots & a_{k+1}(S,\tau) \\ a_{k-n+2}(S,\tau) & a_{k-n+3}(S,\tau) & \cdots & a_{k+2}(S,\tau) \\ \vdots & \vdots & \ddots & \vdots \\ a_k(S,\tau) & a_{k+1}(S,\tau) & \cdots & a_{k+n}(S,\tau) \end{vmatrix}}, \tag{7}$$

where $\Omega_m(*) = \sum_{i=0}^m a_i(S,\tau)p^i$, for $m = 0, 1, \cdots$, and $a_i(S,\tau) = 0$ for $i < 0$.

From $W_{k,n}^D(S,\tau;p) = 1 + \sum_{j=1}^n W_j^D(S,\tau)p^j$ and (7), we recognize that

$$\Omega_{k,n}(S,\tau;p) = \frac{\Omega_k(*) + \sum_{j=1}^n W_j^D(S,\tau)p^j \times \Omega_{k-j}(*)}{1 + \sum_{j=1}^n W_j^D(S,\tau)p^j}, \tag{8}$$

that is, once $W_j^D(S,\tau)$ are determined, $\Omega_{k,n}(S,\tau;p)$ can be received completely without actually solving $W_j^U(S,\tau)$. Setting $p = 1$ provides the [k,n] homotopy-Padé approximation

$$\tilde{P}_{k,n}(S,\tau) = \Omega_{k,n}(S,\tau;1) = \frac{\tilde{P}_k(S,\tau) + \sum_{j=1}^n W_j^D(S,\tau) \times \tilde{P}_{k-j}(S,\tau)}{1 + \sum_{j=1}^n W_j^D(S,\tau)}, \tag{9}$$

where $\tilde{P}_m(S,\tau) = 0$ for $m < 0$.

D Derivation of $\widetilde{V}(x, \widetilde{t}_L(0); b, T_L)$ in Proposition 4.2.3

In the case of occupation time framework, to separate the influence of the barrier level from the dividend value function, we present the solution in R1 and R2 in factorization

form as follows:

(R1): For $x \in (-\infty, 0)$ and $\widetilde{t}_L(0) \in [0, T_L]$,

$$\widetilde{V}(x, \widetilde{t}_L(0); b, T_L) = \frac{h(x, \widetilde{t}_L(0))}{h_0'(b, \widetilde{t}_L(0))}. \tag{10}$$

(R2): For $x \in (0, b]$ and $\widetilde{t}_L(0) \in [0, T_L]$,

$$V(x, 0; b, T_L) = \frac{h_0(x, \widetilde{t}_L(0))}{h_0'(b, \widetilde{t}_L(0))}. \tag{11}$$

Here $h(x, \widetilde{t}_L(0))$ and $h_0(x, \widetilde{t}_L(0))$ are independent of the barrier level b. The reflecting boundary condition at $x = b$ is satisfied automatically. We then obtain the corresponding system for $h(x, \widetilde{t}_L(0))$ in R1 and $h_0(x, \widetilde{t}_L(0))$ in R2, respectively.

1. Region One (R1): For $x \in (-\infty, 0)$ and $\widetilde{t}_L(0) \in [0, T_L]$,

$$\begin{cases} \frac{1}{2}\sigma^2 \frac{\partial^2 h}{\partial x^2} + (\mu + \rho(x)x)\frac{\partial h}{\partial x} + \frac{\partial h}{\partial \widetilde{t}_L} - \delta h = 0, \\ h(x, \widetilde{t}_L(0) = T_L) = 0, \\ h(-\infty, \widetilde{t}_L(0)) = 0, \\ h(0-, \widetilde{t}_L(0)) = h_0(0+, \widetilde{t}_L(0)), \\ \frac{\partial h(x, \widetilde{t}_L(0))}{\partial x}\Big|_{x=0-} = \frac{\partial h_0(x, \widetilde{t}_L(0))}{\partial x}\Big|_{x=0+}. \end{cases} \tag{12}$$

2. Region Two (R2): For $x \in (0, b]$ and $\widetilde{t}_L(0) \in [0, T_L]$,

$$\begin{cases} \frac{1}{2}\sigma^2 \frac{\partial^2 h_0}{\partial^2 x^2} + (\mu + \alpha_0 x)\frac{\partial h_0}{\partial x} - \delta h_0 = 0, \\ h_0(x, \widetilde{t}_L(0) = T_L) = 0, \\ h_0(0+, \widetilde{t}_L(0)) = h(0-, \widetilde{t}_L(0)), \\ \frac{\partial h_0(x, \widetilde{t}_L(0))}{\partial x}\Big|_{x=0+} = \frac{\partial h(x, \widetilde{t}_L(0))}{\partial x}\Big|_{x=0-}. \end{cases} \tag{13}$$

To solve the PDEs defined in the region R1 and R2, we reverse the occupation time by setting $\widetilde{t}_L^* = T_L - \widetilde{t}_L$ and consider the Laplace transform,

$$\hat{h}_i(x) = \int_0^\infty h(x, \widetilde{t}_L^*) e^{-s\widetilde{t}_L^*} \mathrm{d}\widetilde{t}_L^* := \mathcal{L}_s(h(x, \widetilde{t}_L^*)), \quad \text{where} \quad x \in A_i, \tag{14}$$

$$\hat{h}_0(x) = \int_0^\infty h_0(x, \widetilde{t}_L^*) e^{-s\widetilde{t}_L^*} \mathrm{d}\widetilde{t}_L^* := \mathcal{L}_s(h_0(x, \widetilde{t}_L^*)). \tag{15}$$

The subsidiary equations for (12) and (13) are then given by

$$\frac{1}{2}\sigma^2 \frac{\mathrm{d}^2 \hat{h}_i}{\mathrm{d}x^2} + (\mu + \alpha_i x)\frac{\mathrm{d}\hat{h}_i}{\mathrm{d}x} - \delta \hat{h}_i = s\hat{h}_i, \tag{16}$$

$$\frac{1}{2}\sigma^2\frac{\mathrm{d}^2\hat{h}_0}{\mathrm{d}x^2}+(\mu+\alpha_i x)\frac{\mathrm{d}\hat{h}_0}{\mathrm{d}x}-\delta\hat{h}_0=0, \tag{17}$$

with classic solutions

$$\hat{h}_i(x)=\widetilde{C}_{i,1}\Phi_{i,\delta+s}(x)+\widetilde{C}_{i,2}\Psi_{i,\delta+s}(x),\quad \hat{h}_0(x)=\widetilde{C}_{0,1}\Phi_{0,\delta}(x)+\widetilde{C}_{0,2}\Psi_{0,\delta}(x). \tag{18}$$

Based on the corresponding boundary conditions and the continuity of the functions, we obtain

$$\begin{cases} d_{n,1}\widetilde{C}_{n,1}+d_{n,2}\widetilde{C}_{n,2}=0, \\ u_{i,1}\widetilde{C}_{i,1}+u_{i,2}\widetilde{C}_{i,2}-d_{i-1,1}\widetilde{C}_{i-1,1}-d_{i-1,2}\widetilde{C}_{i-1,2}=0, \text{for}\ \ i=1,...,n, \\ u^*_{i,1}\widetilde{C}_{i,1}+u^*_{i,2}\widetilde{C}_{i,2}-d^*_{i-1,1}\widetilde{C}_{i-1,1}-d^*_{i-1,2}\widetilde{C}_{i-1,2}=0, \text{for}\ \ i=1,...,n, \end{cases} \tag{19}$$

where $u_{i,1}, u_{i,2}, d_{i,1}, d_{i,2}, u^*_{i,1}, u^*_{i,2}, d^*_{i,1}, d^*_{i,2}$ are defined in (4.32) and (4.34). It is a system of $2n+1$ equations involving $2n+2$ unknowns. To make it identifiable, we rescale the unknowns by $\widetilde{C}_{0,2}$ and obtain

$$\widetilde{C}^R_{i,1}=\widetilde{C}_{i,1}/\widetilde{C}_{0,2},\quad \widetilde{C}^R_{i,2}=\widetilde{C}_{i,2}/\widetilde{C}_{0,2}, \text{for}\ \ i=1,...,n,\quad \widetilde{C}^R_{0,1}=\widetilde{C}_{0,1}/\widetilde{C}_{0,2}\ \ \widetilde{C}^R_{0,2}=1.$$

$\widetilde{\mathbf{C}}^R=[\widetilde{C}^R_{n,1},\widetilde{C}^R_{n,2},\widetilde{C}^R_{n-1,1},\widetilde{C}^R_{n-1,2},\cdots,\widetilde{C}^R_{1,1},\widetilde{C}^R_{1,2},\widetilde{C}^R_{0,1}]$ is then solvable based on system (19), which gives us

$$\hat{h}_i(x)=\widetilde{C}_{0,2}(\widetilde{C}^R_{i,1}\Phi_{i,\delta+s}(x)+\widetilde{C}^R_{i,2}\Psi_{i,\delta+s}(x)), \hat{h}_0(x)=\widetilde{C}_{0,2}(\widetilde{C}^R_{0,1}\Phi_{0,\delta}(x)+\Psi_{0,\delta}(x)).$$

By inverting the Laplace transform, the solution of (12) and (13) are determined by

$$h(x,\widetilde{t}_L(0))=\sum_{i=1}^{n}\mathcal{L}_s^{-1}[\hat{h}_i(x)]|_{\tau=\widetilde{t}^*_L}\mathbf{1}_{A_i}(x),\quad h_0(x,\widetilde{t}_L(0))=\mathcal{L}_s^{-1}[\hat{h}_0(x)]|_{\tau=\widetilde{t}^*_L}.$$

By recognizing the denominator of the factorization form (10-11) satisfying

$$h_0'(b,\widetilde{t}_L(0))=\widetilde{C}_{0,2}\mathcal{L}_s^{-1}\left[\widetilde{C}^R_{0,1}\left.\frac{\partial\Phi_{0,\delta}}{\partial x}\right|_{x=b}+\left.\frac{\partial\Psi_{0,\delta}}{\partial x}\right|_{x=b}\right]\Bigg|_{\tau=\widetilde{t}^*_L}, \tag{20}$$

we arrive at the dividend value function $\widetilde{V}(x,\widetilde{t}_L(0);b,T_L)$ in Proposition 4.2.3.

Bibliography

[1] Alizadeh, S., Brandt, M., and Diebold, F. (2002). Range-based estimation of stochastic volatility models. *Journal of Finance*, 57, 1047–1091.

[2] Amin, K., and Khanna, A. (1994). Convergence of American option values from discrete to continuous time financial models. *Mathematical Finance*, 4, 289–304.

[3] Asmussen, S., and Taksar, M. (1997). Controlled diffusion models for optimal dividend pay-out. *Insurance: Mathematics and Economics*, 20, 1–15.

[4] Bailey, D.H., and Swarztrauber, P.N. (1991). The fractional Fourier transform and applications. *SIAM Review*, 33, 389–404.

[5] Barone-Adesi, G., and Whaley, R. (1987). Efficient analytical approximation of American option values. *Journal of Finance*, 42, 301–320.

[6] Bernard, C., and Chen, A. (2009). On the regulator-insurer interaction in a structural model. *Journal of Computational and Applied Mathematics*, 233, 3–15.

[7] Bessembinder, H., Coughenour, J.F., Seguin, P.J., and Smoller, M.M. (1995). Mean reversion in equilibrium asset prices: Evidence from the futures term structure. *Journal of Finance*, 50, 361–375.

[8] Bibby, B.M., and Soresen, M. (1996). A hyperbolic diffusion model for stock prices. *Finance and Stochastics*, 1, 25–41.

[9] Black, F., and Scholes, M. (1973). The pricing of options and corporate liabilities. *Journal of Political Economy*, 81, 637–654.

[10] Brennan, M., and Schwartz, E. (1977). The valuation of American put options. *Journal of Finance*, 32, 449–462.

[11] Broadie, M., Chernov, M., and Sundaresan, S. (2007) Optimal debt and equity values in the presence of chapter 7 and chapter 11. *Journal of Finance*, 62, 1341–1377.

[12] Broadie, M., and Detemple, J. (1996). American option valuation: new bounds, approximations and a comparison of existing methods. *Review of Financial Studies*, 9, 1211–1250.

[13] Cadenillas, A., Sarkar, S., and Zapatero, F. (2007). Optimal dividend policy with mean-reverting cash reservoir. *Mathematical Finance*, 17, 81–109.

[14] Cai, J., Gerber, H.U., and Yang, H. (2006). Optimal dividends in an Ornstein-Uhlenback type model with credit and debit interest. *North American Actuarial Journal*, 10, 94–108.

[15] Carr, P. (1998). Randomization and the American put. *Review of Financial Studies*, 11, 597–626.

[16] Carr P., and Madan D. (1999). Option pricing and the fast Fourier transform. *Journal of Computational Finance*, 2, 61–73.

[17] Carr, P., Jarrow, R., and Myneni, R. (1992). Alternative characterizations of American put options. *Mathematical Finance*, 2, 87–106.

[18] Carr, P., Tari, M., and Zariphopolou, T. (1999). Closed form option valuation with smiles. Bank of America Securities Working Paper.

[19] Cetin, U., Jarrow, R., Protter, P., and Yildirim, Y. (2004). Modeling credit risk with partial information. *Annals of Applied Probability*, 14, 1167–1178.

[20] Chen, X., Chadam, J., Jiang, L., and Zheng, W. (2008). Convexity of the exercise boundary of the American put option on a zero dividend asset. *Mathematical Finance*, 18, 185–197.

[21] Chen, A., and Suchanecki, M. (2007). Default risk, bankruptcy procedures and the market value of life insurance liabilities. *Insurance: Mathematics and Economics*, 40, 231–255.

[22] Chernov, M., Gallant, A.R., Ghysels, E., and Tauchen, G. (2003). Alternative models for stock price dynamics. *Journal of Econometrics*, 116, 225–257.

[23] Chourdakis, K. (2004). Option pricing using the fractional FFT. *Journal of Computational Finance*, 8, 1–18.

[24] Cox, J. (1975). Notes on option pricing I: constant elasticity of variance diffusions, working paper, Stanford University, 1975 (reprinted in *Journal of Portfolio Management* 22(1996), 15–17).

[25] Cox, J., Ross, S., and Rubinstein, M. (1979). Option pricing–a simplified approach. *Journal of Financial Economics*, 7, 229–263.

[26] Davydov, D., and Linetsky, V. (2001). Pricing and hedging path dependent options under the CEV process. *Management Science*, 47, 949–965.

[27] Derman, E., and Kani, I. (1994). Riding on a smile. *Risk*, 7, 32–39.

[28] Detemple, J. (2001). American options: symmetry property. In Cvitanic, J., Jouini, E., and Musiela, M. (Eds.), *Option Pricing, Interest Rates and Risk Management*, Cambridge University Press, 2001.

[29] Detemple, J., and Tian, W.T. (2002). The valuation of American options for a class of diffusion processes. *Management Science*, 48, 917–937.

[30] Duan, J., and Pliska, S.R. (2004). Option valuation with co-integrated asset prices. *Journal of Economic Dynamics & Control*, 28, 727–754.

[31] Dupire, B. (1994). Pricing with a smile. *Risk*, 7, 18–20.

[32] Ekström, E., and Johnson, H.E. (2004). Convexity of the optimal stopping boundary for the American put option. *Journal of Mathematical Analysis and Applications*, 299, 147–156.

[33] Ekvall, N., Jennergren, L.P., and Naslund, B. (1997). Currency option pricing with mean reversion and uncovered interest parity: A revision of the Garman-Kohlhagen model. *European Journal of Operational Research*, 100, 41–59.

[34] Emanuel, D., and MacBeth, J. (1982). Further results on the constant elasticity of variance call option pricing model. *Journal of Financial and Quantitative Analysis*, 17, 533–554.

[35] Erhan, B. (2009). On the perpetual American put options for level dependent volatility models with jumps. *Quantitative Finance*, doi: 10.1080/14697680903170817.

[36] Fatone, L., Mariani, F., Recchioni, M.C., and Zirilli, F. (2009). An explicitly solvable multi-scale stochastic volatility model: Option pricing and calibration. *Journal of Futures Markets*, 29, 862–893.

[37] Fouque, J.P., Papanicolaou, G., Sircar, R., and Solna, K. (2003). Multiscale stochastic volatility asymptotics. *SIAM Journal on Multiscale Modeling and Simulation*, 2, 22–42.

[38] Fouque, J.P., Sircar, R., and Solna, K. (2006). Stochastic volatility effects on defaultable bonds. *Applied Mathematical Finance*, 13, 215–244.

[39] Fouque, J.P., Wignall, B.C., and Zhou, X. (2008). Modeling correlated defaults: First passage model under stochastic volatility. *Journal of Computational Finance*, 11, 43–78.

[40] Francois, P., and Morellec, E. (2004). Capital structure and asset prices: some effects of bankruptcy procedures. *Journal of Business*, 77, 387–412.

[41] Galaia, G., Raviv, A., and Wiener, Z. (2007). Liquidation triggers and the valuation of equity and debt. *Journal of Banking and Finance*, 31, 3604–3620.

[42] Gerber, H.U., and Shiu, E.S.W. (2003). Geometric Brownian motion models for assets and liabilites: from pension funding to optimal dividends. *North American Actuarial Journal*, 7, 37–56.

[43] Gerber, H.U., and Shiu, E.S.W. (2004). Optimal dividends: analysis with Brownian motion. *North American Actuarial Journal*, 8, 1–20.

[44] Gerber, H.U., and Shiu, E.S.W. (2006). On optimal dividends: from reflection to refraction. *Journal of Computational and Applied Mathematics*, 186, 4–22.

[45] Geske, R., and Johnson, H.E. (1984). The American put option valued analytically. *Journal of Finance*, 39, 1511–1524.

[46] Griebsch, S., and Wystup, U. (2008). On the valuation of fader and discrete barrier options in Heston's stochastic volatility model. Working paper from SSRN: http://ssrn.com/abstract=1310422.

[47] Heston, S. (1993). A closed-form solution of options with stochastic volatility with applications to bond and currency options. *Review of Financial Studies*, 6, 327–343.

[48] Hugonnier, J. (1999). The Feynman-Kac formula and pricing of occupation time derivatives. *International Journal of Theoretical and Applied Finance*, 2, 153–178.

[49] Hui, C.H., and Lo, C.F. (2006). Currency barrier option pricing with mean reversion. *Journal of Futures Markets*, 26, 939–958.

[50] Jeanblanc-Picqué, M., and Shiryaev, A.N. (1995). Optimization of the flow of dividends, *Russian Mathematical Surveys*, 20, 257–277.

[51] Jiang, L.S., and Dai, M. (1999). Convergence of binomial tree method for American options. *Partial Differential Equations and Their Applications*, Chen, H., and Rodino, L. eds., World Scientific, River Edge, NJ, 106–118.

[52] Jorion, P., and Sweeney, R.J. (1996). Mean reversion in real exchange rates: Evidence and implications for forecasting. *Journal of International Money and Finance*, 15, 535–550.

[53] Karatzas, I., and Shreve, S.E. (1991). *Brownian motion and stochastic calculus*, 2nd Edition, Springer.

[54] Kim, I.J. (1990). The analytic valuation of American puts. *The Review of Financial Studies*, 3, 547–572.

[55] Kimura, T. (2008). Valuing finite-lived Russian options. *European Journal of Operational Research*, 189, 363–374.

[56] Lau, K.W., and Kwok, Y.K. (2004). Anatomy of Option features in convertible bonds. *Journal of Futures Markets*, 24, 513–532.

[57] LeBaron, B. (2001). Stochastic volatility as a simple generator of apparent financial power laws and long memory. *Quantitative Finance*, 1, 621–631.

[58] Leung, K.S., and Kwok, Y.K. (2007). Distribution of occupation times for CEV diffusions and pricing of α-quantile options. *Quantitative Finance*, 7, 87–94.

[59] Leung, K.S., Kwok, Y.K., and Leung, S.Y. (2008). Finite time dividend-ruin models. *Insurance: Mathematics and Economics*, 42, 154–162.

[60] Liao, S.J. (1997). Numerically solving non-linear problems by the homotopy analysis method. *Computational Mechanics*, 20, 530–540.

[61] Liao, S.J. (2004). *Beyond Perturbation: Introduction to the Homotopy Analysis Method*, Chapman & Hall/CRC.

[62] Linetsky, V. (1999). Step options. *Mathematical Finance*, 9, 55–96.

[63] Longstaff, F.A., and Schwartz, E.S. (2001). Valuing American options by simulation: a simple least-squares approach. *Review of Financial Studies*, 14, 113–148.

[64] MacMillan, L. (1986). Analytical approximation for the American put option. *Advances in Future and Option Research*, 1, 119–139.

[65] Merton, R.C. (1973). The theory of rational option pricing. *Bell Journal of Economics and Management Science*, 4, 141–183.

[66] Nelson, D.B., and Ramaswamy, K. (1990). Simple binomial processes as diffusion approximations in financial models. *Review of Financial Studies*, 3, 393–430.

[67] Novikov, A.A. (1979). On conditions for uniform integrability of continuous nonnegative martingales. *Theory of Probability and Its Applications*, 24, 820–824.

[68] Nunes, J.P.V. (2009). Pricing American options under the constant elasticity of variance model and subject to bankruptcy. *Journal of Financial and Quantitative Analysis*, 44, 1231–1263.

[69] Patty, C.W. (1993). *Foundations of Topology*, PWS-KENT Publishing Company, Boston.

[70] Piessens, R. (1971). Gaussian quadrature formulas for the numerical integration of Bromwich's integral and the inversion of the Laplace transform. *Journal of Engineering Mathematics*, 5, 1–9.

[71] Rubinstein, M. (1994). Implied binomial trees. *Journal of Finance*, 49, 771–818.

[72] Shreve, S.E., Lehoczky, J.P., and Gaver, D.P. (1984). Optimal consumption for general diffusions with absorbing and reflecting barriers. *Journal on Control and Optimization*, 22, 55–75.

[73] Sidi, A. (2003). *Practical Extrapolation Methods: Theory and Applications*, Cambridge University Press.

[74] Slater, L.J. (1996). *Confluent Hypergeomteric Functions*, Cambridge University Press, Cambridge, U.K.

[75] Sorensen, C. (1997). An equilibrium approach to pricing foreign currency options. *European Financial Management*, 3, 63–84.

[76] Sundaresan, S.M. (2000). Continuous-time methods in finance: a review and an assessment. *Journal of Finance*, 55(4), 1569–1622.

[77] Sweeney, R.J. (2006). Mean reversion in G-10 nominal exchange rates. *Journal of Financial and Quantitative Analysis*, 41, 685–708.

[78] Wong, H.Y., and Chan, C.M. (2007). Lookback options and dynamic fund protection under multiscale stochastic volatility. *Insurance: Mathematics and Economics*, 40, 357–385.

[79] Wong, H.Y., and Chan, C.M. (2008). Turbo warrants under stochastic volatility. *Quantitative Finance*, 8, 739–751.

[80] Wong, H.Y., and Kwok, Y.K. (2003). Multi-asset barrier options and occupation time derivatives. *Applied Mathematical Finance*, 10, 245–266.

[81] Wong, H.Y., and Lau, K.Y. (2008). Path-dependent currency options with mean reversion. *Journal of Futures Markets*, 28, 275–293.

[82] Wong, H.Y., and Lo, Y.W. (2009). Option pricing with mean reversion and stochastic volatility. *European Journal of Operational Research*, 197, 179–187.

[83] Wong, H.Y., and Zhao, J. (2008). An artificial boundary method for American option pricing under the CEV model. *SIAM Journal on Numerical Analysis*, 46, 2183–2209.

[84] Wong, H.Y., and Zhao, J. (2010). Currency option pricing: mean reversion and multi-scale stochastic volatility. *The Journal of Futures Markets*, doi: 10.1002/fut.20452.

[85] Wu, L.X., and Kwok, Y.K. (1997). A front-fixing finite difference method for the valuation of American options. *Journal of Financial Engineering*, 6, 83–97.

[86] Yildirim, Y. (2006). Modeling default risk: a new structural approach. *Finance Research Letters*, 3, 165–172.

[87] Zhao, J., and Wong, H.Y. (2010). A closed-form solution to American options under general diffusion processes. *Quantitative Finance*, doi: 10.1080/14697680903193405.

[88] Zhu, S.P. (2006). An exact and explicit solution for the valuation of American put options. *Quantitative Finance*, 6(3), 229–242.

[89] Zwillinger, D. (1992). *Handbook of Differential Equations*, Boston: Academic Press.